



Max-Planck-Institut für Metallforschung
Stuttgart

**Nitriding of Iron-based Alloys; residual stresses and
internal strain fields**

Nicolás Vives Díaz

Dissertation
an der

Universität Stuttgart

Bericht Nr. 207
November 2007



Max-Planck-Institut für Metallforschung
Stuttgart

**Nitriding of Iron-based Alloys; residual stresses and
internal strain fields**

Nicolás Vives Díaz

Dissertation
an der

Universität Stuttgart

Bericht Nr. 207
November 2007

Nitriding of Iron-based Alloys; residual stresses and internal strain fields

von der Fakultät Chemie der Universität Stuttgart
zur Erlangung der Würde eines Doktors der
Naturwissenschaften (Dr. rer. nat.) genehmigte Abhandlung

vorgelegt von

Nicolás Vives Díaz

aus Rosario/Argentinien

Hauptberichter:	Prof. Dr. Ir. E. J. Mittemeijer
Mitberichter:	Prof. Dr. F. Aldinger
Mitprüfer:	Prof. Dr. E. Roduner

Tag der Einreichung:	30.07.2007
Tag der mündlichen Prüfung:	05.11.2007

MAX-PLANCK-INSTITUT FÜR METALLFORSCHUNG, STUTTGART
INSTITUT FÜR METALLKUNDE DER UNIVERSITÄT, STUTTGART

2007

Contents

1. Introduction	9
1.1. General introduction	9
1.2. Microstructural development upon nitriding of iron-based alloys. Occurrence of “excess nitrogen” and residual macro- and micro-stresses.....	10
1.3. Aim and outlook of the thesis.....	12
References	14
2. The morphology of nitrided iron-chromium alloys; influence of chromium content and nitrogen supersaturation.....	15
2.1. Introduction; two types of precipitate morphology	16
2.2. Experimental.....	17
2.2.1. Specimen preparation.....	17
2.2.2. Nitriding	17
2.2.3. X-ray Diffraction (XRD)	18
2.2.4. Microscopy	18
2.2.5. Electron probe microanalysis (EPMA).....	19
2.2.6. Micro-hardness measurement.....	19
2.3. Results and discussion	19
2.3.1. Phase analysis	19
2.3.2. Morphology.....	19
2.3.3. Micro-hardness measurements.....	23
2.3.4. Concentration-depth profiles.....	24
2.4. Morphological consequences of chromium content and nitrogen supersaturation changing with depth.....	28
2.5. Conclusions	31
Acknowledgements	32
References	32
3. Influence of the microstructure on the residual stresses of nitrided iron-chromium alloys.....	35
3.1. Introduction	36
3.2. Experimental procedures and data evaluation.....	37
3.2.1. Specimen preparation	37
3.2.2. Nitriding	38
3.2.3. Phase characterization using X-ray diffraction (XRD).....	38
3.2.4. Microscopy.....	39
3.2.5. Electron-probe microanalysis.....	39
3.2.6. Hardness measurements.....	39
3.2.7. Determination of residual stress-depth profile using XRD.....	39
3.3. Results and discussion	42
3.3.1. Phase analysis.....	42
3.3.2. Morphology of the nitrided zone; two types of precipitation morphology.	42
3.3.3. Hardness-depth profiles.....	42
3.3.4. Nitrogen concentration-depth profiles.....	44
3.3.5. Residual stress-depth profiles.....	46
3.4. General discussion; the build up and relaxation of stress.....	50
3.5. Conclusions.....	54
3.6. Appendix; correction of the measured stress for stress relaxation upon	

removing layers from the nitrated specimen.....	55
Acknowledgements	57
References	57
4. Nitride precipitation and coarsening in Fe–2 wt%. V alloys; XRD and (HR)TEM study of coherent and incoherent diffraction effects caused by misfitting nitride precipitates in a ferrite matrix	59
4.1. Introduction	60
4.2. Experimental	61
4.2.1. Specimen preparation	61
4.2.2. Nitriding; denitriding and annealing experiments.....	62
4.2.3. Transmission Electron Microscopy (TEM).....	63
4.2.4. X-ray diffraction (XRD).....	63
4.2.4.1. Texture measurements	63
4.2.4.2. 2θ -scans	64
4.3. Results and preliminary discussion	65
4.3.1. As-nitrated specimens	65
4.3.1.1. Phase analysis using X-ray diffraction (XRD)	65
4.3.1.2. Analysis of the microstructure using TEM and HRTEM	65
4.3.2. Nitrated and annealed specimens	69
4.3.2.1. Phase analysis using X-ray diffraction (XRD)	70
4.3.2.2. Effects of denitriding	71
4.3.2.3. Analysis of the microstructure using TEM and HRTEM	72
4.3.3. Stoichiometry of the nitrated platelets; evidence of absorbed nitrogen of types I, II and III	76
4.3.4. Analysis of the X-ray diffraction profiles	78
4.3.4.1. Diffraction model	78
4.3.4.2. Results of the fitting and discussion	80
4.4. General discussion: “sidebands” and coarsening	84
4.5. Conclusions	86
Acknowledgements	87
References	87
5. Zusammenfassung	89
5.1. Einleitung	89
5.2. Experimentelles	90
5.3. Ergebnisse und Diskussion	91
5.3.1. Mikrostruktur der Nitrierschicht von Fe-Cr Legierungen	91
5.3.2. Der Einfluss des Cr Gehaltes und des Überschussstickstoffes auf die Mikrostruktur der Nitrierschichten in Fe-Cr Legierungen	93
5.3.3. Einfluss der Mikrostruktur nitrierter Schichten in Fe-Cr Legierungen auf die Eigenspannungen	93
5.3.4. Nitridausscheidungen und Ausscheidungsvergrößerungen in Fe-2 Gew. % V Legierungen	96
Curriculum Vitae	99
Danksagung	101

Chapter 1

Introduction

1.1 General introduction

Nitriding is a thermochemical treatment widely used to modify and improve the mechanical and corrosion properties of iron and iron-based alloys. Nitriding consists of the inward diffusion of nitrogen into the specimen; the nitrogen is absorbed through the surface of the material. There are several methods to achieve this goal: plasma nitriding, salt-bath nitriding and gaseous nitriding are among the most common ones. Gaseous nitriding possesses the fundamental advantage of providing an accurate control of the chemical potential in the nitriding atmosphere, which is accomplished by mass-flow controllers. The nitriding atmosphere is a mixture of hydrogen (H_2) and ammonia (NH_3) gas. Ammonia gas dissociates at the surface of the iron-based alloy at temperatures in the range 450-590 °C and the thereby produced nitrogen enters the material through its surface. As a result of the nitriding process a nitrided zone develops, which, depending on the nitriding conditions (nitriding time, nitriding temperature and nitriding potential [1]), can usually be subdivided into a compound layer adjacent to the surface, composed of iron nitrides; and a diffusion zone, beneath the compound layer, see Fig 1.1.

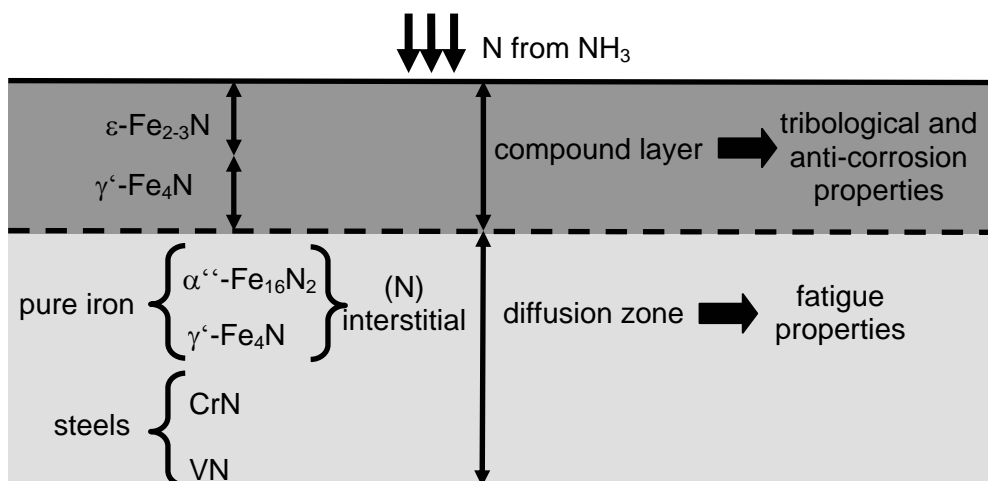


Fig. 1.1: Schematic representation of the surface of a nitrided specimen of iron/iron-based alloy. The nitriding parameters used in this thesis allow the formation of a diffusion zone only; no iron-nitrides were formed.

In the diffusion zone nitrogen can be dissolved (on a fraction of the octahedral interstitial sites of the ferrite lattice) or precipitated as internal nitrides MeN_x , if nitride forming elements (as, for example, Ti, Al, V, Cr) are present. The improvement of the tribological and anticorrosion properties can be mainly attributed to the compound layer at the surface of the specimen [2], while enhancement of the fatigue properties is ascribed to the diffusion zone [3].

1.2 Microstructural development upon nitriding of iron-based alloys.

Occurrence of “excess nitrogen” and residual macro- and micro-stresses

Chromium and vanadium are often used as alloying elements in nitriding steels because of their relatively strong interaction with nitrogen. Sub-microscopical, coherent nitrides develop during the initial stage of the nitriding process; the precipitation of these nitrides is associated with the occurrence of a relatively high hardness. This high hardness is a consequence of the strain fields surrounding the precipitates, which are induced by the misfit between the nitride particles and the ferrite matrix, and which hinder the movement of dislocations, see Fig. 1.2. It has been observed [4,5] that upon nitriding iron-chromium and iron-vanadium alloys a surplus uptake of nitrogen occurs: “excess nitrogen”. Excess nitrogen is the amount of nitrogen that exceeds the normal capacity of nitrogen uptake of the alloy. This normal capacity consists of two contributions: (1) the amount of nitrogen dissolved in the octahedral interstices of the unstrained ferrite, and (2) the amount of nitrogen incorporated in the alloying element nitride precipitates. The difference between the total amount of nitrogen in the nitrided zone and this normal capacity is defined as “excess nitrogen”. Three types of “excess” nitrogen can be distinguished: (1) nitrogen trapped at dislocations (in particular for deformed alloys), (2) nitrogen adsorbed at the precipitate/matrix interfaces and (3) nitrogen which is additionally dissolved in the strained ferrite matrix.

Upon continued nitriding, coarsening of the nitride particles already formed occurs, and consequently several phenomena take place: loss of coherency, decrease of the misfit strain energy and of the nitride/ferrite interfacial area, and loss of nitrogen supersaturation. The coarsening process can occur in two ways: (i) “continuous coarsening” implies the growth of larger particles at the cost of the smaller ones; (ii) “discontinuous coarsening” involves the development of a lamellar structure consisting of alternate ferrite and nitride lamellae. Both reactions can occur simultaneously and lead to a decrease of hardness and disappearance of

long-range strain fields, effects that are particularly pronounced for the lamellar microstructure. The mechanism of coarsening in the nitrated zone depends on the alloying element content and the alloying element: for both chromium and vanadium, it holds (approximately) that in the concentration range 0-2 wt.% alloying element mainly continuous coarsening takes place, whereas in the range between 2-10 wt.% alloying element a mixture of both mechanisms can be observed. For the nitrated zones of iron alloys with more than 10 wt.% alloying element content, only discontinuous coarsening can be observed [6].

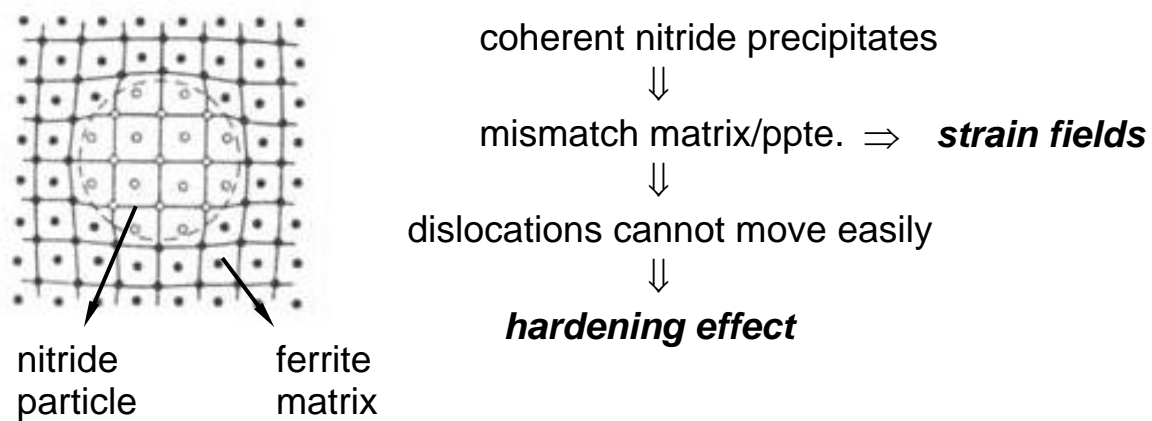


Fig. 1.2: Schematic representation of the precipitation of a coherent nitride particle and the corresponding occurrence of strain fields in the surrounding ferrite matrix, which leads to a hardening effect.

The development of residual macrostresses during nitriding is related to the difference in specific volume between the matrix and the nitrides, and can be described (in an extremely simplified way) as follows: consider first an unnitrided specimen (see Fig. 1.3a), during nitriding nitrogen is absorbed through the surface and diffuses through the sample. Nitrogen combines with the nitride-forming elements and subsequently nitrides precipitate. As there is a difference in specific volume between the matrix and the nitrides, the nitrated layer would tend to expand (see Fig. 1.3b). However, the nitrated layer is attached to the sample, so it cannot expand freely; the matrix counterbalances the expansion by means of compressive stresses, which develop in the nitrated layer. At the same time, to maintain the mechanical equilibrium of the nitrated specimen, small tensile stresses develop in the unnitrided core (see Fig. 1.3c).

A peculiar phenomenon related with the influence of the microstresses on the microstructure of the nitrated iron-based alloy is the occurrence of sidebands on the X-ray diffraction peaks of ferrite instead of separate nitride reflections. The occurrence of sidebands

can be understood considering the different contributions to the X-ray diffraction observed in systems in early stages of precipitation.

The phenomenon of sidebands is directly related to the existence of streaks along the $\langle 100 \rangle$ directions in electron diffraction patterns and a tweed contrast in the microstructure of the nitrated specimens [7, 8]. It is assumed that the tweed contrast, the streaks and the sidebands arise from an arrangement of closely spaced thin plates on cubes planes of the matrix; these plates are a few atomic layers thick and cause a tetragonal distortion of the surrounding ferrite matrix.

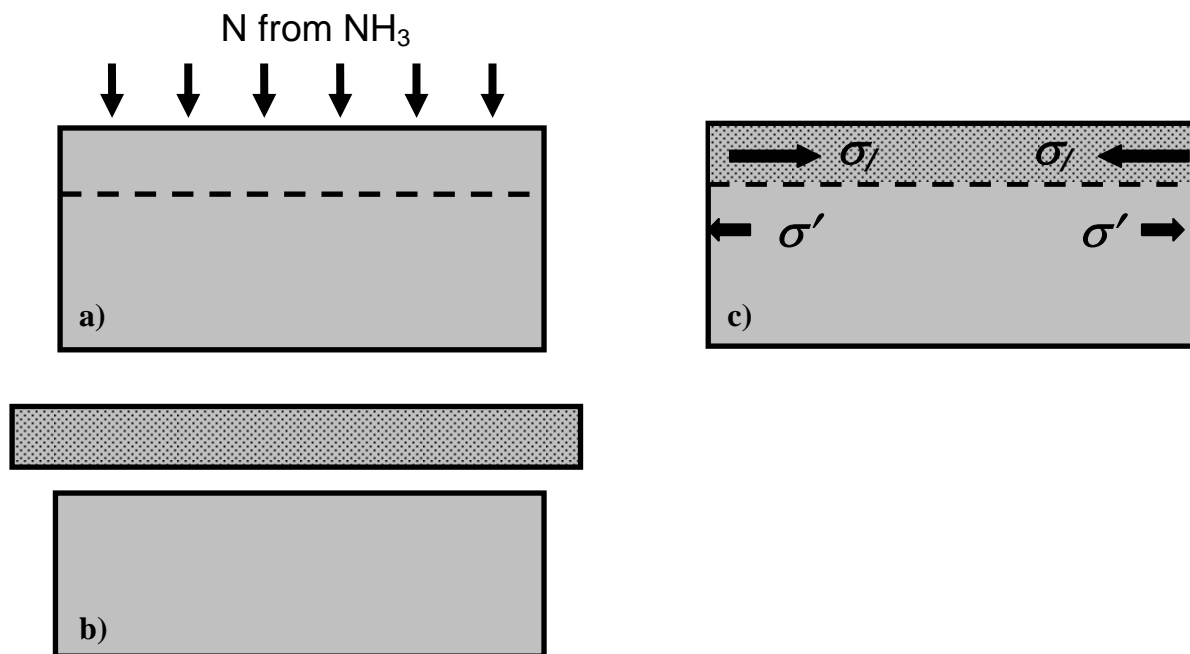


Fig. 1.3: Schematic representation of the development of residual macrostresses in nitrated iron-based alloys. (a) Nitrogen from the decomposition of ammonia is absorbed through the surface of the specimen and diffuses inward. (b) Nitrogen combines with the alloying element(s) and nitride precipitates develop. Due to the mismatch between the ferrite and the nitride particle lattices the nitrated zone tends to expand. (c) As the nitrated zone is attached to the whole specimen it cannot expand freely, therefore a compressive stress arises in the nitrated zone in order to counterbalance the desired expansion; tensile stress is generated in the un-nitrated zone in order to maintain the mechanical equilibrium of the specimen.

1.3 Aim and outlook of the thesis

Considering the background described in the previous Sections, the aims of this thesis can be summarized as follows:

1. To explore the influence of nitrogen supersaturation and alloying element content on the microstructure of nitrated iron-chromium alloys.

2. To explain the relation between the microstructure and the development of residual macrostresses in nitrided iron-chromium alloys.
3. To provide fundamental understanding for the phenomenon of peculiar diffraction effects as sidebands and for the microstructural evolution of nitrided iron-vanadium alloys.

In Chapter 2 the influence of the nitrogen supersaturation and the chromium content of the alloy on the microstructure and, consequently, on the mechanical properties of the nitrided iron-chromium alloys has been studied. It has been recognized that the chromium content, but in particular the nitrogen supersaturation, have a cardinal role in the development of the microstructure after nitriding. It has been demonstrated that the increase of the lamellar spacing with depth in the nitrided zone is ascribed to the decrease of nitrogen supersaturation in the ferrite matrix with depth. Near the surface, where the nitrogen supersaturation is maximum, the driving force for discontinuous coarsening is maximal, causing more abundant nucleation of α -Fe/CrN lamellae colonies of relatively small lamellar spacing. The microstructural development of the nitrided iron-chromium specimens is also related to the content of alloy element; at higher chromium contents it is possible that the growth rate of the discontinuously coarsened region is equal to or larger than the nitriding rate. Therefore, the entire nitrided zone of alloys with relatively high chromium content has experienced the discontinuous coarsening reaction.

Chapter 3 is concerned with the development of residual macrostresses upon nitriding of iron-chromium alloys. The residual stress depth-profiles measured for several nitrided specimens depend strongly on the microstructure of the nitrided zone; two different behaviours have been observed for specimens with relatively low and relatively high chromium content.

Chapter 4 is devoted to the characterization of nitrided Fe-2 wt.% V alloy by means of X-ray diffraction (XRD) and transmission electron microscopy (TEM; conventional and high resolution). The experimental diffractograms of the nitrided specimens have been fitted using the hypothesis of tetragonal distortion. The results indicate that sidebands are indeed the contribution of the tetragonally distorted matrix surrounding the extremely small VN platelets. Annealing experiments performed with nitrided specimens showed the high stability of the microstructure; coarsening occurs at relatively high temperatures and the size of most of the particles after coarsening remained relatively small.

References

- [1] E.J. Mittemeijer, J.T. Slycke: Surf. Eng. 12 (1996) 152.
- [2] H.C.F. Rozendaal, P.F. Colijn: Surf. Eng. 1 (1985) 30.
- [3] Mittemeijer, E.J.; J. Heat Treat. 3 (1983) 114.
- [4] P.M. Hekker, H.C.F. Rozendaal, E.J. Mittemeijer: J. Mat. Sci. 20 (1985) 718.
- [5] S.S. Hosmani, R.E. Schacherl, E.J. Mittemeijer: Acta Mater. 17 (2005) 2069.
- [6] R.E. Schacherl, P.C.J. Graat, E.J. Mittemeijer: Z. Metallkd. 93 (2002) 468.
- [7] M. Gouné, T. Belmonte, A. Redjaimia, P. Weisbecker, J.M. Fiorani, H. Michel: Mat. Sci. Eng. A 351 (2003) 23.
- [8] D.H. Jack: Acta Metall. 24 (1976).

Chapter 2

The morphology of nitrided iron-chromium alloys; influence of chromium content and nitrogen supersaturation

N.E. Vives Díaz, R.E. Schacherl and E.J. Mittemeijer

Abstract

Different iron-chromium alloys (4, 8, 13 and 20 wt.% Cr) were nitrided in NH_3/H_2 gas mixtures at 580 °C. The nitrided microstructure was investigated by X-ray diffraction, light microscopy, hardness measurements and scanning electron microscopy. Composition depth-profiles of the nitrided zone were determined by electron probe microanalysis. Various microstructures develop, depending on the nitriding conditions and the alloy composition (chromium content). The initial development of coherent, sub-microscopical CrN nitrides leads to a state of hydrostatic stress allowing the uptake of excess nitrogen dissolved in the ferrite matrix. It is shown that the outcome of the subsequent discontinuous coarsening process, which leads to a lamellar microstructure, has a close relation to the nitrogen supersaturation. As a result, the occurrence of a distinct gradient in hardness across the nitrided zone can be understood.

2.1 Introduction; two types of precipitate morphology

The nitriding of iron-based alloys is an important and widely used thermochemical surface treatment used to improve the tribological, anti-corrosion and/or fatigue properties of iron and iron-based alloys [1-3]. The nitriding process consists of the inward diffusion of nitrogen. This nitrogen can be provided by several methods. In this project gas nitriding has been applied: nitrogen from dissociated NH_3 at temperatures in the range 450-590 °C enters the material through its surface. As a result a nitrided zone develops, which, depending on the nitriding conditions, can be composed of a compound layer of iron nitrides adjacent to the surface, and a diffusion zone, beneath the compound layer, where, in the case an alloying element M with affinity for nitrogen (M: Ti, Al, V, Cr) has been dissolved in the iron matrix, MN_x nitrides can precipitate [4,5].

The precipitates in the matrix cause a large increase of the hardness [6-21], which depends on the chemical composition of the precipitates, their coherency with the matrix, their size and morphology.

Chromium is often used as an alloying element in nitriding steels [13-22]. The initial stage of chromium-nitride formation corresponds to the development of sub-microscopical, coherent precipitates, which are associated with a relatively high hardness [13, 14, 23]. This is a consequence of the strain fields surrounding the precipitates, which are induced by the misfit between the CrN particles and the ferrite matrix, and hinder the movement of dislocations [14]. It has been observed [14] that upon nitriding Fe-Cr alloys a surplus uptake of nitrogen occurs: “excess nitrogen”. Excess nitrogen is the amount of nitrogen that exceeds the normal capacity of nitrogen uptake. This normal capacity consists of two contributions: (1) the amount of nitrogen dissolved in the octahedral interstices of the unstrained ferrite, and (2) the amount of nitrogen incorporated in the alloying element nitride precipitates. The difference between the total amount of nitrogen in the nitrided zone and this normal capacity is defined as “excess nitrogen”. Three types of “excess” nitrogen are distinguished: (1) nitrogen trapped at dislocations (in particular for deformed alloys [7, 8]), (2) nitrogen adsorbed at the precipitate/matrix interfaces and (3) nitrogen which is (additionally) dissolved in the strained ferrite matrix [14, 24].

Continued nitriding leads to coarsening of the initially formed sub-microscopical CrN particles, which is associated with loss of coherency, a decrease of the misfit-strain energy and reduction of CrN/ferrite interfacial area and, consequently, loss of nitrogen supersaturation (enhanced dissolution) in the ferrite matrix [25]. The coarsening process can

occur in two ways: (i) “continuous coarsening” implies the growth of larger particles at the cost of the smaller ones; (ii) “discontinuous coarsening” involves the replacement of the initially fine (coherent or partly coherent) CrN precipitates by a lamellae-like morphology consisting of ferrite and CrN lamellae [14, 18, 26]. Both types of coarsening can occur simultaneously and lead to a decrease of hardness, which is particularly pronounced for the development of the lamellar structure.

Although a series of investigations were devoted to the nitriding of iron-chromium alloys [13-22], fundamental knowledge on the relation between the nitriding parameters and the developing microstructure, especially the precipitation morphology, lacks. The present work is an investigation of the relation between the hardness, the morphology and the nitrogen content, in particular the nitrogen supersaturation, of several iron-chromium alloys, nitrided under different conditions. It is shown that the nitrogen supersaturation within the nitrided zone has a pronounced influence on the final microstructure.

2.2 Experimental

2.2.1 Specimen preparation

Iron alloys with 4 wt.%, 8 wt.%, 13 wt.% and Fe-20 wt.% Cr were prepared of pure iron with a purity of 99.98 wt.% and pure Cr with a purity of 99.999 vol. % in an inductive furnace. The alloy melts were cast into cylindrical moulds of 10 mm \varnothing , 80-100 mm length. The ingots were cut into pieces. Each piece was rolled down to a sheet of about 1.1 mm thickness. The sheets were subsequently machined down to 1 mm thickness, in order to achieve a flat surface. From these sheets rectangular specimens (10×20 mm²) were cut. Next the specimens were ground and polished to remove the grooves on the surface resulting from the machining process, cleaned using ethanol in an ultrasonic bath, and then encapsulated in a quartz tube under an inert atmosphere (Ar, 300 mbar). Subsequently, the specimens were annealed at 700 °C during 2 hours.

2.2.2 Nitriding

The samples were suspended at a quartz fibre in a vertical quartz tube nitriding furnace. The nitriding atmosphere consisted of a mixture of pure NH₃ (>99.998 vol.%) and pure H₂ (99.999 vol. %). The fluxes of both gases were regulated with mass flow controllers. All samples were nitrided at T = 580 °C using a nitriding potential $r_N = 0.104 \text{ atm}^{-1/2}$; one extra sample of Fe-20 wt.% Cr was also nitrided using a nitrided potential $r_N = 0.043 \text{ atm}^{-1/2}$.

Samples of Fe-4 wt.% Cr were nitrided for 1.5 and 6 h; samples of Fe-8 wt.% Cr were nitrided for 1.5, 6 and 24 h; samples of Fe-13 wt.% Cr were nitrided for 6 and 24 h, and samples of Fe-20 wt.% Cr were nitrided for 24 h. After nitriding, the samples were quenched in water and cleaned ultrasonically with ethanol. The nitrided specimens were subjected to X-ray diffraction analysis (see Section 2.2.3). Next, pieces were cut from the specimens for cross-sectional analysis. To embed the specimens, Polyfast, a conductive, polymer-based embedding material, was used. Subsequently the cross sections were ground and polished down to 1 μm diamant paste. For the light optical and scanning electron microscopy investigations the polished cross sections were etched with Nital (HNO_3 dissolved in ethanol) using different HNO_3 concentrations (expressed as % vol.) depending on the alloy (Nital 1% for Fe-4 wt.% Cr, Nital 2.5% for Fe-8 wt.% Cr and Fe-13 wt.% Cr, and Nital 4% for Fe-20 wt.% Cr). Specimens used for electron-probe microanalysis were only ground and polished.

2.2.3 X-ray Diffraction (XRD)

Phase analysis of the nitrided specimens was performed by means of XRD using a Siemens D500 diffractometer, equipped with a Cu tube and a graphite monochromator in the diffracted beam (to select Cu K_α radiation: $\lambda=1.54056 \text{ \AA}$). The diffraction-angle (2θ) range $10^\circ \leq 2\theta \leq 140^\circ$ was scanned with a step size of 0.04° in 2θ . Phase identification was performed comparing the position of the measured peaks with the data derived from the JCPDS data base [27] and the software Carine, based on data from Pearson [28].

2.2.4 Microscopy

The cross sections were investigated with light optical microscopy and scanning electron microscopy (SEM). The applied light optical microscope was a Leica DMRM. The SEM investigations were performed with a Jeol JSM 6300F microscope operated at 3 or 5 KV. The interlamellar spacing was determined as an average from measurements performed on a number of SEM micrographs recorded at the same depth; these micrographs were taken at lateral distances of about 500 μm . The interlamellar spacing was thus determined near to the surface of the specimen and near to the largest depth where discontinuous coarsening had occurred. The measured values were corrected for the variation of the angle of inclination of the lamellae with respect to the surface of the cross section examined, using the correction procedure proposed in [29].

2.2.5 Electron probe microanalysis (EPMA)

To determine the composition-depth profiles in the nitrated zones EPMA was performed using a Cameca SX100 instrument. A focused electron beam at an accelerating voltage of 15 kV and a current of 100 nA was applied. The element contents in the specimen cross-section was determined from the intensity of the characteristic Fe K β , Cr K β , N K α and O K α X-ray emission peaks at points along lines (4-5) across the cross-sections (single measurement points at a distance of 2 or 3 μm , depending on the sample). The intensities obtained for the nitrated samples were divided by the intensities obtained from standard samples of pure Fe (Fe K β), pure Cr (Cr K β), andradite/Ca₃Fe₂(SiO₄)₃ (O K α) and γ' -Fe₄N (N K α). Concentration values were calculated from the intensity ratios applying the $\Phi(\rho z)$ approach according to Pouchou and Pichoir [30].

2.2.6 Micro-hardness measurement

Hardness measurements using Vicker's method were performed using a Leica VHMT MOT device, applying a load of 50 g and a loading time of 30 s. The measured hardness-depth profiles were determined along lines with an inclination angle between 30 and 45° with respect to the surface of the sample (but results are given as a function of depth beneath the surface). At least two to four scans were measured for each specimen.

2.3 Results and discussion

2.3.1 Phase analysis

Diffraction patterns recorded after nitriding (see examples shown in Figs. 2.1a and 2.1b) reveal that the nitrated zones of all specimens are composed of α -Fe and CrN (penetration depth of the Cu K α radiation is 1- 2 μm).

2.3.2 Morphology

The nitrated specimens can be divided in two groups, according to the morphology observed in the light-optical and scanning electron microscopical examination. *The first group* consists of nitrated specimens with relatively low chromium content: nitrated Fe-4 wt.% Cr and Fe-8 wt.% Cr alloys. These specimens exhibit near the surface dark grains with a lamellar morphology. In this region the originally fine, sub-microscopical CrN precipitates have

transformed by a discontinuous coarsening reaction (see Section 2.1). Below this region, mainly bright grains are observed, which contain the fine sub-microscopical coherent precipitates (see Fig 2.2a). These latter precipitates cannot be resolved using light-optical or scanning electron microscopy. Evidence of their existence can be obtained comparing diffractograms recorded from the surface and from the region where these coherent CrN precipitates are present, see Fig. 2.2c. The pronounced broadening of the ferrite reflection is due to micro-stresses produced by the fine, coherent CrN particles; the coherent precipitates diffract with the matrix and thus no separate nitride peaks occur at this stage (see also [10, 31]). In the transition zone between the discontinuous coarsened region and the region containing submicroscopical precipitates, tiny regions revealing the initiation of discontinuous coarsening at grain boundaries can be observed, e.g. in the specimen of Fe-4 wt.% Cr nitrided for 1.5 h (see Fig. 2.2d).

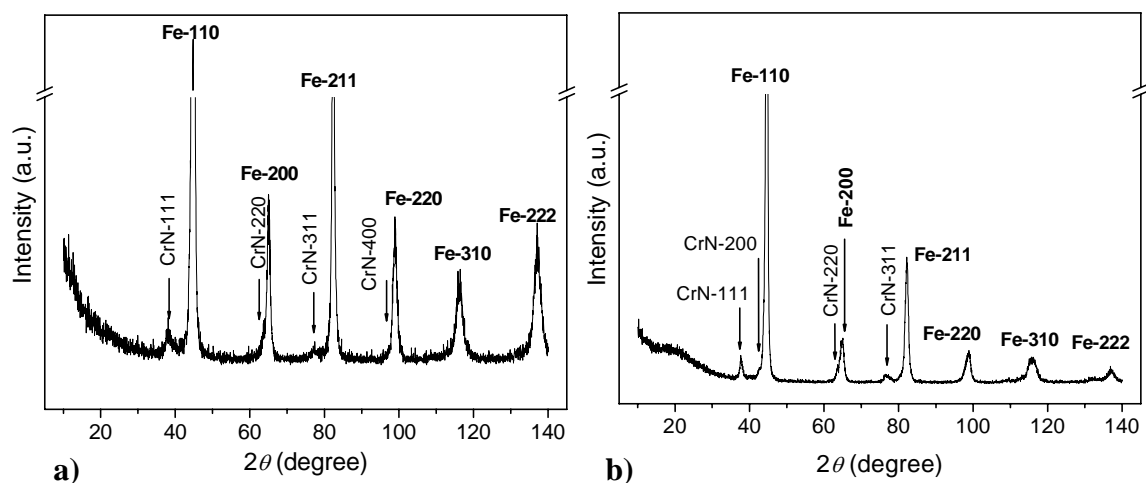


Fig. 2.1: X-ray diffractograms recorded from iron-chromium specimens nitrided at 580 °C with $r_N = 0.104 \text{ atm}^{-1/2}$. All specimens are composed of α -Fe (ferrite) and CrN. The peak positions of α -Fe and CrN have been indicated. **(a)** Fe-8 wt.% Cr alloy nitrided for 1.5 h; **(b)** Fe-13 wt.% Cr alloy nitrided for 6 h.

The second group consists of nitrided specimens with relatively high chromium content: Fe-13 wt.% Cr and Fe-20 wt.% Cr alloys. The entire nitrided zone of these samples has experienced the discontinuous coarsening reaction; see Fig. 2.2b.

The thickness of the nitrided zone depends on the alloy composition, nitriding potential, nitriding temperature and nitriding time. It was found that, for specimens of the same alloy and nitrided under the same conditions, the squared thickness of the nitrided zone depends linearly on the nitriding time (“parabolic growth law”). Higher chromium contents leads to slower nitriding, i.e. thinner nitrided zones, than for alloys with lower chromium content, for

the same nitriding time, in agreement with [17-20], see Fig. 2.3. This result suggests already why for relatively high chromium contents the entire nitrated zone has experienced the discontinuous coarsening (see above): the relatively low migration rate for the nitriding front, in the alloys with relatively high chromium content, allows the discontinuous coarsening reaction front to catch up with the nitriding front (see discussion in Section 2.4).

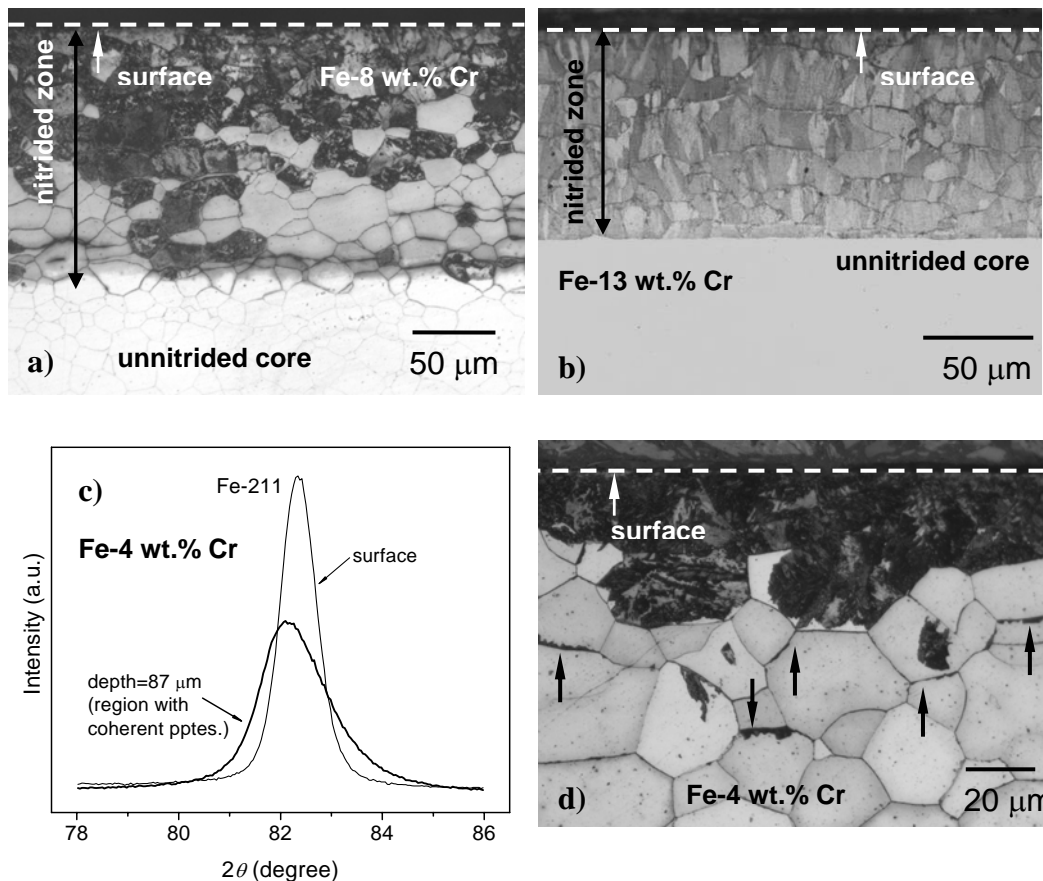


Fig. 2.2: Morphological variety of the nitrated zone. **(a)** Light optical micrograph of a specimen of Fe-8 wt.% Cr nitrided for 6 h showing a nitrated zone with a region adjacent to the surface that has experienced the discontinuous coarsening reaction and a region near the transition nitrated zone/un-nitrated core with coherent, sub-microscopical CrN precipitates; **(b)** specimen of Fe-13 wt.% Cr nitrided for 6 h showing a nitrated zone that has been entirely subjected to the discontinuous coarsening reaction. **(c)** X-ray diffractograms recorded at different depths from the specimen Fe-4 wt.% Cr alloy nitrided for 1.5 h, the broadening of the reflection at depth = 87 μm is caused by the precipitation of fine, coherent CrN particles; **(d)** specimen of Fe-4 wt.% Cr nitrided for 6 h, where tiny regions revealing the initiation of discontinuous coarsening at the grain boundaries can be observed (see arrows). All specimens were nitrided at 580 °C and $r_N = 0.104 \text{ atm}^{-1/2}$.

Detailed examination of the lamellae morphology in the nitrated zone has been performed by SEM. For specimens of relatively low chromium content, nitrated Fe-4 wt.% Cr and Fe-8 wt.% Cr alloys, the micrographs (shown in Figs. 2.4a-d for the nitrated specimen of Fe-8 wt.% Cr alloy) depict a region in the nitrated zone near the surface of the specimen (Figs. 2.4a-b) and a region at the largest depth where discontinuous coarsening had occurred (Figs.

2.4c-d). For specimens of relatively high chromium content, nitrated Fe-13 wt.% Cr and Fe-20 wt.% Cr alloys, the micrographs (shown in Figs. 2.5a-d for the nitrated specimen of Fe-13 wt.% Cr alloy) depict a region in the nitrated zone near the surface of the specimen (Figs. 2.5a-b) and a region at the transition nitrated zone/un-nitrated core (for these alloys of relatively high chromium content the discontinuous coarsened region comprises the entire nitrated zone; cf. Section 2.1).

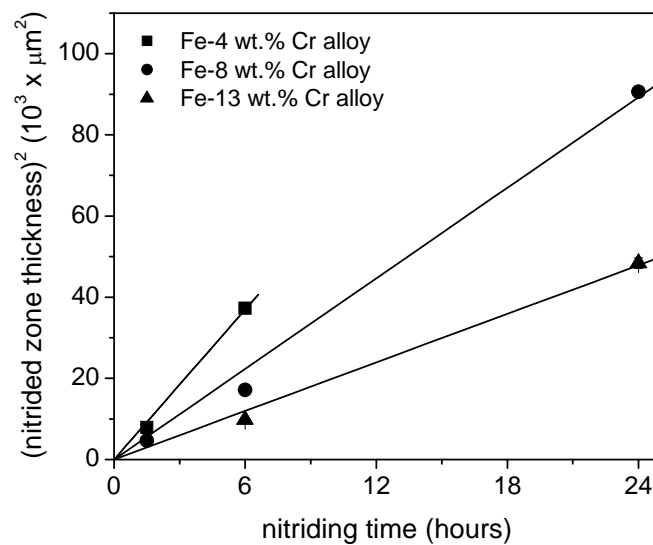


Fig. 2.3: Growth of the nitrated zone for specimens of Fe-4 wt.% Cr, Fe-8 wt.% Cr and Fe-13 wt.% Cr alloys nitrated at 580 °C with $r_N = 0.104 \text{ atm}^{-1/2}$. The nitrated zone thickness was measured as the depth from the surface to the location where the nitrogen content reaches half of the nitrogen content at the surface. Error bars are smaller than the symbols in the figure. The fitted straight lines in this graph of squared thickness of the nitrated zone versus nitriding time at constant nitriding temperature and at constant nitriding potential indicate that a “parabolic growth law” holds (in this case without apparent incubation time, as the lines run through the origin).

For the specimens of low chromium content (nitrated Fe-4 wt.% Cr and Fe-8 wt.% Cr alloys) small colonies of α -Fe and CrN lamellae of relatively small lamellar spacing were observed near the surface, whereas large colonies of larger lamellar spacing were observed at the largest depth where discontinuous coarsening had occurred (see Fig. 2.4).

Similarly for specimens with relatively high chromium content (nitrated Fe-13 wt.% Cr and Fe-20 wt.% Cr alloys): near the surface small colonies of small lamellar spacing occur, whereas larger colonies of distinctly larger lamellar spacing are observed in regions near the nitrated zone/un-nitrated core transition (see Fig. 2.5). A peculiar feature was observed for the nitrated specimen of Fe-20 wt.% Cr alloy: a globular structure occurs near the surface of the specimen, up to a depth of about 1 μm (see Fig. 2.6). This morphology resembles the

morphology of globular pearlite, which is obtained in steels after applying a spheroidization heat treatment [32]. The occurrence of this globular morphology in particular in this specimen, can be ascribed to the relatively long nitriding time used for this specimen (24 h); spheroidization in steels takes place faster in pearlite regions with small lamellar spacing, as pertains to the region adjacent to the surface in this specimen.

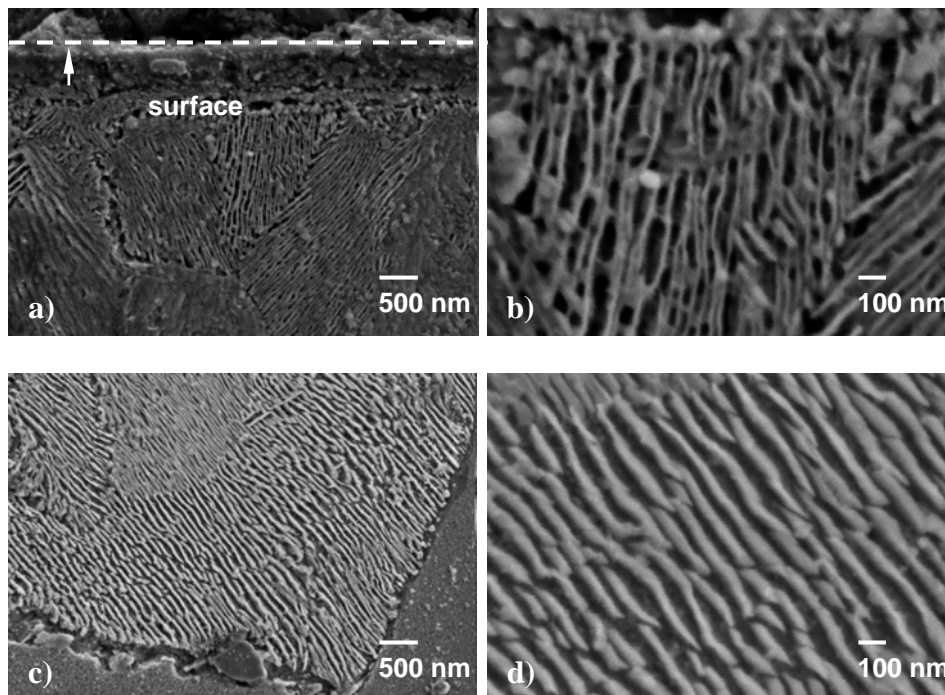


Fig. 2.4: Lamellar morphology in the discontinuously coarsened part of the nitrided zone of a nitrided iron-chromium alloy of relatively low chromium content (specimen of Fe-8 wt.% Cr alloy, nitrided for 6 h at 580 °C with $r_N = 0.104 \text{ atm}^{-1/2}$). (a) overview of the surface region, where a number of colonies of α -Fe/CrN lamellae are observed; (b) detail of one colony in the same region as (a); (c) at the transition between the region composed mainly of discontinuously transformed grains and the region composed mainly of ferrite grains containing coherent, sub-microscopical CrN precipitates; (d) detail of one colony in the same region as (c).

2.3.3 Micro-hardness measurements

The hardness-depth profiles of specimens with low chromium show that near the surface, i.e. in regions where mainly discontinuously coarsened grains are present, a relatively low hardness occurs; whereas at larger depths, where mainly continuous, sub-microscopical CrN particles are present, the hardness is relatively high, see Fig. 2.7.

The hardness-depth profiles of specimens of high chromium content show a continuous decrease in hardness from the surface to the transition nitrided zone/unnitrided core, see Fig. 2.8. The absence of a region of high hardness at the bottom of the nitrided zone is obviously due to the absence of grains containing sub-microscopical CrN precipitates in the nitrided alloys of high chromium content (see Section 2.3.2).

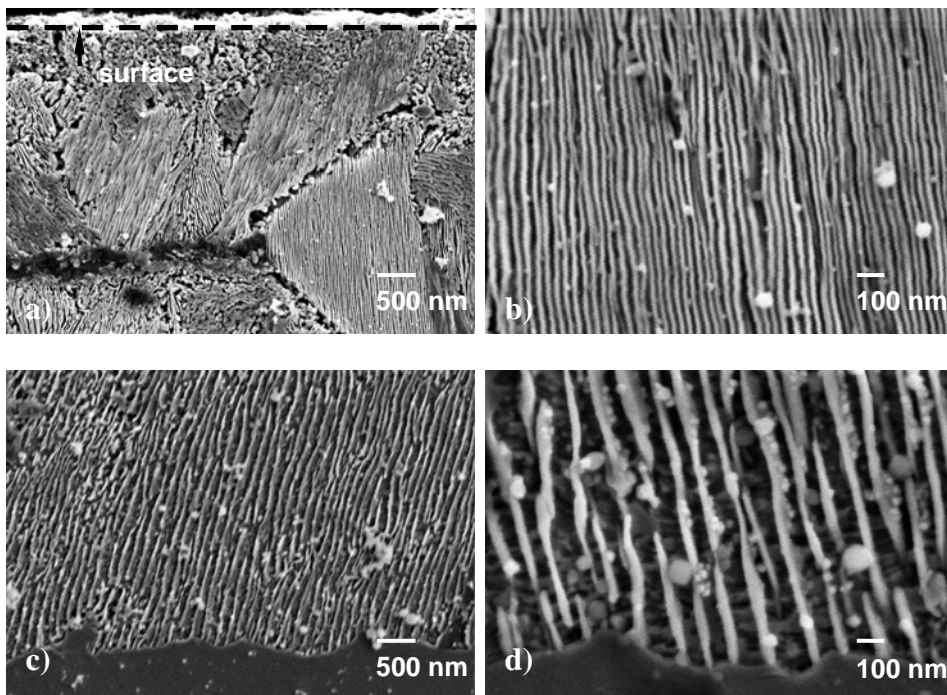


Fig. 2.5: Lamellar morphology in the the nitrided zone of a nitrided iron-chromium alloy of relatively high chromium content (specimen of Fe-13 wt.% Cr alloy, nitrided for 24 h at 580 °C with $r_N = 0.104 \text{ atm}^{-1/2}$) (a) overview of the surface region, where a number of colonies of $\alpha\text{-Fe/CrN}$ lamellae are observed; (b) detail of one colony in the same region as (a); (c) near the transition nitrided zone/unnitrided core; (d) detail of one colony in the same region as (c).

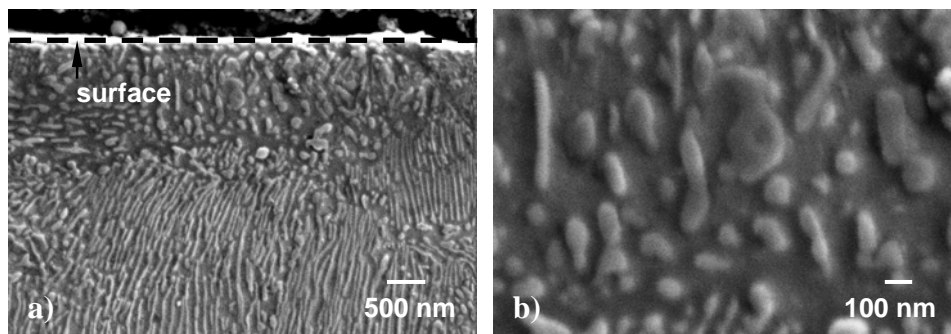


Fig. 2.6: Micrographs taken from the nitrided zone adjacent to the surface of a specimen of Fe-20 wt.% Cr (nitrided for 24 h at 580 °C with $r_N = 0.043 \text{ atm}^{-1/2}$) (a) overview; (b) detail revealing the globular nature of the microstructure of the nitrided zone close to the surface of the specimen.

2.3.4 Concentration depth-profiles

Representative nitrogen concentration-depth profiles, as measured by EPMA, are shown in Figs. 2.9a-d for nitrided alloys of different chromium content. The square data points are the measured total amounts of nitrogen. The “normal” nitrogen content (that is the equilibrium nitrogen content dissolved at interstitial sites in unstressed ferrite matrix plus the nitrogen

incorporated in stoichiometric CrN; cf. Section 2.1) has been indicated by the horizontal dashed line. The positive difference between the square data points and the dashed line represents the amount of “excess nitrogen” (cf. Section 2.1).

For nitrided iron-chromium alloys the predominant part of the excess nitrogen is dissolved in the misfit-strain fields surrounding the coherent, sub-microscopical CrN particles, which are created during nitriding [14, 24].

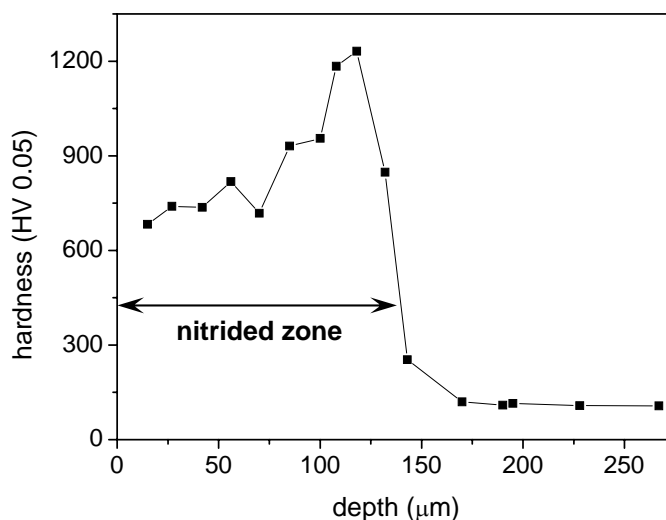


Fig. 2.7: Hardness depth-profile of a specimen of Fe-8 wt.% Cr (nitrided for 6 h at 580 °C with $r_N = 0.104 \text{ atm}^{-1/2}$), with a nitrided zone consisting of grains transformed by the discontinuous coarsening reaction (surface region) and grains containing coherent, sub-microscopical CrN precipitates (near the nitrided zone/unnitrided core transition).

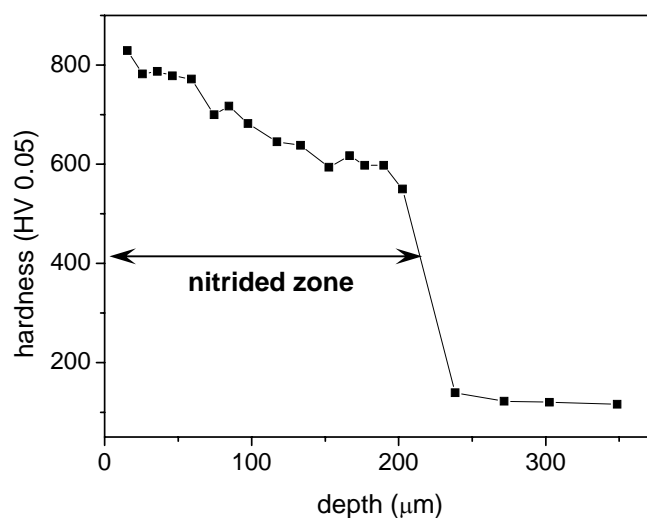


Fig. 2.8: Hardness depth-profile of a specimen of Fe-13 wt.% Cr (nitrided for 24 h at 580 °C with $r_N = 0.104 \text{ atm}^{-1/2}$). The nitrided zone is fully composed of grains which have experienced the discontinuous coarsening reaction.

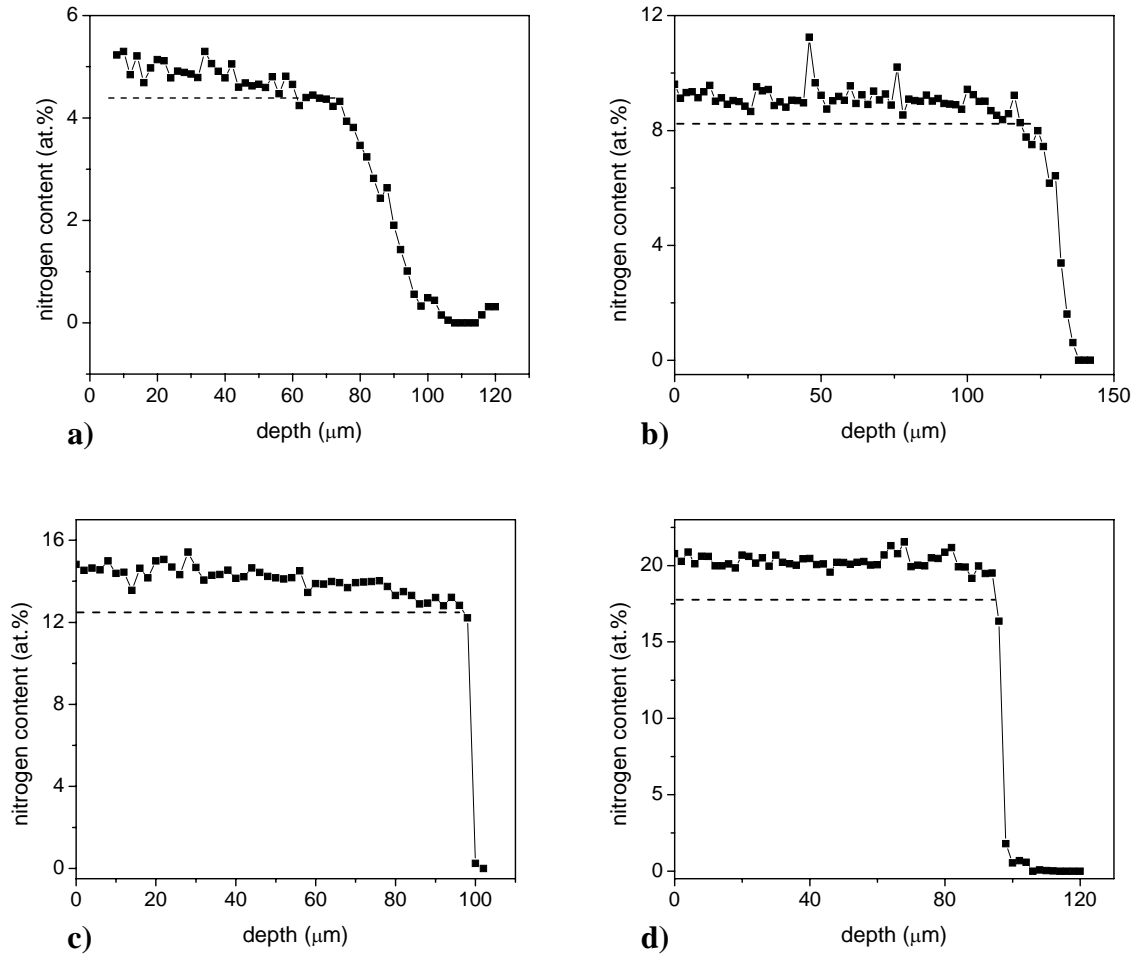


Fig. 2.9: Nitrogen concentration-depth profiles (results of EPMA). (a) Fe-4 wt.% Cr alloy nitrided for 1.5 h; (b) Fe-8 wt.% Cr alloy nitrided for 6 h; (c) Fe-13 wt.% Cr alloy nitrided for 6 h; (d) Fe-20 wt.% Cr alloy nitrided for 24 h. All specimens were nitrided at 580 °C and $r_N = 0.104 \text{ atm}^{-1/2}$. The horizontal lines indicate the “normal” nitrogen uptake as defined in the text.

The nitriding potential of the gas atmosphere determines the equilibrium amount of nitrogen dissolved in ferrite. Only the surface adjacent region of the solid substrate can be in (local) equilibrium with the outer gas atmosphere. Therefore, the amount of excess nitrogen, $[N]_{\text{exc}}$, was calculated taking the average value of the three first measurements of nitrogen content near the surface of the specimens, $[N]_{\text{tot}}$, using the following relation:

$$[N]_{\text{exc}} = [N]_{\text{total}} - [N]_{\text{CrN}} - [N]_{\alpha}^0 \quad \text{Eq. (2.1)}$$

where $[N]_{\text{CrN}}$ is the amount of nitrogen incorporated in the stoichiometric CrN (assuming that all chromium precipitates to form CrN^*) and $[N]_{\alpha}^0$ is the value of equilibrium nitrogen dissolved in unstressed ferrite ($[N]_{\alpha}^0 = 0.4 \text{ at.}\%$ at 580 °C [34]). The results have been gathered in Table 2.1.

* De-nitriding experiments performed by our group in a project to determine the absorption isotherms of nitrided Fe-20 wt.% Cr alloys confirm the stoichiometry of the CrN precipitates [33].

Table 2.1: Various contributions to the total amount of nitrogen in the surface adjacent region of the nitrided zone (EPMA results); $T = 580\text{ }^{\circ}\text{C}$, $r_{\text{N}} = 0.104\text{ atm}^{-1/2}$.

alloy	Fe-4 wt.% Cr		Fe-8 wt.% Cr			Fe-13 wt.% Cr		Fe-20 wt.% Cr
nitriding time (h)	1.5	6	1.5	6	24	6	24	24
total nitrogen, $[\text{N}]_{\text{tot}}$ (at.%)	5.3	5	9.8	9.5	9.4	14.7	14.3	20.8
“normal” nitrogen, $[\text{N}]_{\text{nor}}$ (at.%)	4.4	4.4	8.2	8.2	8.3	12.6	12.4	17.6
“excess” nitrogen, $[\text{N}]_{\text{exc}}$ (at.%)	0.9	0.6	1.6	1.3	1.1	2.1	1.9	3.2

The amount of excess nitrogen increases with increasing chromium content, because the higher the chromium content, the larger the volume fraction of nitrides that precipitates upon nitriding, which increases the capacity for uptake of nitrogen due to the more pronounced straining of the ferrite matrix and the larger amount of nitride/matrix interface. The amount of excess nitrogen decreases with increasing nitriding time, because upon discontinuous coarsening the capacity for the uptake of excess nitrogen is lost (see also discussion below).

Upon discontinuous coarsening relaxation of long range misfit-strain fields and decrease of the nitride/matrix interface area occurs. Thereby, the capacity for excess nitrogen uptake severely decreases. There are three possibilities for the originally, excess nitrogen within the discontinuously coarsened region: (1) it diffuses inward, to contribute to the nitriding of deeper layers in the specimen; (2) it diffuses outward (only possible in regions adjacent to the surface of the specimen) or (3) it precipitates as nitrogen gas (development of pores at the grain boundaries, see [14, 18]). Processes (1) and, in particular, (2) could account for the apparent presence of the remaining excess nitrogen in the discontinuously coarsened region and the decrease of excess nitrogen at the surface of the specimens with increasing nitriding time.

In nitrided specimens of low chromium content (Fe-4 wt.% Cr alloy) the change in nitrogen content at the nitrided zone/unnitrided core transition is smoother (less abrupt) than for nitrided specimens of high chromium content (cf. Figs. 2.9a and 2.9d). This is due to the different “strength” of the nitrogen-chromium interaction in these alloys [5]. For iron-chromium alloys of relatively high chromium content (in the present case: Fe-13 wt.% Cr and Fe-20 wt.% Cr alloys) a strong nitrogen-chromium interaction occurs, which leads to an easy,

immediate nucleation of CrN precipitates; i.e. all nitrogen at the nitriding front reacts with chromium to form CrN. Therefore, a sharp transition nitrated zone/unnitrided core is observed for alloys of relatively high chromium content (see Figs. 2.9c and 2.9d). For alloys of relatively low chromium content (in the present case: Fe-4 wt.% Cr and Fe-8 wt.% Cr alloys) an intermediate nitrogen-chromium interaction occurs, i.e. not all nitrogen at the nitriding front combines with chromium to form CrN. Consequently, the transition nitrated zone/unnitrided core is less abrupt than for the strong interaction case (see Figs. 2.9a and 2.9b; see also discussion in [8]).

2.4 Morphological consequences of chromium content and nitrogen supersaturation changing with depth

The results of the morphological analysis (cf. Section 2.3.2) can be presented schematically as in Fig. 2.10. Specimens of low chromium content (see Fig. 2.10a) have a nitrated zone microstructure with a region of discontinuously coarsened grains near the surface (low hardness [Fig. 2.7], separate CrN reflections [Fig. 2.1a], relatively narrow α -Fe reflections [Fig. 2.2c]) and a region of coherent, sub-microscopical CrN precipitates (high hardness [Fig. 2.7], no separate CrN reflections and considerably broadened α -Fe reflections [Fig. 2.2c]). Specimens of high chromium content (see Fig. 2.10b) have a nitrated zone that has entirely experienced the discontinuous coarsening (separate CrN reflections [Fig. 2.1b] and a hardness that decreases from the surface to the nitrated zone/unnitrided core transition [Fig. 2.8]).

Considering the increase of lamellar spacing with depth (see Figs. 2.5a and 2.5c) it may be concluded that the observed hardness profiles for specimens with high chromium content (see for example Fig. 2.8) are due to the increase of lamellar spacing with depth (cf. Hall-Petch relation). The effect is pronounced: 829 H_V at the surface and 550 H_V at the transition nitrated zone/unnitrided core for a specimen of Fe-13 wt.% Cr nitrated for 24 h at 580 °C (see Fig. 2.8); which corresponds to an increase of lamellar spacing of 39 nm, in the nitrated zone adjacent to the surface, to 83 nm, at the transition nitrated zone/unnitrided core. For fully pearlitic steels it was observed that the hardness depends primarily on the interlamellar spacing, whereas the pearlitic colony size plays a subordinate role [35].

A lamellar spacing depending on depth was also observed for the low chromium content specimens, but the effect is less outspoken (cf. small extent of the discontinuously coarsened region), see Fig. 2.7.

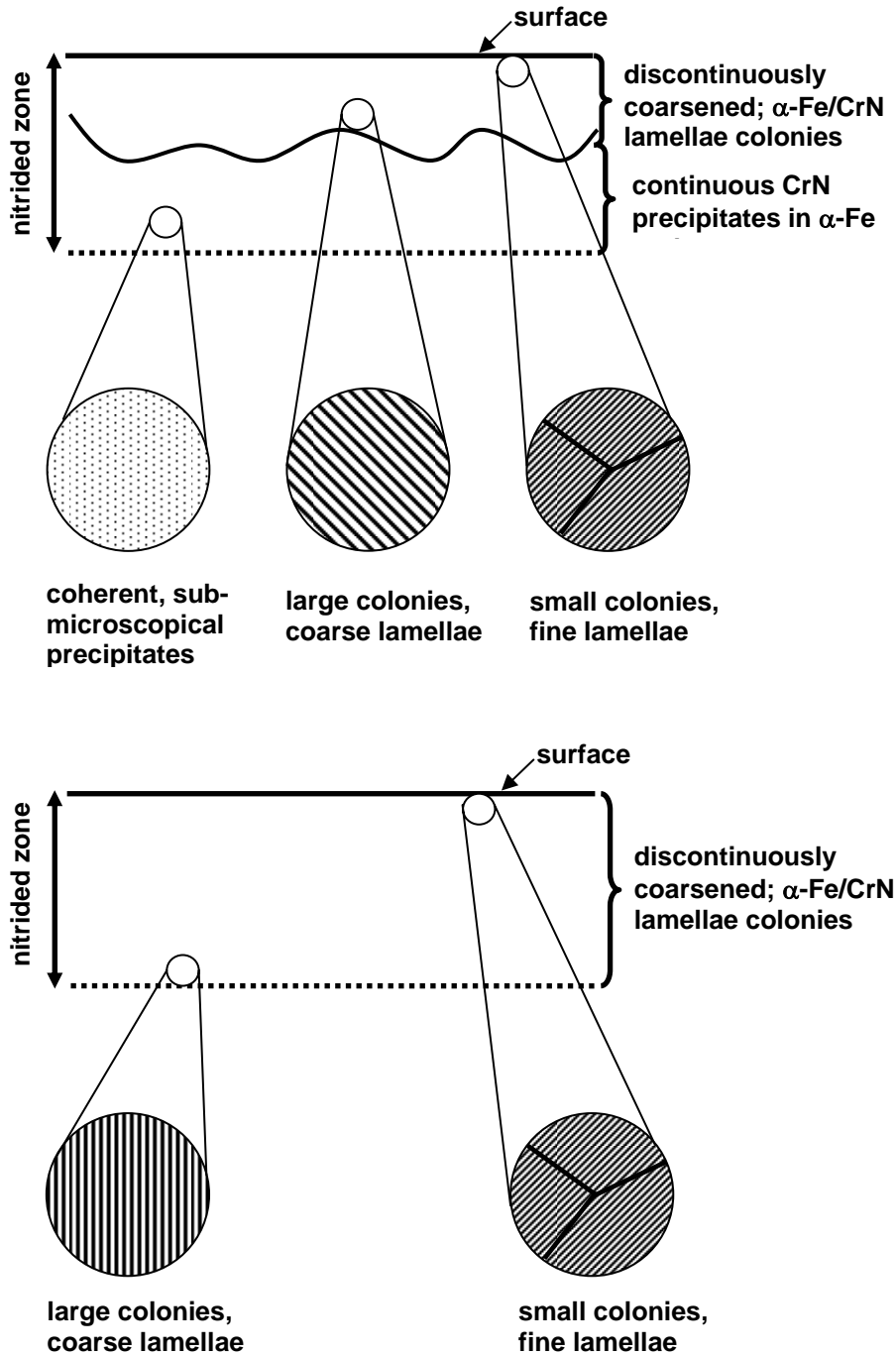


Fig. 2.10: (a) Schematic picture of the morphology of the nitrided zone of iron-chromium alloys of relatively low chromium content (Fe-4 wt.% and Fe-8 wt.% Cr). The nitrided zone is composed of discontinuously coarsened grains near the surface and ferritic grains with coherent, sub-microscopical CrN precipitates beneath the discontinuously coarsened layer. Near the surface small colonies with fine α -Fe/CrN lamellae occur, whereas large colonies of coarse lamellae are observed near the transition from the region composed predominantly of discontinuously coarsened grains to the region composed predominantly of ferritic grains containing coherent precipitates. (b) Schematic picture of the morphology of the nitrided zone of iron-chromium alloys of relatively high chromium content (Fe-13 wt.% and Fe-20 wt.% Cr). The nitrided zone is completely composed of discontinuously coarsened grains. Near the surface small colonies of fine α -Fe/CrN lamellae are observed, whereas large colonies of coarse lamellae are observed near the nitrided zone/un-nitrided core transition.

The microstructural development of the nitrated zone of iron-chromium specimens is dominated by two processes taking place at different rates:

- i.* growth of the nitrated zone: in the most simple case the nitrating depth is proportional with (a) (nitrating time)^{1/2} [20, 36] and with (b) (dissolved chromium concentration)⁻¹ [5, 20, 36] (see also Fig. 2.3);
- ii.* growth of the discontinuously coarsened region: discontinuous coarsening is an ageing process occurring during nitrating in the nitrated zone that proceeds from the oldest part of the nitrated zone (the surface) to the youngest part of the nitrated zone (transition nitrated zone/unnitrated core). The rate of growth of the discontinuously coarsened region is largely independent of the chromium content of the alloy.

The nitrating rate can be larger than the growth rate of the discontinuously coarsened region for alloys of low chromium content, in particular in an early stage of the nitrating process (see item *i* above and see Fig. 2.2a). However, at higher chromium contents it is feasible that the growth rate of the discontinuously coarsened region is equal to or larger than the nitrating rate. Thus it can be understood that the entire nitrated zone of nitrated alloys of high chromium content has experienced the discontinuous coarsening reaction (see Fig. 2.2b). Furthermore, the nitrogen supersaturation (see data of $[N]_{exc}$ in Table 2.1) increases with chromium content, which can be expected to increase the rate of discontinuous coarsening (cf. [14]). Consequently, the degree of discontinuous coarsening is more pronounced in alloys of high chromium content, as observed (cf. Fig 2.2b).

The origin for the dependence of lamellar spacing on depth can then be as follows. The driving force for the discontinuous coarsening is the larger, the larger the nitrogen supersaturation [14, 25, 26]. The nitrogen supersaturation is higher near the surface than in deeper layers within the nitrated zone; see for example Fig. 2.9 (this is a consequence of the necessity to maintain a nitrogen flux throughout the nitrated zone during nitrating). Hence, the driving force for the discontinuous coarsening is higher near the surface than in deeper layers. Thus, upon occurrence of the discontinuous coarsening reaction in the nitrated zone, a larger number of lamellar colonies of smaller lamellar spacing are nucleated near the surface, as compared with the discontinuous coarsening reaction occurring at larger depths. This proposed interpretation is schematically presented in Fig. 2.11.

For specimens of low chromium content, where only regions of the nitrated zone adjacent to the surface of the specimen experienced the discontinuous coarsening reaction, the variation of nitrogen supersaturation across the discontinuously coarsened region is relatively

small, leading to a less pronounced increase in lamellar spacing with increasing depth, as observed.

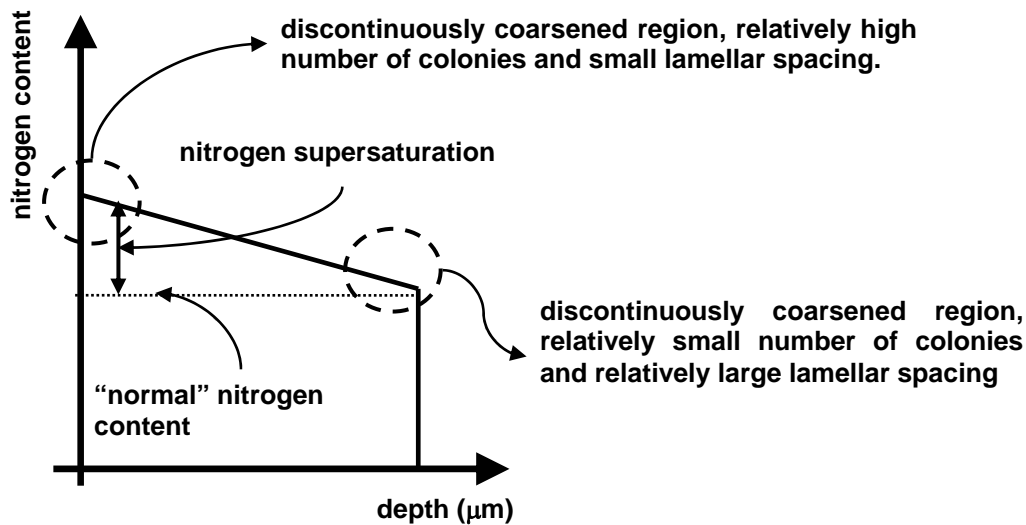


Figure 11: Schematic drawing of the nitrogen concentration-depth profile of a nitrided specimen with indication of the corresponding morphology, for a specimen with a nitrided zone that has entirely experienced the discontinuous coarsening reaction.

2.5 Conclusions

1. Upon nitriding ferritic iron-chromium alloys two types of precipitation morphologies can occur.
 - For low chromium content alloys (Fe-4 wt.% Cr and Fe-8 wt.% Cr alloys): (i) near the transition nitrided zone/unnitrided core (youngest part of the nitrided zone), the nitrided zone is composed of coherent, sub-microscopical CrN precipitates (high hardness, no separate CrN reflections in the X-ray diffraction pattern, strongly broadened ferrite-matrix reflections); (ii) adjacent to the surface the nitrided zone has experienced a discontinuously coarsening reaction and is composed of colonies of alternate α -Fe/CrN lamellae (relatively low hardness, separate CrN reflections, relatively narrow ferrite-matrix reflections).
 - For high chromium content alloys (Fe-13 wt.% Cr and Fe-20 wt.% Cr alloys): the nitrided zone has experienced entirely the discontinuous coarsening reaction.
2. The lamellar spacing in the discontinuously coarsened (part of the) nitrided zone increases with depth; the number density of lamellae colonies decreases with depth.
3. The nitrogen concentration depth-profiles reveal a nitrogen supersaturation decreasing with depth within the nitrided zone.

4. The increase of the lamellar spacing with depth in the nitrided zone is ascribed to the decrease of nitrogen supersaturation in the ferrite matrix with depth. Near the surface, where the nitrogen supersaturation is maximum, the driving force for discontinuous coarsening is maximal, causing more abundant nucleation of α -Fe/CrN lamellae colonies of relatively small lamellar spacing.
5. The increase of lamellar spacing with depth induces a pronounced decrease of hardness with depth in the nitrided zone.

Acknowledgements

We wish to thank Mr. J. Köhler and Mr. P. Kress for assistance with the nitriding experiments, Mrs. S. Haug for assistance with the EPMA experiments and Mrs. S. Kuehnemann for assistance with SEM analysis.

References

- [1] ASM Handbook, volume 4, ASM International, Metals Park, Ohio (1991).
- [2] D. Liedtke: Wärmebehandlung von Eisenwerkstoffen. Nitrieren und Nitrocarburieren, Expert Verlag, Renningen (2006).
- [3] E.J. Mittemeijer (Ed): Mat. Sci. Forum 102-104 (1992) 223.
- [4] K.H. Jack, in: Proc. Conf. on Heat Treatment, The Metals Society, London (1975) 39.
- [5] B.J. Lightfoot, D.H. Jack, in: Proc. Conf. on Heat Treatment, The Metals Society, London (1975) 59.
- [6] D.H. Jack: Acta Metall. 24 (1979) 137.
- [7] M.H. Biglari, C.M. Brakman, E.J. Mittemeijer, S. van der Zwaag: Phil. Mag. A 72 (1995) 931.
- [8] M.H. Biglari, C.M. Brakman, M.A.J. Somers, W.G. Sloof, E.J. Mittemeijer: Z. Metallkd 84 (1993) 124.
- [9] M. Pope, P. Grieveson, K.H. Jack: Scan. J. Metall. 2 (1973) 29.
- [10] T.C. Bor, A.T.W. Kempen, F.D. Tichelaar, E.J. Mittemeijer, E. van der Giessen: Phil. Mag. A 82 (2002) 971.
- [11] M. Gouné, T. Belmonte, A. Redjaimia, P. Weisbecker, J.M. Fiorani, H. Michel: Mat. Sci. Eng. A 351 (2003) 23.
- [12] S.S. Hosmani, R.E. Schacherl, E.J. Mittemeijer: Acta Mater. 35 (2005) 2069.
- [13] B. Mortimer, P. Grieveson, K.H. Jack: Scand. J. Metall. 1 (1972) 203.

- [14] P.M. Hekker, H.C.F. Rozendaal, E.J. Mittemeijer: *J. Mat. Sci.* 20 (1985) 718.
- [15] P.C. van Wiggen, H.C.F. Rozendaal, E.J. Mittemeijer: *J. Mat. Sci.* 20 (1985) 4561.
- [16] C. Alves Jr., J. de Anchieta Rodrigues, A.E. Martinelli: *Mat. Sci. Eng. A* 279 (2000) 10.
- [17] R.E. Schacherl, P.C.J. Graat, E.J. Mittemeijer, in: *Proceedings of the symposium on nitriding (April 2002, Aachen, Germany)*, Arbeitsgemeinschaft Wärmebehandlung und Werkstofftechnik (AWT), Schlangenbad, Germany (2002) 51.
- [18] R.E. Schacherl, P.C.J. Graat, E.J. Mittemeijer: *Z. Metallkd.* 93 (2002) 468.
- [19] R.E. Schacherl, P.C.J. Graat, E.J. Mittemeijer: *Metall. Mater. Trans. A* 35 (2004) 3387.
- [20] S.S. Hosmani, R.E. Schacherl, E.J. Mittemeijer: *Mater. Sci. Tech.* 21 (2005) 113.
- [21] M. Sennour, P.H. Jouneau, C. Esnouf: *J. Mat. Sci.* 39 (2004) 4521.
- [22] M. Sennour, C. Jacq, C. Esnouf: *J. Mat. Sci.* 39 (2004) 4533.
- [23] E.J. Mittemeijer, A.B.P. Vogels, P.J. van der Schaaf: *J. Mat. Sci.* 12 (1980) 3129
- [24] M.A.J. Somers, R.M. Lankreijer, E.J. Mittemeijer: *Phil. Mag. A* 59 (1989) 353.
- [25] E.J. Mittemeijer: *J. Metals* 37 (1985) 16.
- [26] D.B Williams, E.P. Butler: *Int. Metals Rev.* 3 (1981) 153.
- [27] JCPDS-International Center for Diffraction Data (1999), PCPDFWIN, Version 202
- [28] P. Villars (Ed.): *Pearson's Handbook. Desk edition. Crystallographic data for intermetallic phases.* ASM International, Metals Park, Ohio (1997).
- [29] R. Lück: *Z. Metallkd.* 66 (1975) 488.
- [30] J.L. Pouchou, F. Pichoir: *La Recherche Aérospatiale* 3 (1984) 167.
- [31] N.E. Vives Díaz, S.S. Hosmani, R.E. Schacherl, E.J. Mittemeijer: Chapter 4
- [32] G. Krauss: *Principles of heat treatment of steel.* ASM International, Metals Park, Ohio (1980).
- [33] S.S. Hosmani, R.E. Schacherl, E.J. Mittemeijer: in preparation
- [34] E.J. Mittemeijer, M.A.J. Somers: *Surf. Eng.* 13 (1997) 483.
- [35] J.M. Hyzak, I.M. Bernstein: *Metall. Trans. A* 7 (1976) 1217.
- [36] J.L. Meijering, in: *Advances in materials research*, Wiley Interscience, New York (1971).

Chapter 3

Influence of the microstructure on the residual stresses of nitrated iron-chromium alloys

N.E. Vives Díaz, R.E. Schacherl, L.F. Zagonel and E.J. Mittemeijer

Abstract

Different iron-chromium alloys (4, 8, 13 and 20 wt.% Cr) were nitrated in a NH_3/H_2 gas mixture at 580 °C for various times. The nitrated microstructure was characterized by X-ray diffraction, light microscopy and hardness measurements. Composition depth-profiles of the nitrated zone were determined by electron probe microanalysis. Residual stress-depth profiles of the nitrated specimens were measured using the (X-ray) diffraction $\sin^2\psi$ method in combination with cumulative sublayer removals and correction for corresponding stress relaxations. Unusual, nonmonotonous changes of stress with depth could be related to the microstructure of the nitrated zone. A model description of the evolution of the residual stress as function of depth and nitriding time was given.

3.1 Introduction

Residual stresses are self-equilibrating stresses existing in materials at uniform temperature and without external loading [1]. Residual stresses often arise in materials during processing steps, such as heat treatment or machining [2]. One of the most important and widely used thermochemical surface treatments to bring about a beneficial state of residual stress is nitriding, in particular nitriding of iron and iron-based alloys. Nitriding is used to improve the tribological, anti-corrosion and/or fatigue properties of iron and iron-based alloys [3-5]. The nitriding process involves the inward diffusion of nitrogen provided by a surrounding, nitrogen containing atmosphere. In this project gas nitriding has been applied: ammonia gas dissociates at the surface of the iron-based alloy at temperatures in the range 450-590 °C and the thereby produced nitrogen enters the material through its surface. As a result of the nitriding process a nitrided zone develops, which, depending on the nitriding conditions [6-8], can usually be subdivided into a compound layer adjacent to the surface, composed of iron nitrides [9]; and a diffusion zone, beneath the compound layer [10]. In the diffusion zone nitrogen can be dissolved (i.e. present on [a fraction of] the octahedral sites of the ferrite lattice) or precipitated as internal nitrides MeN_x , if nitride forming elements (Ti, Al, V, Cr) are present [11-13]. The improvement of the tribological and anticorrosion properties can be mainly attributed to the compound layer at the surface of the specimen [14], while enhancement of the fatigue properties is ascribed to the diffusion zone [15].

Nitriding leads to the generation of pronounced residual internal stresses in the diffusion zone [16]. The origins of residual stresses have been ascribed to compositional changes, thermal effects, lattice defects and the formation of precipitates [17]. Residual stresses have a crucial influence on the (mechanical) properties of nitrided specimens. This holds particularly for the fatigue properties: the presence of compressive residual stresses parallel to the surface in the surface-adjacent regions of the specimen can prevent crack initiation and crack growth [1, 16]. An increase in the fatigue limit of around 90% was found for nitrided, unnotched workpieces, in comparison with unnitrided specimens; for notched workpieces the enhancement of the fatigue resistance can (even) be much larger [17]. Hence, fundamental understanding of the development of the state of residual (internal) stress during nitriding is of cardinal importance for technological applications of nitrided components.

Chromium is often used as an alloying element in nitriding steels because of its relatively strong nitrogen-chromium interaction [16]. During the nitriding process, initially sub-microscopical, coherent CrN precipitates develop, which is associated with the occurrence of a relatively high hardness. This high hardness is a consequence of the strain fields surrounding

the precipitates, which are induced by the misfit between the CrN particles and the ferrite matrix, and hinder the movement of dislocations [11]. Upon continued nitriding, coarsening of the CrN particles already formed occurs, which is associated with loss of coherency, a decrease of the misfit strain energy and CrN/ferrite interfacial area and loss of nitrogen supersaturation [11-13, 16, 18]. The coarsening process can occur in two ways: (i) “continuous coarsening” implies the growth of larger particles at the cost of the smaller ones; (ii) “discontinuous coarsening” involves the development of a lamellar structure consisting of alternate ferrite and CrN lamellae. Both reactions can occur simultaneously and lead to a decrease of hardness and disappearance of long-range strain fields, effects that are particularly pronounced for the lamellar microstructure [12, 13, 19]. The mechanism of coarsening in the nitrided zone depends on the chromium content of the alloy. In the concentration range 0-2 wt.% Cr mainly the continuous coarsening takes place; in the range 2-10 wt.% Cr a mixture of both mechanisms can be observed; above 10 wt.% Cr only discontinuous coarsening can be observed [12, 19].

Although some work on the development of stresses in nitrided iron-based alloys has been performed [14, 20-22], fundamental knowledge on the relation between the development of residual stress and the microstructure (precipitation morphology) of nitrided, in particular chromium-alloyed, iron-based alloys lacks. This work is intended to describe and to provide an explanation for the complicated residual stress-depth profiles which develop upon nitriding of iron-chromium alloys.

3.2 Experimental procedures and data evaluation

3.2.1 Specimen preparation

Iron alloys with 4 wt.%, 8 wt.%, 13 wt.% and Fe-20 wt.% Cr were prepared of pure iron with a purity of 99.98 wt.% and pure Cr with a purity of 99.999 vol. % by melting in an inductive furnace. The alloy melts were cast into cylindrical moulds of 10 mm Ø, 80-100 mm length. The ingots were cut in pieces. Each piece was rolled down to sheets of about 1.1 mm thickness. The sheets were subsequently machined down to 1 mm thickness, in order to achieve a flat surface. From these sheets rectangular specimens (10×20 mm²) were cut. Next the specimens were ground and polished to remove the grooves on the surface resulting from the machining process using specially devised specimen holders (see Section 3.2.7), cleaned using ethanol in an ultrasonic bath, and then encapsulated in a quartz tube under an inert

atmosphere (Ar, 300 mbar). Subsequently, the specimens were annealed at 700 °C during 2 hours, during which full recrystallization of the specimens was realized.

3.2.2 Nitriding

The specimens were suspended at a quartz fibre in a vertical quartz tube nitriding furnace. The nitriding atmosphere consisted of a mixture of pure NH₃ (>99.998 vol.%) and H₂ (99.999 vol. %). The fluxes of both gases were regulated with mass flow controllers. Specimens of all alloys were nitrided at T = 580 °C using a nitriding potential [7] $r_N = 0.104 \text{ atm}^{-1/2}$; besides, an extra specimen of Fe-20 wt.% Cr was nitrided at T = 580 °C using a nitrided potential $r_N = 0.043 \text{ atm}^{-1/2}$. Under these conditions no iron nitrides are formed. Specimens of Fe-4 wt.% Cr were nitrided for 1.5 and 6 h; specimens of Fe-8 wt.% Cr were nitrided for 1.5, 6 and 24 h; specimens of Fe-13 wt.% Cr were nitrided for 6 and 24 h, and the specimens of Fe-20 wt.% Cr were nitrided for 24 h. After nitriding, the specimens were quenched in water and cleaned ultrasonically in an ethanol bath. The nitrided specimens were subjected to X-ray diffraction experiments for phase identification (see Section 3.2.3). Next, pieces were cut from the specimens for cross-sectional analysis. To embed the specimens, Polyfast, a conductive, polymer-based embedding material, was used. Subsequently the cross sections were ground and polished down to 1 μm diamond paste. For the light optical microscopy investigations the polished cross sections were etched with Nital (HNO₃ dissolved in ethanol) using different HNO₃ concentrations depending on the alloy (Nital 1% for Fe-4 wt.% Cr, Nital 2.5% for Fe-8 wt.% Cr and Fe-13 wt.% Cr, and Nital 4% for Fe-20 wt.% Cr). Specimens used for electron-probe microanalysis (see Section 2.5) were only ground and polished.

3.2.3 Phase characterization using X-ray diffraction (XRD)

Phase analysis of the nitrided specimens was performed by means of XRD using a Siemens D500 diffractometer (Bragg-Brentano configuration), equipped with a Cu tube and a graphite monochromator in the diffracted beam (Cu K_α radiation: $\lambda=1.54056 \text{ \AA}$). The diffraction angle, 2θ , in the range $10^\circ \leq 2\theta \leq 140^\circ$ was scanned with a step size of 0.04° in 2θ . Phase identification was performed comparing the position of the measured peaks with the data derived from the JCPDS data base [23] and the software Carine, based on data from Pearson [24].

3.2.4 Microscopy

The cross sections were investigated with light optical microscopy using a Leica DMRM microscope. The micrographs were recorded with a digital camera (Jenoptik Progress 3008).

3.2.5 Electron-probe microanalysis (EPMA)

To determine the composition-depth profiles in the nitrided zones EPMA was performed using a Cameca SX100 instrument. A focused electron beam at an accelerating voltage of 15 kV and a current of 100 nA was applied. The iron, chromium, nitrogen and oxygen contents in the specimen cross-section were determined from the intensity of the characteristic Fe K β , Cr K β , N K α and O K α X-ray emission peaks at points along lines (4-5) across the cross-sections (single measurement points at a distance of 2 or 3 μm , depending on the specimen). The intensities obtained for the nitrided specimens were divided by the intensities obtained from standard specimens of pure Fe (Fe K β), pure Cr (Cr K β), andradite/Ca₃Fe₂(SiO₄)₃ (O K α) and γ '-Fe₄N (N K α). Concentration values were calculated from the intensity ratios applying the $\Phi(\rho z)$ approach according to Pouchou and Pichoir [25].

3.2.6 Hardness measurements

Hardness measurements using Vicker's method were performed using a Leica VHMT MOT device, applying a load of 50 g and a loading time of 30 s. At least two to four hardness-depth profiles were measured for each specimen; the hardness-depth profiles were measured, on the specimen cross-sections, at a certain inclination angle (between 30° and 45°) with respect to the surface to improve the depth resolution. The distance between the hardness indents amounts to 10 to 25 μm , depending on the actual size of the indent (as determined by the local microstructure of the nitrided zone), such distance is sufficient to avoid overlap of the plastically deformed zones surrounding the indents. The obtained hardness data are shown as a function of the distance from the surface of the nitrided specimens.

3.2.7 Determination of residual stress-depth profiles using XRD

The residual stress-depth profiles of the different nitrided specimens were determined by means of XRD, using the $\sin^2\psi$ method [2, 26, 27], in combination with sublayer removal. In the traditional $\sin^2\psi$ method the specimen is tilted at different angles (i.e. the direction of the diffraction vector is varied with respect to the specimen surface normal) and (partial)

diffractograms, around a particular reflection, are recorded. When a state of (residual) stress is present in the specimen, the peak position of the reflection studied is different for different angles of tilt. Then, using Bragg's law and applying continuum mechanics, it is in principle possible to calculate the state of residual stress in the specimen. For the traditional X-ray diffraction methods to measure residual stress, the tilting of the specimen implies that the penetration depth changes in dependence on the angle of specimen tilt. This dependence of penetration depth on angle of tilt can lead to inaccurate assessment of residual stress values if stress- and/or composition-depth profiles occur within the probed depth range in the specimen under study [28, 29]. Therefore, a method that allows to measure at constant penetration depth is crucial for the accurate determination of the stress-depth profiles. In order to measure at constant penetration depth, a modification of the traditional $\sin^2 \psi$ method was adopted here, which consists of combining specific tilting and rotating angles of the specimen during the diffraction stress analysis. A comprehensive description of this method can be found in [30].

A Philips MRD diffractometer, equipped with an Eulerian cradle, a graphite monochromator in the diffracted beam and a Cu X-ray tube (Cu K_α radiation, $\lambda = 1.54056 \text{ \AA}$), was employed to record the Fe-211 reflections. Measurements were performed for tilt angles ψ in the range $34^\circ \leq \psi \leq 66^\circ$ in steps of 4° , which implies the incorporation of nine points in the $\sin^2 \psi$ plot (see further below). The lattice strains were calculated from the peak position of the Fe-211 reflection. Texture (pole figure) measurements performed in this work, using the Fe-211 reflection, revealed that the specimens possess a weak rotationally symmetric (with respect to the surface normal) texture, implying that at each value of tilt angle ψ sufficient diffracted intensity is generated.

For a macroscopically isotropic specimen, and under the supposition of a plane, rotationally symmetric state of mechanical stress, the lattice strain is independent of the angle of rotation φ (the rotation angle around the sample surface normal) and the stress parallel to the surface $\langle \sigma_{//}^S \rangle$ can be calculated using [27]:

$$\varepsilon_{\psi}^{hkl} = \left(2 S_1^{hkl} + \frac{1}{2} S_2^{hkl} \sin^2 \psi \right) \langle \sigma_{//}^S \rangle \quad \text{Eq. (3.1)}$$

where ε_{ψ}^{hkl} is the lattice strain in the direction of the diffraction vector pertaining to the angle ψ (the inclination angle of the diffraction vector with respect to the sample surface normal),

S_1^{hkl} and $\frac{1}{2}S_2^{hkl}$ are the hkl -dependent X-ray elastic constants, which are independent of φ and ψ and $\langle \sigma_{//}^S \rangle$ is the stress parallel to the surface of the specimen.

The lattice strain is calculated from the measured lattice spacing d_{ψ}^{hkl} according to:

$$\varepsilon_{\psi}^{hkl} = \frac{d_{\psi}^{hkl} - d_0^{hkl}}{d_0^{hkl}} \quad \text{Eq. (3.2)}$$

where d_0^{hkl} is the strain-free lattice spacing, which is obtained by interpolation in the d_{ψ}^{hkl} - $\sin^2 \psi$ plot at the $\sin^2 \psi$ value calculated by setting $\varepsilon_{\psi}^{hkl} = 0$ in Eq. (3.1).

The stress $\langle \sigma_{//}^S \rangle$ can now be calculated from the slope of a plot of the lattice strain versus $\sin^2 \psi$. The value of $\frac{1}{2}S_2^{hkl}$ (6.21 TPa^{-1}) was calculated using the experimentally determined bulk elastic constants of ferrite listed in [2].

In order to measure the residual stress as function of depth, sublayers were removed consecutively by polishing in a controlled way. To this end, special specimen holders for each individual specimen were fabricated. The specimen was placed in a rectangular cavity, specially machined such so that it is slightly wider than the specimen. At the bottom of the cavity there is a magnet, used to fix the specimen in the holder. The purpose of designing such specimen holders was to fasten the specimen, assuring that it remains flat, and to achieve homogeneous removal of material during the subsequent polishing procedure. The thickness of the specimens was measured at the centre point of the specimen using a special caliper, so that the thickness of the sublayer removed could be calculated. The polishing steps were performed using a TegraPol-35 automatic polishing and grinding machine from Struers; several specimens could be polished simultaneously. The polishing procedure was as follows:

1. polishing using 1 μm diamond powder solution;
2. the last 2 or 3 μm before reaching the aimed for specimen thickness, were polished down using $\frac{1}{4} \mu\text{m}$ diamond powder solution;
3. etching with Nital 0,5 % during one minute removing up to 1 μm of material (to remove any material that might have experienced plastic deformation by polishing);
4. specimen thickness measurement.

Before a diffraction stress analysis was performed, the specimen was cleaned in an ultrasonic bath with ethanol.

When stressed layers are removed from a specimen, the stress in the remaining material relaxes to a new equilibrium configuration. Therefore, all stress values measured upon successive sublayer removals must be corrected for such stress relaxation in order to obtain the true stress-depth profile that existed in the specimen before the sublayers were removed (for details concerning the correction method, see Appendix, Section 3.6).

3.3 Results and Discussion

3.3.1 Phase analysis

Diffraction patterns recorded after nitriding reveal that the region adjacent to the surface of the nitrided zones of all specimens is composed of α -Fe and CrN (e.g. see Figs. 3.1a-d; penetration depth of the Cu K_{α} radiation is 1- 2 μm).

3.3.2 Morphology of the nitrided zone; two types of precipitation morphology

The nitrided specimens can be divided in two groups, according to the morphology observed in the light optical examination (cf. Section 3.1). The first group consists of nitrided specimens of relatively low chromium content (Fe-4 wt.% Cr and Fe-8 wt.% Cr alloys). These specimens exhibit near the surface dark grains with a lamellar morphology (α -Fe/CrN lamellae) and below this region mainly bright grains are observed (see Figs. 3.5b, 3.6b, 3.6d and 3.6f).

The second group of specimens consists of nitrided specimens of relatively high chromium content (Fe-13 wt.% Cr and Fe-20 wt.% Cr alloys); the entire nitrided zones of these specimens are composed of dark grains showing a lamellar morphology (see Figs. 3.7b, 3.7d and 3.8b).

3.3.3 Hardness-depth profiles

The hardness characteristics of the nitrided zone of specimens with relatively low chromium content are similar: near the surface, in regions where mainly discontinuously coarsened grains are present, the hardness is relatively low; whereas at larger depths, where mainly continuous, sub-microscopical CrN particles are present (cf. Section 3.1), the hardness is relatively high. The transition between the small hardness regime to the high hardness regime takes place over a relatively short distance; see Fig. 3.2.

On the other hand, an almost continuous decrease of hardness, from the surface to the transition nitrided zone/unnitrided core, occurs in the case of specimens of relatively high chromium content; see Fig. 3.3. There appears to be no indication of the presence of continuous precipitates (in the bottom part of the nitrided zone): cf. hardness values in Figs. 3.2 and 3.3. The decrease of the hardness from the surface towards the interface of the nitrided zone to the unnitrided core of the specimen can be ascribed to the variation of the interlamellar spacing (from small to large) across the nitrided zone [19].

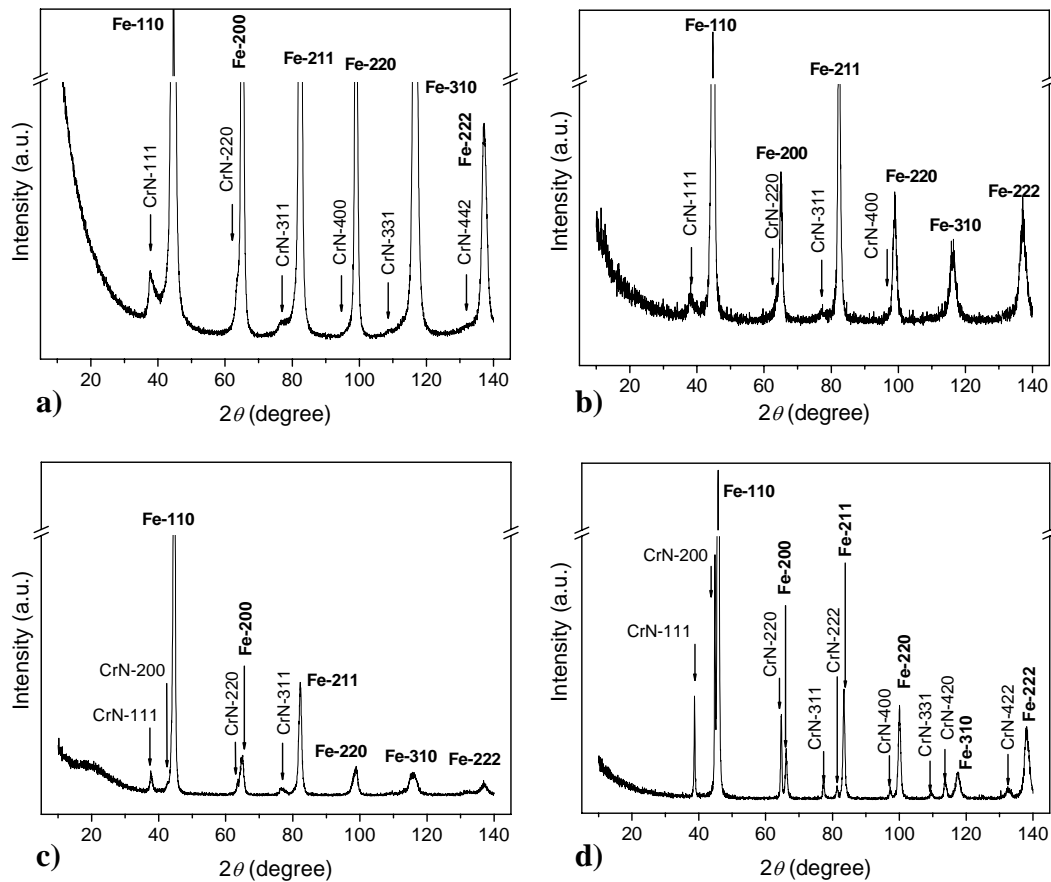


Fig. 3.1: Selected X-ray diffractograms recorded at the surface of specimens of iron-chromium alloys nitrided at 580 °C. After nitriding the nitrided zones of all specimens are composed of α -Fe and CrN (the penetration depth pertaining to the diffractograms is 1-2 μm [cf. Section 3.2.5]). **(a)** specimen of Fe-4 wt.% Cr alloy nitrided for 1.5 h and $r_N = 0.104 \text{ atm}^{-1/2}$; **(b)** specimen of Fe-8 wt.% Cr alloy nitrided for 1.5 h and $r_N = 0.104 \text{ atm}^{-1/2}$; **(c)** specimen of Fe-13 wt.% Cr alloy nitrided for 6 h and $r_N = 0.104 \text{ atm}^{-1/2}$; **(d)** specimen of Fe-20 wt.% Cr alloy nitrided for 24 h and $r_N = 0.043 \text{ atm}^{-1/2}$.

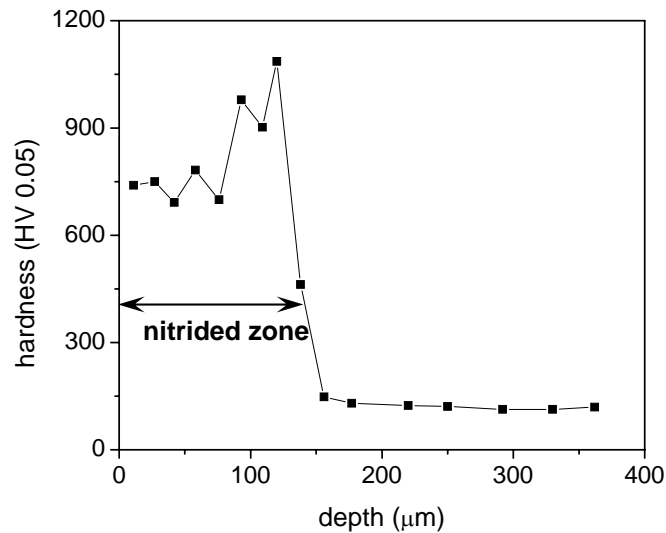


Fig. 3.2: Hardness depth-profile of a specimen of Fe-8 wt.% Cr nitrided for 6 h at 580 °C and $r_N = 0.104 \text{ atm}^{-1/2}$, with a nitrided zone consisting of grains transformed by the discontinuous coarsening reaction (surface region) and grains containing coherent, sub-microscopical CrN precipitates (near the nitrided zone/unnitrided core transition).

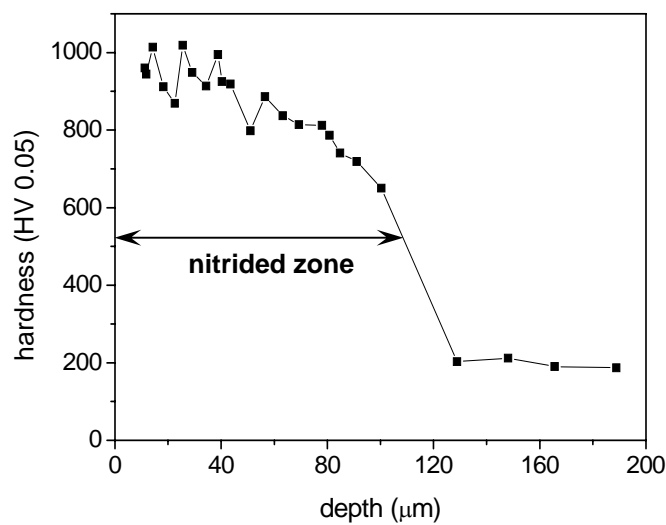


Fig. 3.3: Hardness depth-profile of a specimen of Fe-20 wt.% Cr nitrided for 24 h at 580 °C and $r_N = 0.043 \text{ atm}^{-1/2}$. The nitrided zone is fully composed of grains which have experienced the discontinuous coarsening reaction.

3.3.4 Nitrogen concentration-depth profiles

Nitrogen concentration-depth profiles, as measured by EPMA, are shown in Fig. 3.4 for nitrided alloys of different chromium content (and different precipitation morphology, cf. Section 3.3.2). The square data points represent the measured total amounts of nitrogen. The “normal” nitrogen content (defined as the equilibrium nitrogen content dissolved at interstitial

sites in an unstressed ferrite matrix, plus the nitrogen incorporated in stoichiometric CrN) has been indicated by the horizontal dashed line. The positive difference between the square data points and the dashed line represents the amount of “excess nitrogen” [31].

The nitriding potential of the gas atmosphere determines the equilibrium amount of nitrogen dissolved in ferrite. Only the surface adjacent region of the solid substrate can be in (local) equilibrium with the outer gas atmosphere. Therefore, the amount of excess nitrogen, $[N]_{exc}$, was calculated taking the average value of the three first measurements of nitrogen content near the surface of the specimens, $[N]_{tot}$, using the following relation:

$$[N]_{exc} = [N]_{tot} - [N]_{CrN} - [N]_{\alpha}^0 \quad \text{Eq. (3.3)}$$

where $[N]_{CrN}$ is the amount of nitrogen incorporated in the stoichiometric CrN (assuming that all chromium precipitates to form CrN^{\dagger}) and $[N]_{\alpha}^0$ is the equilibrium value of nitrogen dissolved in stress-free ferrite ($[N]_{\alpha}^0 = 0.4$ at.% at 580 °C [33]). The results have been gathered in Table 3.1.

All nitrogen concentration-depth profiles reveal the existence of a significant gradient of nitrogen concentration in the nitrided zone; the nitrogen concentration decreases from the surface to the transition nitrided zone/unnitrided core (see Fig. 3.4).

Table 3.1: Excess nitrogen contents, $[N]_{exc}$, (derived from EPMA measurements) in the nitrided zone near the surface of the specimens of different chromium content and nitrided for various times at 580 °C, $r_N = 0.104 \text{ atm}^{-1/2}$. $[N]_{nor}$ is the equilibrium nitrogen content dissolved at interstitial sites in an unstressed ferrite matrix, plus the nitrogen incorporated in stoichiometric CrN; $[N]_{exc}$ is the difference between the total nitrogen in the surface region of the specimen, as measured by EPMA, and $[N]_{nor}$.

alloy	Fe-4 wt.% Cr		Fe-8 wt.% Cr			Fe-13 wt.% Cr		Fe-20 wt.% Cr
	1.5	6	1.5	6	24	6	24	24
nitriding time (h)	1.5	6	1.5	6	24	6	24	24
$[N]_{nor}$ (at.%)	4.4	4.4	8.2	8.2	8.3	12.6	12.4	17.6
$[N]_{exc}$ (at.%)	0.9	0.6	1.6	1.3	1.1	2.1	1.9	3.2

[†] This composition of the precipitates has been corroborated by de-nitriding experiments performed by our group in a project to determine the absorption isotherms of nitrided Fe-20 wt.% Cr alloys [32].

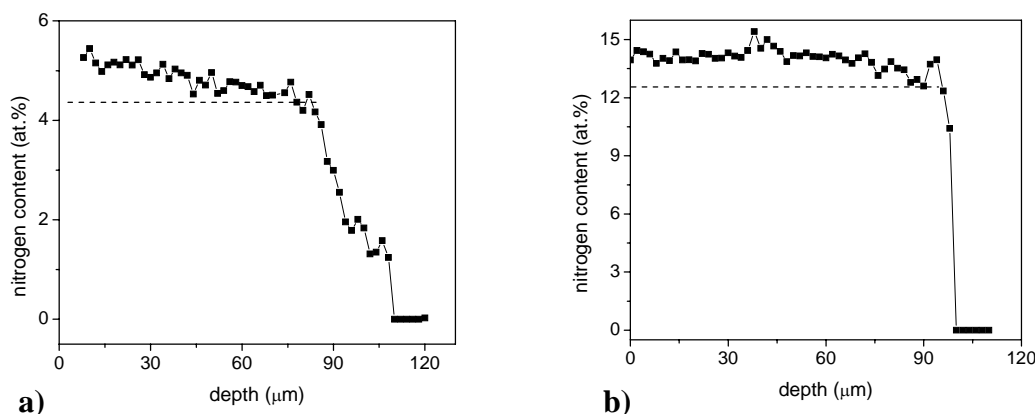


Fig. 3.4: Nitrogen concentration-depth profiles (EPMA measurements). **(a)** Fe-4 wt.% Cr alloy nitrided for 1.5 h (profile representative of alloys with low chromium content); **(b)** Fe-13 wt.% Cr alloy nitrided for 6 h (profile representative of alloys with high chromium content). Both specimens were nitrided at 580 °C and $r_N = 0.104 \text{ atm}^{-1/2}$. The horizontal dashed lines indicate the “normal” nitrogen uptake.

3.3.5 Residual stress-depth profiles

The residual stress-depth profile of a specimen of relatively low chromium content alloy (Fe-4 wt.% Cr alloy nitrided for 1.5 h at 580 °C) is presented in Fig. 3.5a. The stress (parallel to the surface) decreases from the surface towards the unnitrided core. Tensile stresses occur in the region where mainly discontinuously transformed grains are present; compressive stresses occur in the region where coherent nitrides are the predominant type of precipitation. A maximum compressive stress of ~ 680 MPa was measured near the transition nitrided zone/unnitrided core. Beyond the transition nitrided zone/unnitrided core, the stress increases and eventually becomes tensile.

The residual stress-depth profiles of specimens of Fe-8 wt.% Cr alloy nitrided for 1.5, 6 and 24 h at 580 °C are shown in Figs. 3.6a, 3.6c and 3.6e, respectively. The residual stress-depth profile of the specimen nitrided for 1.5 h indicates the existence of compressive stresses across the whole nitrided zone, except *at* the specimen surface where a tensile stress (~ 215 MPa) was measured. The maximum compressive stresses occur in the bottom part of the nitrided zone, where grains with sub-microscopical, coherent precipitates are present. A low tensile stress prevails in the unnitrided core close to the nitrided zone/unnitrided core transition. The stress-depth profiles of the specimens nitrided for 6 and 24 h show that in the nitrided zone a zone I has developed, with mainly discontinuously coarsened grains and exhibiting tensile stresses. In zone II, where a significant part of the grains contains sub-microscopical, coherent CrN precipitates, the stress decreases and becomes eventually compressive, reaching a minimum (maximum compressive stress) at the transition nitriding

zone/unnitrided core. Beyond the transition nitrided zone/unnitrided core, the stress increases and eventually becomes tensile.

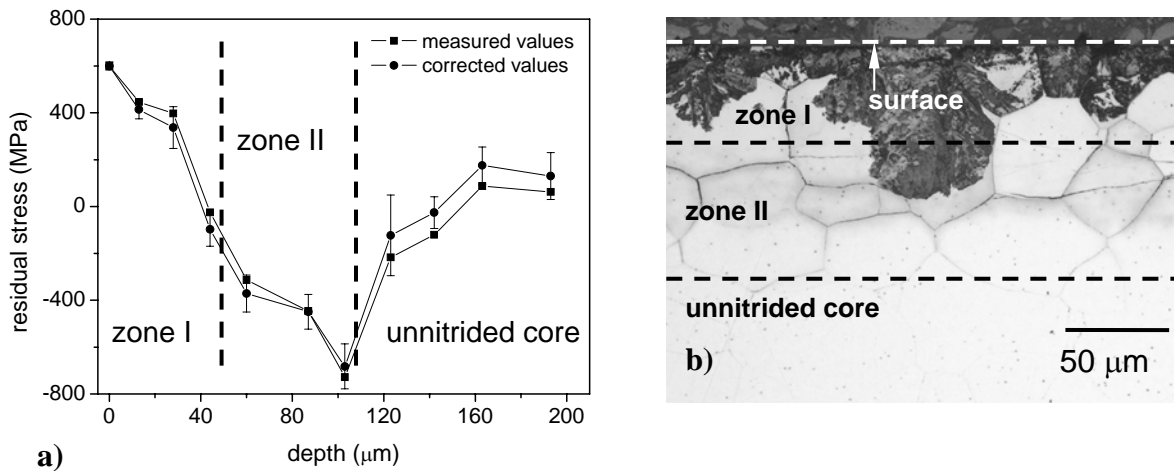


Fig. 3.5: (a) Residual stress depth-profile measured for a specimen of Fe-4 wt.% Cr alloy nitrided for 1.5 h at 580 °C and $r_N = 0.104 \text{ atm}^{-1/2}$; (b) corresponding light optical micrograph of the nitrided zone, zone I corresponds to the region where discontinuously coarsened grains are predominant, zone II corresponds to the region where continuous precipitates are predominant.

The residual stress-depth profiles obtained for specimens of relatively high chromium content alloys (Fe-13 wt.% Cr nitrided for 6 and 24 h, see Figs. 3.7a and 3.7c) show that there are mainly compressive stresses parallel to the surface in the nitrided zone. In the specimen of Fe-13 wt.% Cr nitrided for 6 h (see Fig. 3.7a) the compressive stress has (again) a maximum near the transition nitrided zone/unnitrided core. Near the surface the compressive stresses are of relatively moderate value. At the surface a tensile stress was measured. The last statement also holds for the specimen of Fe-13 wt.% Cr nitrided for 24 h (see Fig. 3.7c). In this case the maximum compressive stress occurs just beneath the surface; for larger depths the compressive stress decreases gradually, and the stress becomes eventually tensile near the transition nitrided zone/unnitrided core.

The residual stress-depth profile obtained for the specimen of Fe-20 wt.% Cr alloy nitrided for 24 h (see Fig. 3.8a) shows that tensile stresses occur in a surface adjacent layer, followed by moderate compressive stresses over the remainder of the nitrided zone.

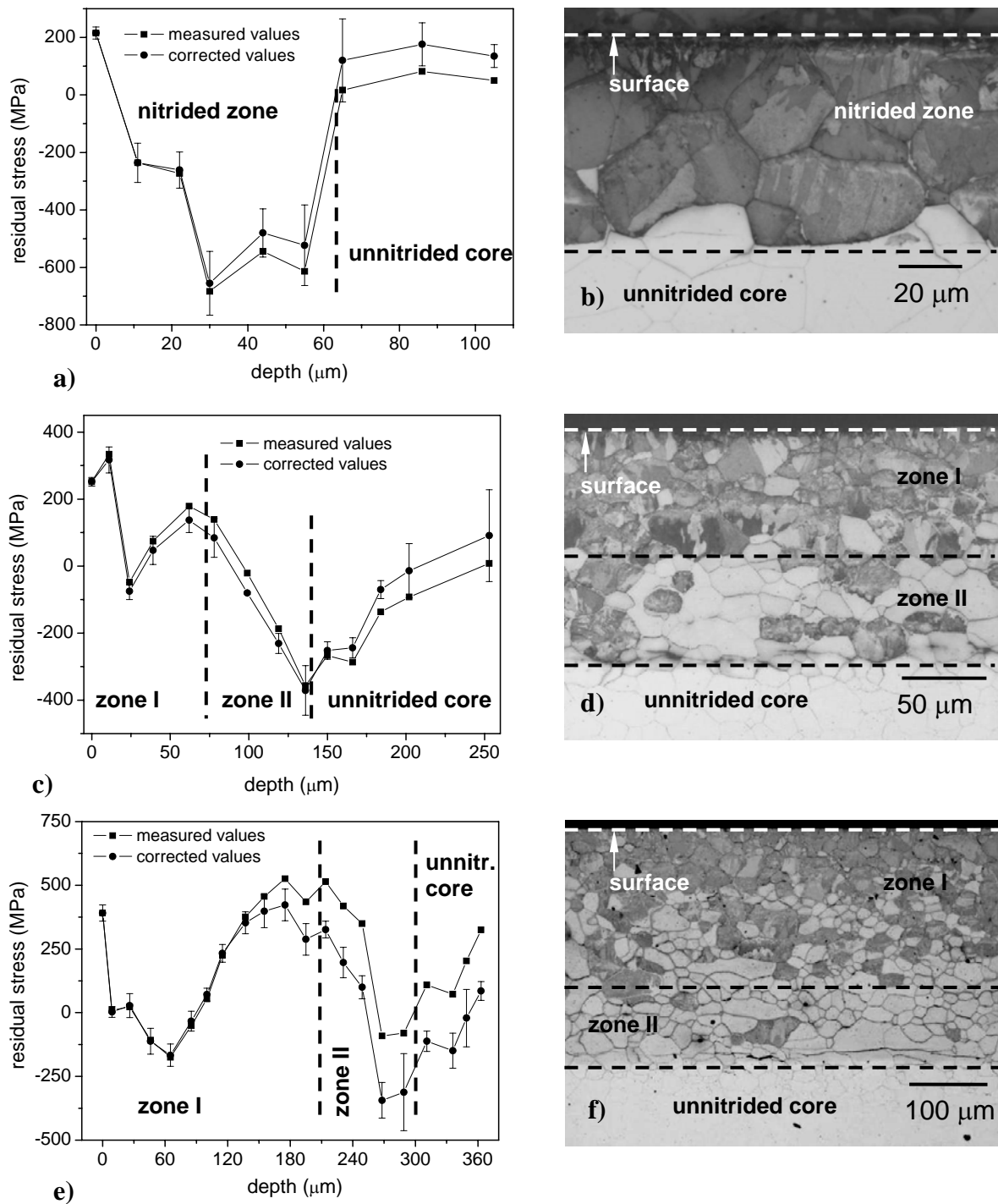


Fig. 3.6: (a) Residual stress depth-profile measured for a specimen of Fe-8 wt.% Cr alloy nitrided for 1.5 h; (b) corresponding light optical micrograph of the nitrided zone, which in this case is mainly composed of discontinuously coarsened grains, continuous precipitates are present at the transition between the nitrided zone and the unnitrided core; (c) residual stress depth-profile measured for a specimen of Fe-8 wt.% Cr alloy nitrided for 6 h; (d) corresponding light optical micrograph of the nitrided zone, zone I corresponds to the region where discontinuously coarsened grains are predominant, zone II corresponds to the region where continuous precipitates are predominant; (e) residual stress depth-profile measured for a specimen of Fe-8 wt.% Cr alloy nitrided for 24 h; (f) corresponding light optical micrograph of the nitrided zone, zone I corresponds to the region where discontinuously coarsened grains are predominant, zone II corresponds to the region where continuous precipitates are predominant. All specimens were nitrided at 580 °C and $r_N = 0.104 \text{ atm}^{-1/2}$.

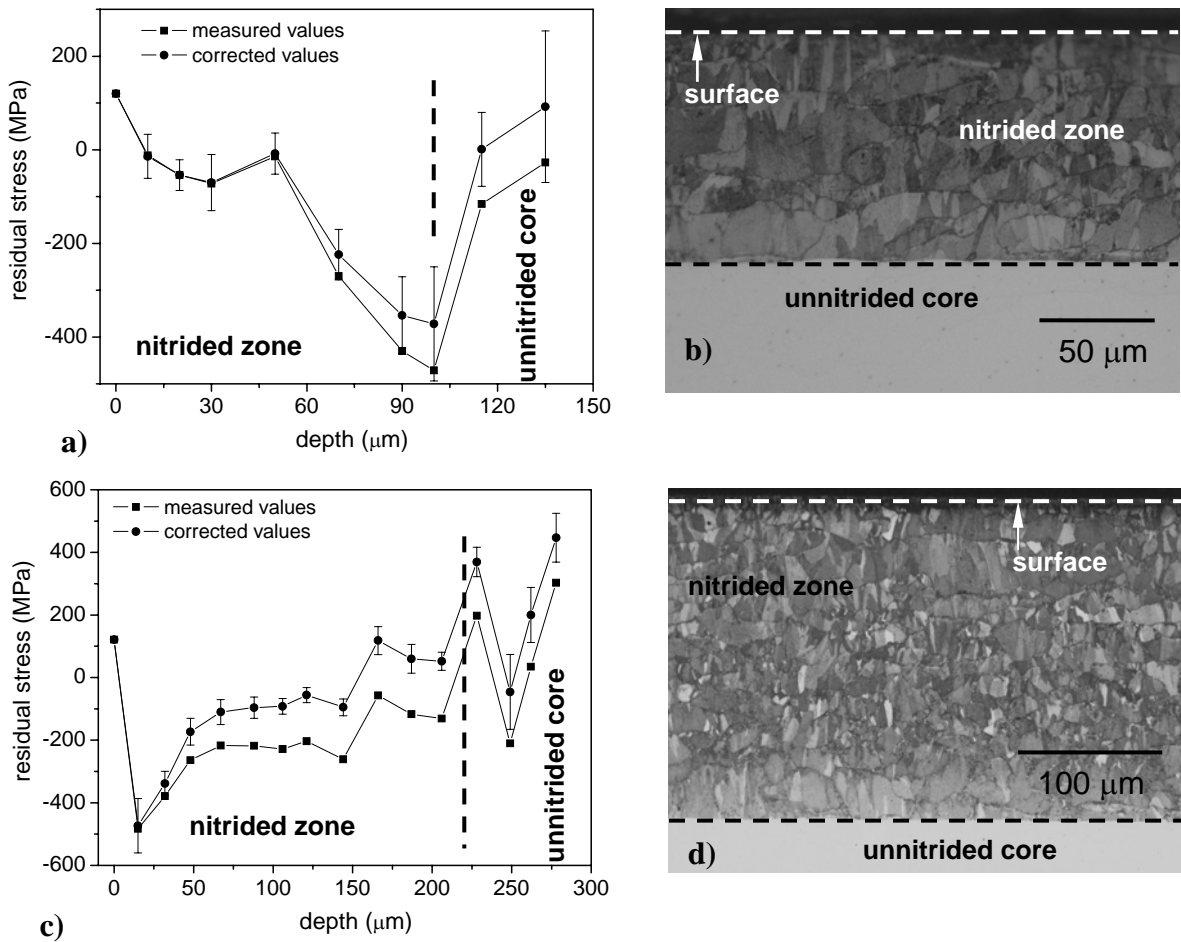


Fig. 3.7: (a) Residual stress depth-profile measured for a specimen of Fe-13 wt.% Cr alloy nitrided for 6 h; (b) corresponding light optical micrograph of the nitrided zone, which in this case is only composed of discontinuously coarsened grains; (c) residual stress depth-profile measured for a specimen of Fe-13 wt.% Cr alloy nitrided for 24 h; (d) corresponding light optical micrograph of the nitrided zone, which in this case is only composed of discontinuously coarsened grains. Both specimens were nitrided at 580 °C and $r_N = 0.104 \text{ atm}^{-1/2}$.

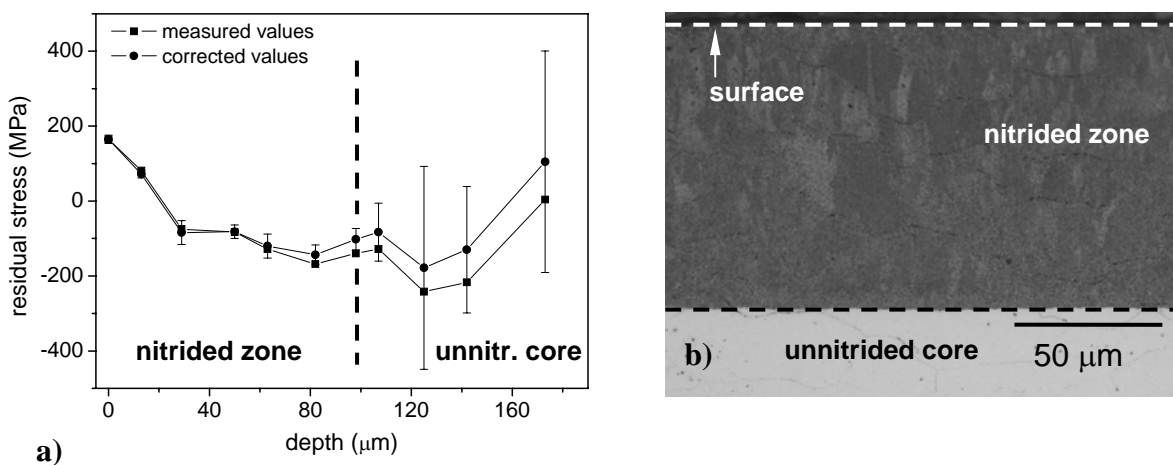


Fig. 3.8: (a) Residual stress depth-profile measured for a specimen of Fe-20 wt.% Cr alloy nitrided for 24 h at 580 °C and $r_N = 0.043 \text{ atm}^{-1/2}$; (b) corresponding light optical micrograph of the nitrided zone, which in this case is only composed of discontinuously coarsened grains.

It may be thought that, for an infinitely sharp interface between the nitrided zone and the unnitrided core, removal of the entire nitrided zone should lead to a state of *measured* zero stress in the remaining unnitrided core. However, the sublayer removals have only been performed on one side of the specimen; the nitrided zone at the other side is still there, influencing the state of stress in the unnitrided core. Note that the thicknesses of the whole specimens range between 700-1000 μm . Further, an infinitely sharp interface between the nitrided zone and the unnitrided core does not occur for, in any case, the low chromium content specimens.

The residual stress-depth profiles presented above were measured for the ferrite (matrix) phase and taken as representative for the planar state of mechanical stress in the surface region of the specimen. This supposition could be supported in this work by separate measurement of the stress in the CrN phase. To this end the CrN-311 reflection was employed in a $\sin^2\psi$ procedure similar to the one described in Section 3.2.7. Measurements were performed at the surface of a specimen of Fe-20 wt.% Cr nitrided for 24 h at 580 °C and $r_N = 0.104 \text{ atm}^{-1/2}$. The residual stress measured for the CrN phase is 146 MPa, which, in view of the uncertainty inherent to the values of the X-ray elastic constants used (cf. Section 3.2.7), indeed is practically the same value as measured for the ferrite phase (165 MPa; cf. Fig. 3.8a), which validates the above supposition.

3.4 General discussion; the build up and relaxation of stress

To interpret the dependences of the residual stress in the nitrided zone on depth (beneath the surface) and nitriding time, it is necessary first to provide an understanding for the microstructural development of the nitrided zone.

The microstructural development of the nitrided zone is governed by two processes occurring at different rates:

- i.* The growth of the nitriding zone. In the most simple case the nitriding depth is proportional with (a) (nitriding time)^{1/2} and with (b) (dissolved chromium concentration)⁻¹ [34, 35], and thus the rate of growth of the nitrided zone decreases with increasing time and with increasing chromium content.
- ii.* The growth of the discontinuously coarsened region. Discontinuous coarsening is an ageing process occurring during nitriding in the nitrided zone. Obviously the discontinuous coarsening proceeds from the oldest part of the nitrided zone (the surface) to the youngest part of the nitrided zone (transition nitrided

zone/unnitrided core). The rate of growth of the discontinuously coarsened region is largely independent of the chromium content of the alloy (or even increases with chromium content, see below).

Now, whereas the growth rate of the discontinuously coarsened region can be smaller than the nitriding rate for the (beginning of) nitriding in alloys with low chromium content (cf. Fig. 3.5b), it is conceivable that at (sufficiently) high chromium content the growth rate of the discontinuously coarsened region is equal to or larger than the nitriding rate (see point (i) above). Thus it can be understood that in nitrided alloys with high chromium content the entire nitrided zone has experienced the discontinuous coarsening reaction (cf. Figs. 3.7b, 3.7d and 3.8b). Moreover, the nitrogen supersaturation (see data concerning “excess nitrogen”, $[N]_{\text{exc}}$, in Table 3.1) increases with chromium content, which can be expected to speed up the rate of discontinuous coarsening.

The residual stress-depth profiles determined for nitrided specimens of low chromium content alloys (Fe-4 wt.% Cr and Fe-8 wt.% Cr alloys) exhibit similar features: compressive stress occurs in the bottom part of the nitrided zone where sub-microscopical, coherent nitrides are predominant, whereas tensile stress occurs in the region near the surface, which is the oldest part of the nitrided zone and where discontinuously coarsened grains prevail.

To understand the measured residual stress-depth profiles in specimens of low chromium content the following model is proposed:

- (a) During the first stage of nitriding iron-chromium alloys, CrN precipitates as coherent, sub-microscopical particles. Due to the mismatch of the lattices of ferrite and CrN, the precipitation of nitride particles tends to expand (laterally) the nitrided zone, which is opposed by the unnitrided core, and as a result a compressive residual (macro-) stress, parallel to the surface, is generated in the ferrite matrix of the nitrided zone (see Fig. 3.9a).
- (b) Upon the occurrence of discontinuous coarsening, the coherent, sub-microscopical CrN precipitates are replaced by incoherent, relatively large CrN lamellae. At the same time, relaxation of the (initial) compressive stress occurs in the part of the nitrided zone which experiences the discontinuous coarsening reaction. This relaxation can be most pronounced near the surface as there expansion perpendicular to the “free” surface can occur, implying that moderate levels of compressive stress can be maintained at some depth from the surface in the region where discontinuous coarsening occurred. Then, upon continued nitriding, coherent, sub-microscopical CrN particles are formed at larger depths beneath the

surface (see the finely dotted area in Fig. 3.9b), i.e. at the transition nitrified zone/un-nitrified core. Consequently, compressive stress develops in this region, as explained in (a). Then, as a consequence of the requirement of mechanical equilibrium of the specimen (cf. Figs. 3.5a and 3.6a; see also Fig. 3.9b):

- a tensile stress contribution is generated in the surface-adjacent regions of the nitrified zone, and
- a tensile stress arises in the un-nitrified core in regions adjacent to the transition nitrified zone/un-nitrified core.

On the above basis, the evolution with nitriding time of the residual stress profile of specimens exhibiting a nitrified zone composed of a discontinuously coarsened region (zone I in Figs. 3.5b, 3.6d and 3.6f) and a region where largely only coherent, sub-microscopical nitrified occur (zone II in Figs. 3.5b, 3.6d and 3.6f) can be discussed. In an advanced stage of nitriding, the emergence of pronounced (cf. Figs 3.6c and 3.6e) compressive stress in the region (at pronounced depths) where (largely) only coherent, sub-microscopical nitrides occur, can be compensated, because of the requirement of mechanical equilibrium, by tensile stresses in the regions (especially) immediately above and immediately beneath (un-nitrified core, see (c) above) this region. This picture may explain (see the sketch in Fig. 3.9c) the eventual development of a residual stress-depth profile in zone I characterized by tensile stress in the surface adjacent region and moderate compressive stress in the region beneath it, *followed by tensile stress in the region adjacent to zone II*; see Figs 3.6c and 3.6e.

The entire nitrified zone of specimens of high chromium content (Fe-13 wt.% Cr and Fe-20 wt.% Cr alloys) has experienced the discontinuous coarsening reaction (the nitrified zone growth rate is smaller than the growth rate of the discontinuously coarsened zone [see (i) and (ii) above]). As discussed under (b) above, the relaxation near the surface (upon discontinuous coarsening) can be most pronounced as the specimen at this location can expand “freely” in the direction perpendicular to the surface. Then, upon continued nitriding (see the coarsely hatched area in Fig. 3.10) it is likely for specimens of relatively high chromium content that residual stress profiles develop exhibiting a tensile stress near the surface and a (still, but relatively moderate) compressive stress in deeper parts of the nitrified zone (see Fig. 3.10 and cf. Figs. 3.7a and 3.8a). Indeed, the values of compressive stress occurring in the bottom parts of the nitrified zone are much larger if in these depth ranges coherent, sub-microscopical nitride precipitates are present, as compared to the presence of the discontinuously coarsened microstructure (cf. Fig. 3.6a for a Fe-4 wt.% Cr specimen and Fig. 3.8a for a Fe-20 wt.% Cr specimen).

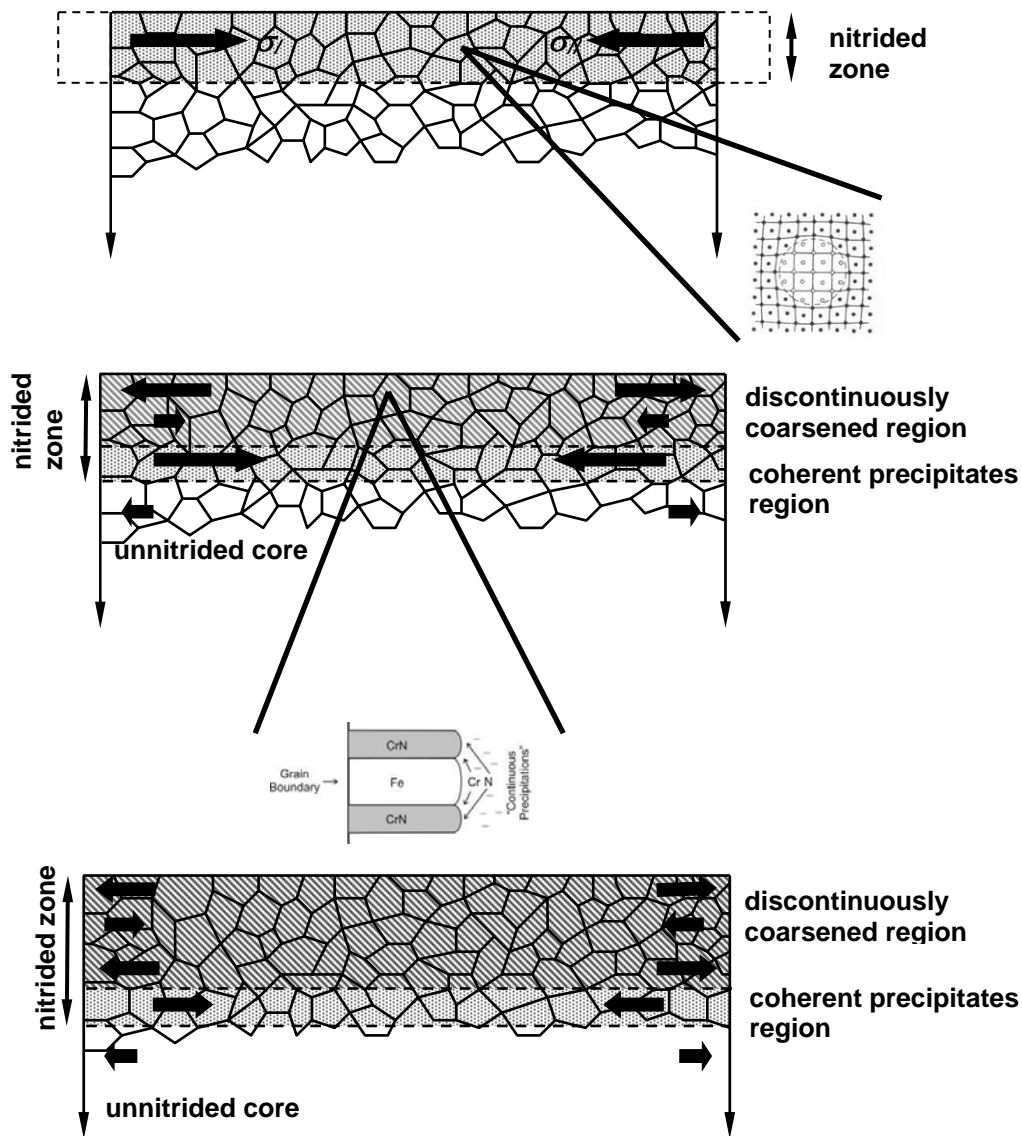


Fig. 3.9: Schematic representation of stress development upon nitriding of specimens with low chromium content. **(a)** First stage of nitriding: precipitation of coherent nitrides occurs, which tends to expand the nitrided layer, but this expansion is opposed by the unnitrided core and development of compressive residual stress parallel to the surface occurs within the nitrided layer; only coherent nitrides are present at this stage. **(b)** Upon continued nitriding discontinuous coarsening takes place: the coherent, sub-microscopical CrN precipitates in the supersaturated ferrite matrix are replaced by incoherent, relatively large α -Fe/CrN lamellar colonies under simultaneous (partial) relaxation of compressive stress in the discontinuously coarsened region. The relaxation may be complete near the surface; moderate levels of compressive stress may be maintained at some depth from the surface. Upon further nitriding coherent, sub-microscopical CrN precipitates are formed in the bottom part of the nitrided zone, generating compressive stress at this location (finely dotted area in **(b)**; see also **(a)**). Preservation of mechanical equilibrium requires the generation of a tensile stress contribution in the already discontinuously coarsened upper part of the nitrided zone, and of tensile stress in the unnitrided core adjacent to the nitrided zone. **(c)** In an advanced stage of nitriding, the development of pronounced compressive stress at relatively large depth where coherent, sub-microscopical nitrides occur, will lead to (according to the mechanism described under **(b)**) the development of a residual stress depth-profile characterized by tensile stress in the surface adjacent layer and moderate compressive stresses in the region beneath it, followed by tensile stress in the region adjacent to the transition between the discontinuously coarsened region and the coherent precipitates region.

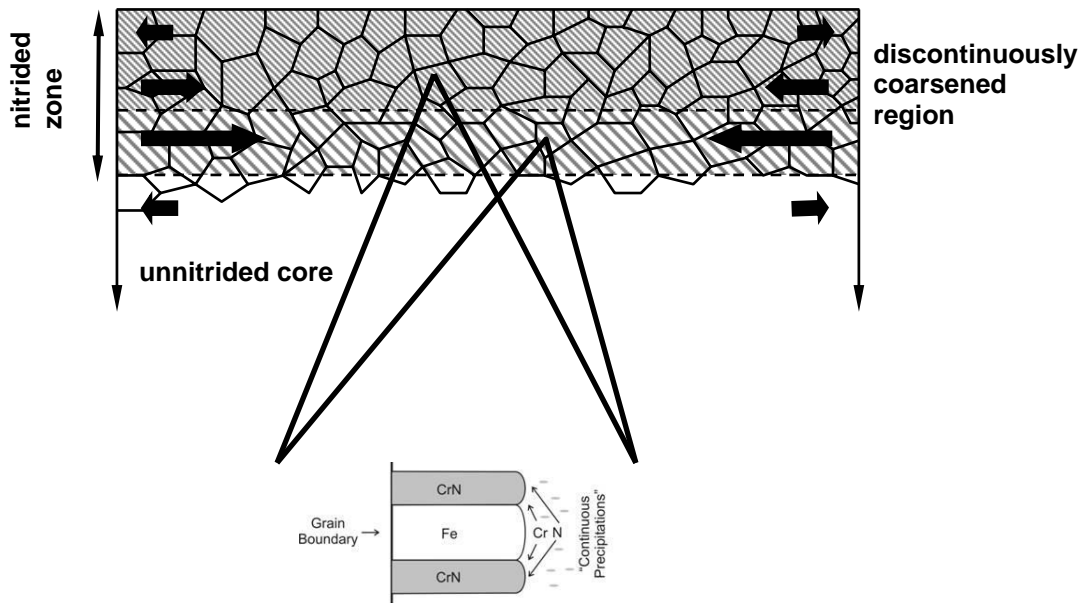


Fig. 3.10: Schematic representation of stress development upon nitriding of specimens with high chromium content. For these alloys the growth rate of the discontinuously coarsened region is equal to or larger than the nitriding rate: the entire nitrided zone consists of α -Fe/CrN lamellar colonies. The relaxation upon discontinuous coarsening in the surface region is complete (expansion of the specimen perpendicular to the surface is possible) leading, upon continued nitriding (see the coarsely hatched area), to the occurrence of tensile stress in this region. The relaxation upon discontinuous coarsening in deeper parts of the nitrided zone is more constrained and (moderate) compressive stress values (still) occur there.

3.5 Conclusions

1. Upon nitriding of iron-based iron-chromium alloys of low and high chromium content complex residual (macro) stress-depth profiles develop in the nitrided zone, which show a direct relation with gradients in the microstructure.
2. The microstructural development of the nitrided zone of iron-chromium alloys is governed by two processes occurring at different rates: (1) the growth of the nitrided zone and (2) the growth of the discontinuously coarsened region. For iron-chromium alloys with low chromium content the growth rate of the discontinuously coarsened region can be smaller than the nitriding rate. Therefore the nitrided zone of these alloys consists of a discontinuously coarsened region adjacent to the surface of the specimen and a region with coherent, sub-microscopical CrN precipitates underneath. For iron-chromium alloys with sufficiently high chromium content the growth rate of the discontinuously coarsened region is equal to or larger than the nitriding rate, and consequently the nitrided zone of these alloys is completely composed of discontinuously coarsened grains.

3. The occurrence of discontinuous coarsening is associated with (partial) relaxation of the (initial) compressive stress, most pronouncedly at the “free” surface. Upon continued nitriding of high chromium content alloys this leads to a residual stress-depth profile exhibiting a tensile stress near the surface and a (still, but relatively moderate) compressive stress in deeper parts of the nitrided zone.
4. For low chromium content alloys, in an advanced stage of nitriding, the emergence of large compressive stress in the region (at pronounced depths) where mainly coherent, sub-microscopical nitrides occur, can be compensated by tensile stress contributions in the regions immediately above and immediately beneath (unnitrided core) this region. Consequently a residual stress-depth profile develops characterized by two different zones: zone I (region adjacent to the surface) with tensile stress in the surface adjacent region and moderate compressive stress in the region beneath it (cf. conclusion 3), followed by tensile stress in the region adjacent to zone II; and zone II where stress becomes more compressive with increasing depth.

3.6 Appendix; correction of the measured stress for stress relaxation upon removing layers from the nitrided specimen

In order to trace the stress-depth profile, consecutive sublayer removal was performed in steps, by means of polishing the specimen. Upon layer removal a redistribution of stress occurs in the specimen. Hence, it is necessary to correct the stress value measured upon sublayer removal for the relaxation due to the removal of the sublayer.

A correction method can be proposed, assuming elastic relaxation only. For the case of a flat plate, the following equation is used to correct the measured residual stress (see Fig. 3.A-1) [36]:

$$\sigma(z_i) = \sigma_m(z_i) + 2 \int_{z_i}^H \frac{\sigma_m(z) dz}{z} - 6 z_j \int_{z_i}^H \frac{\sigma_m(z) dz}{z^2} \quad \text{Eq. (A-1)}$$

where $\sigma(z_i)$ is the original residual stress in the specimen (without that any sublayer has been removed) at the distance z_i to the bottom of the specimen; $\sigma_m(z_i)$ is the measured stress at the distance z_i to the bottom of the specimen (i.e. upon sublayer removal); $\sigma_m(z)$ is the function that describes the measured residual stress as a function of the distance z to the

Acknowledgements

We wish to thank Messrs. J. Köhler and Dipl.-Ing. P. Kress for assistance with the nitriding experiments and Mrs. S. Haug for assistance with the EPMA experiments.

References

- [1] E. Macherauch, K.H. Kloos, in: *Residual Stresses in Science and Technology*, volume 1, DGM Informationsgesellschaft, Oberursel (1987).
- [2] I.C. Noyan, J.B. Cohen, in: *Residual Stresses. Measurement by diffraction and interpretation*, Springer-Verlag, New York (1987).
- [3] *ASM Handbook*, volume 4, ASM International, Metals Park, Ohio (1991).
- [4] D. Liedtke: *Wärmebehandlung von Eisenwerkstoffen. Nitrieren und Nitrocarburieren*, Expert Verlag, Renningen (2006).
- [5] E.J. Mittemeijer (Ed): *Mat. Sci. Forum*; 102-104 (1992) 223.
- [6] E. Lehrer: *Z. Elektrochem.* 36 (1930) 383.
- [7] E.J. Mittemeijer, J.T. Slycke: *Surf. Eng.* 12 (1996) 152.
- [8] K.H. Jack in: *Proc. Conf. on Heat Treatment*, The Metals Society, London (1975) 39.
- [9] S.S. Hosmani, R.E. Schacherl, E.J. Mittemeijer: *Int. J. Mat. Res.* 11 (2006) 1545.
- [10] S.S. Hosmani, R.E. Schacherl, E.J. Mittemeijer: *Mat. Sci. Tech.* 21 (2005) 113.
- [11] P.M. Hekker, H.C.F. Rozendaal, E.J. Mittemeijer: *J. Mat. Sci.* 20 (1985) 178.
- [12] R.E. Schacherl, P.C.J. Graat, E.J. Mittemeijer: *Z. Metallk.* 93 (2002) 468.
- [13] S.S. Hosmani, R.E. Schacherl, E.J. Mittemeijer: *Acta Mater.* 17 (2005) 2069.
- [14] H.C.F. Rozendaal, P.F. Colijn, E.J. Mittemeijer: *Surf. Eng.* 1 (1985) 30.
- [15] E.J. Mittemeijer: *J. Heat Treat.* 3 (1983) 114.
- [16] E.J. Mittemeijer: *J. Metals* 37 (1985) 16.
- [17] E.J. Mittemeijer, in: *Case-hardened steels: microstructural and residual stress effects; Proceedings of the symposium sponsored by the Heat Treatment Committee of the Metallurgical Society of AIME held at the 112th AIME Annual Meeting*, The Metallurgical Society of AIME, New York (1984) 161.
- [18] D.B. Williams, E.P. Butler: *Inter. Metals Rev.* 3 (1981) 153.
- [19] N.E. Vives Díaz, R.E. Schacherl, E.J. Mittemeijer: Chapter 2.
- [20] E.J. Mittemeijer, A.B.P. Vogels, P.J. van der Schaaf: *J. Mat. Sci.* 15 (1980) 3129.
- [21] E.J. Mittemeijer, H.C.F. Rozendaal, P.F. Colijn, P.J. van der Schaaf, Th. Furnée, in: *Proc. of Heat Treatment '81*, The Metals Society, London (1983) 107.

- [22] P.C. van Wiggan, H.C.F. Rozendaal, E.J. Mittemeijer: *J. Mat. Sci.* 20 (1985) 4561.
- [23] JCPDS-International Center for Diffraction Data (1999), PCPDFWIN, Version 202
- [24] P. Villars, (Ed.): *Pearson's Handbook. Desk edition. Crystallographic data for intermetallic phases.* ASM International (1997).
- [25] J.L. Pouchou, F. Pichoir: *La Recherche Aérospatiale* no 1984-3 13.
- [26] V. Hauk (Ed.) in: *Structural and residual stress analysis by nondestructive methods,* Elsevier, Amsterdam (1997).
- [27] U. Welzel, J. Ligot, P. Lamparter, A.C. Vermeulen, E.J. Mittemeijer: *J. Appl. Cryst.* 38 (2005) 1.
- [28] M.A.J. Somers, E.J. Mittemeijer: *Met. Trans. A* 21 (1990) 189.
- [29] T. Christiansen, M.A.J. Somers: *Mat. Sci. Forum* 443-44 (2004) 91.
- [30] A. Kumar, U. Welzel, E.J. Mittemeijer: *J. Appl. Cryst.* 39 (2006) 633.
- [31] M.A.J. Somers, R.M. Lankreijer, E.J. Mittemeijer: *Phil. Mag. A* 59 (1989) 353.
- [32] S.S. Hosmani, R.E. Schacherl, E.J. Mittemeijer: in preparation.
- [33] E.J. Mittemeijer, M.A.J. Somers: *Surf. Eng.* 13 (1997) 483.
- [34] B.J. Lightfoot, D.H. Jack, in: *Proc. Conf. on Heat Treatment,* The Metals Society, London (1975) 59.
- [35] J.L. Meijering, in: *Advances in materials research,* Wiley Interscience, New York 5 (1971) 1.
- [36] M.G. Moore, W.P. Evans: *SAE Transactions* 66 (1958) 340.

Chapter 4

Nitride precipitation and coarsening in Fe-2 wt.% V alloys; XRD and (HR)TEM study of coherent and incoherent diffraction effects caused by misfitting nitride precipitates in a ferrite matrix

N.E. Vives Díaz, S.S. Hosmani, R.E. Schacherl and E.J. Mittemeijer

Abstract

Specimens of Fe-2.23 at.% V alloy were nitrided in a NH_3/H_2 gas mixture at 580 °C. The nitrided microstructure was investigated by X-ray diffraction (XRD), and (conventional and high resolution) transmission electron microscopy (HR)TEM. For specimens homogeneously nitrided during relatively short times no separate VN reflections developed but instead sidebands associated with ferrite reflections, most pronouncedly for the α -Fe-200 reflection, appeared. The diffractograms measured for the different specimens were interpreted as the result of coherent diffraction of the nitride platelets with the surrounding ferrite matrix, which is tetragonally distorted: the distorted ferrite matrix and the nitride platelets are represented by a single b.c.t. lattice, whereas the remaining part of the ferrite is described by a b.c.c. lattice. Analysis of the microstructure of the nitrided specimens using (HR)TEM investigations confirmed the existence of very tiny VN platelets, coherent with the surrounding matrix. Annealing at elevated temperatures (uphill 750 °C) after nitriding led to (moderate) coarsening of the nitride precipitates. The coarsening is associated with the occurrence of local disruptions/bending of lattice planes in the VN platelet. This effect causes that the VN platelets appear segmented in the diffraction contrast images. The specific changes in the X-ray diffractograms, as function of the stage of aging, could be consistently described as consequence of the transition from coherent to incoherent diffraction of the nitride platelets with reference to the surrounding ferrite matrix.

4.1 Introduction

Nitriding is one of the most widely used thermochemical surface treatments to improve the fatigue properties of iron-based (ferritic) workpieces [1-3]. The nitriding process consists of the inward diffusion of nitrogen, which subsequently combines with alloying elements Me, as Cr, V, Al and Ti, to produce alloying-element nitrides [4,5]. The precipitation of these nitrides is directly (hardness increase) and indirectly (development of residual stress-depth profile) responsible for the pronounced improvement of the fatigue resistance [6]. The nature of the initial stages of the alloying-element nitride precipitation process has been discussed controversially [4, 7].

Upon nitriding iron-based Fe-Ti [8-10], Fe-V [11-13] and Fe-Cr [14] alloys, plate-like nitride precipitates develop with the nitride-platelet faces parallel to the “cube” planes of ferrite (α -Fe): $\{001\}_{\alpha\text{-Fe}}$. The platelets (typical thickness around 5 nm [11]) are oriented with respect to the ferrite matrix according to the Bain orientation relationship given by: $\{001\}_{\alpha\text{-Fe}} // \{001\}_{\text{nitride}}$; $\langle 100 \rangle_{\alpha\text{-Fe}} // \langle 110 \rangle_{\text{nitride}}$: the relative misfit between the precipitate and the matrix in the direction parallel to the platelet is relatively small (typically 2%), whereas the relative misfit in the direction perpendicular to the platelet is very large (typically 44%) [7].

Recent work has highlighted the occurrence of various kinds of nitrogen present in the nitrided specimen (see Fig. 4.1 and Refs. [15-16]):

- (i) Type I: nitrogen strongly bonded to the nitride precipitates. This nitrogen cannot be (easily) removed by denitriding in a reducing atmosphere (usually pure H_2);
- (ii) Type II: nitrogen *adsorbed* at the nitride/matrix interface. This nitrogen is less strongly bonded than type I nitrogen and (with the exception of nitrided iron-aluminum alloys) can be removed by denitriding.
- (iii) Type III: nitrogen dissolved in the octahedral interstitial sites of the ferrite matrix. Note that a strained ferrite matrix (due to the presence of the misfitting nitride precipitates) is able to dissolve more nitrogen than unstrained ferrite [7]. Type III nitrogen is easily removed by denitriding.

Diffraction analysis of nitrided iron-based alloys has revealed that, (even) for fully nitrided specimens, separate MeN (i.e. CrN, VN, AlN, TiN) reflections are not observed and that the ferrite (matrix) reflections are extremely broadened and distorted: the nitriding induced ferrite diffraction line-profile shape changes have sometimes been described as the emergence of “sidebands” which, for example, would possibly hint at a spinodal

decomposition mechanism [9] or the periodicity of a “tweed like” microstructure [12]. On the other hand, it is proposed in this paper that coherency of diffraction effects can be responsible for the phenomena observed.

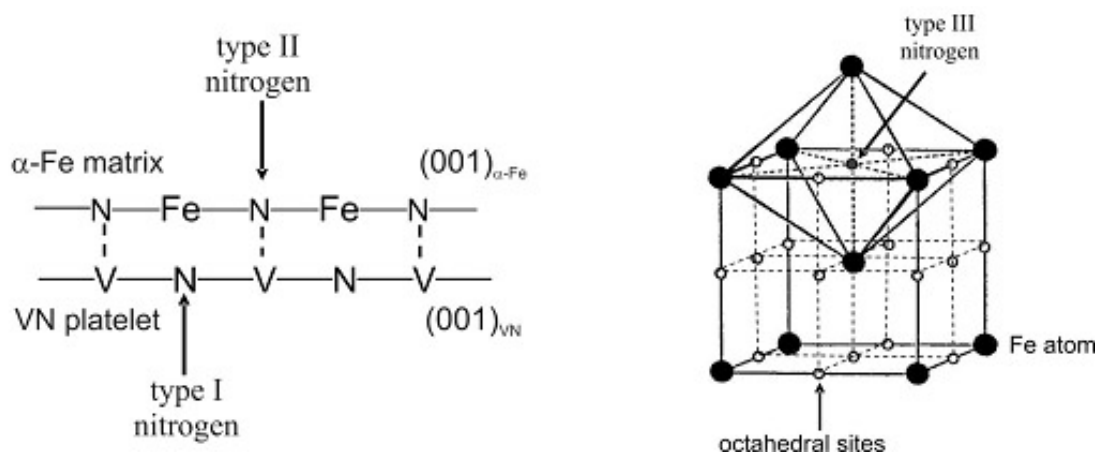


Fig. 4.1: Schematic representation of the three types of absorbed nitrogen. (a) type I nitrogen is bonded to vanadium in the VN platelets; at the interface between the ferrite and the VN platelet nitrogen atoms (type II) are adsorbed in the octahedral interstices of the ferrite in direct contact with the vanadium atoms in the VN platelet; (b) type III nitrogen is dissolved in the octahedral interstices of the ferrite matrix.

Against the above background, an evaluation of diffraction effects induced by the microstructure of nitrated iron-based alloys appears appropriate. If a consistent interpretation is achieved, at the same time significant insight into the initial stage of nitride precipitation is obtained, possibly confirming interpretations of (nitrogen) mass-uptake data in terms of atomistic models as shown in Fig. 4.1. As a model system, here an iron-vanadium alloy (2.23 at.% V) has been chosen. Previous work on this alloy system has shown that distracting complications as due to “discontinuous coarsening” [13, 17] and occurrence of non-equilibrium nitride crystal structures [18] do not occur.

4.2 Experimental

4.2.1 Specimen preparation

Alloys of nominal composition Fe-2 wt.% V (actual composition: Fe-2.04 wt.% V / Fe-2.23 at.% V) were prepared from pure Fe (99.98 wt.%) and pure V (99.80 wt.%) by melting in an Al₂O₃ crucible in an inductive furnace under Ar atmosphere (99.999 vol.%). After casting the Fe-2.23 at.% V alloy had a cylindrical shape with a diameter of 10 mm and a length of 100 mm. The cast rods were cold rolled to sheets with a thickness of 1.0 mm. These sheets were annealed at 700 °C for 2 h (within the α -phase region in the Fe-V phase diagram) to obtain a

recrystallized grain structure. After this annealing procedure the sheets were cold rolled to foils with a thickness of 0.2 mm. The obtained foils were cut into square pieces of 20×20 mm². These foil pieces were annealed at 700 °C during 2 hours under H₂ atmosphere to obtain a recrystallized grain structure. Before nitriding the specimens were ground, polished (last step: 1 μm diamond paste) and cleaned in an ultrasonic bath filled with ethanol.

4.2.2 Nitriding; denitriding and annealing experiments

For nitriding, the specimens were suspended at a quartz fibre in a vertical quartz tube nitriding furnace. The nitriding atmosphere consisted of a mixture of pure ammonia (NH₃) (>99.998 vol.%) and hydrogen (H₂) (99.999 vol. %). The flux of both gases (500 ml/s; linear gas flow rate: 1.35 cm/s) was regulated with mass flow controllers. After nitriding, the specimens were quenched and cleaned with ethanol in the ultrasonic bath. All specimens were nitrided at 580 °C and at a nitriding potential [19] $r_N = \frac{P_{NH_3}}{P_{H_2}^{3/2}} = 0.104 \text{ atm}^{-1/2}$ (where P_{NH_3} and P_{H_2} are the partial pressures of ammonia and hydrogen in the nitriding atmosphere). One specimen nitrided for 4 hours at 580 °C was subsequently denitrided during 48 hours at 700 °C under hydrogen atmosphere (500 ml/s). Four specimens nitrided for 10 hours at 580 °C (two of these specimens were denitrided after nitriding, as described above) were subjected to several annealing treatments: one nitrided specimen and one nitrided + denitrided specimen were annealed at 750 °C for 10 h; one nitrided specimen and one nitrided + denitrided specimen were annealed at 580 °C for 10 h, then again at 580 °C for another 20 h, and subsequently at annealing temperatures increasing from 580 to 740 °C in steps of 20 °C for 20 h each time, and finally at 750 °C for 20 h.

After nitriding, pieces were cut from the specimens for cross-sectional analysis. The specimens were embedded using Konduktomet (Buehler GmbH), a conductive, polymer-based embedding material. Subsequently the cross sections were ground and polished down to 1 μm diamond paste. For the light optical microscopy investigations the polished cross sections were etched with Nital 2.5 % (2.5 % vol. HNO₃ dissolved in ethanol) for about 5 s. The light optical microscopy analysis, the hardness-depth profiles and the electron probe micro-analysis demonstrated that all specimens (i.e. including the small nitriding time of 2 h (at 580 °C)) were through nitrided; hence, the nitrided zone coincides with the whole cross-section of the specimens. It should thus be recognized that for the foils considered nitriding times beyond 2 h (at 580 °C) must be interpreted as aging times at 580 °C.

4.2.3 Transmission Electron Microscopy (TEM)

Discs with a diameter of 3 mm were cut from the nitrated specimens and from the nitrated + annealed specimens after the last annealing treatment (see end of Section 4.2.2). The discs were subsequently subjected to ion milling at 4 kV and 1 mA in order to thin the specimens such that a region transparent to the electron beam is produced in the middle of the disc. During ion milling the specimens were cooled using nitrogen gas.

The microstructure of all specimens was investigated by means of bright and dark field diffraction-contrast images, and also recording the corresponding electron diffraction patterns, mostly with the foil surface oriented perpendicular to the $\langle 100 \rangle$ direction of the ferrite matrix, which is a convenient orientation of the specimen in order to investigate diffraction effects of precipitates oriented according to the Bain orientation relationship.

Conventional transmission electron microscopy (TEM) characterization was performed using a Jeol JEM 2000 FX microscope operated at 200 kV and a Philips CM 200 microscope, operated also at 200 kV. For high resolution analysis of the specimens (HRTEM) a Jeol ARM 1250 microscope operated at 1250 kV was utilized.

4.2.4 X-ray diffraction (XRD)

4.2.4.1 Texture measurements

The ferritic matrix of the specimens investigated generally possesses a crystallographic texture. Furthermore, a specific orientation relationship (Bain, see above) occurs between the nitride precipitates and the ferrite matrix. Therefore, in order to best detect specific ferrite reflections and specific nitride reflections, it is necessary to choose appropriate sets of tilt (ψ , the inclination angle of the diffraction vector with respect to the specimen surface normal) and rotation (φ , the angle of rotation around the specimen surface normal) angles in order to achieve maximum diffracted intensity.

For the determination of the texture of the ferrite matrix a Philips MRD diffractometer, provided with an Eulerian cradle and a Cu tube (Cu K_{α} radiation, λ : 1.54056 Å) was used. The 2θ angle was kept fixed and the texture measurements were performed for the ranges $0^{\circ} \leq \psi \leq 87^{\circ}$ (step size: 3°) and $0^{\circ} \leq \varphi \leq 360^{\circ}$ (step size: 3°), for the Fe-110, Fe-200 and Fe-211 reflections. All specimens were obtained from the same ingot and have the same texture. The obtained pole figures were analyzed using the X'Pert Texture software by Philips. The texture is not rotationally symmetric with respect to the angle φ (see Fig. 4.2).

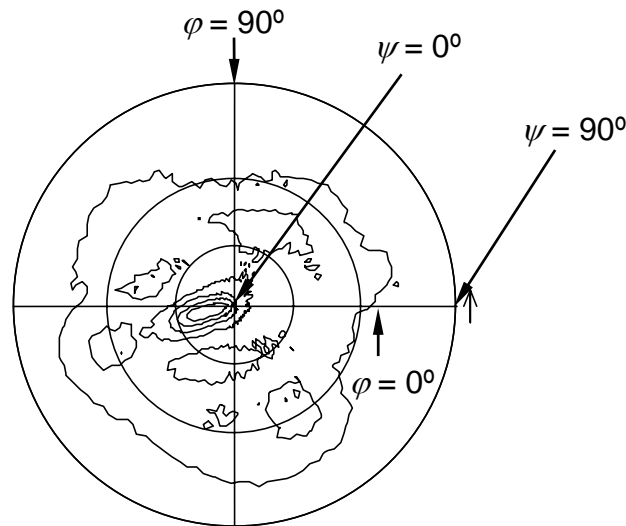


Fig. 4.2: Pole figure recorded from the specimen of Fe-2.23 at.% V nitrided for 10 h corresponding at 580 °C and $r_N = 0.104 \text{ atm}^{-1/2}$, recorded using the Fe-200 reflection.

4.2.4.2 2θ -scans

(a) *Analysis of “ferrite” reflections.* On the basis of the measured texture, sets of tilt (ψ) and rotation (ϕ) angles were selected to record the Fe-110, Fe-200 and Fe-211 reflections, encompassing a diffraction angle, 2θ , range from 30° to 95°. The same Philips MRD diffractometer (with an Eulerian cradle) as in Section 4.2.4.1 was used.

(b) *Analysis of VN reflections.* Because (i) the VN particles are oriented with respect to the ferrite matrix according to the Bain orientation relationship and (ii) the ferrite matrix exhibits a specific crystallographic texture, maximum intensity for a specific VN reflection can be expected only at specific combinations of tilt (ψ) and rotation (ϕ) angles. For example, if ψ and ϕ are chosen such that the Fe-200 reflection has a maximum intensity, then also a maximum intensity for the VN-200 reflection is expected. However, choice of the VN-200 reflection to prove separate (incoherent) diffraction by the VN precipitates is inappropriate, because of the strong overlap (in a 2θ scan) with the Fe-110 reflection. A suitable choice provides the VN-111 reflection: relatively high intensity and no appreciable overlap with other (ferrite) reflections in a 2θ scan. To detect the VN-111 reflection the following procedure was employed: (1) the specimen was positioned using the tilt and rotation angles to obtain maximum intensity for the Fe-200 reflection; (2) the specimen was further tilted over another 54.74°, which is the angle between the lattice planes $\{100\}_{\text{VN}}$ and $\{111\}_{\text{VN}}$; (3) at this tilt angle, and at the diffraction angle 2θ corresponding to the VN-111 reflection ($2\theta =$

37.687°) a φ -scan was performed, in order to obtain the rotation angle which provides maximum diffracted intensity for VN-111; (4) then, at the ψ and φ angles thus determined a 2θ -scan in the diffraction angle-range around the VN-111 reflection was performed.

4.3 Results and preliminary discussion

4.3.1 As-nitrided specimens

4.3.1.1 Phase analysis using X-ray diffraction (XRD)

The X-ray diffractograms recorded from nitrided iron-based alloys can be divided in two groups: (1) diffractograms recorded for nitriding times up to 10 h at 580 °C showing only (strongly) broadened, distorted ferrite reflections and no separate nitride reflections; (2) diffractograms recorded for nitriding times beyond 15 h at 580 °C showing both ferrite reflections and nitride reflections.

Diffractograms recorded around the 2θ position of the Fe-200 reflection from specimens nitrided up to 10 h show peculiar diffraction contributions near the ferrite peak, which cannot be attributed to separate VN reflections, see Figs. 4.3a-c.

Upon prolonging nitriding (nitriding time longer than 15 h), the diffraction profiles in the same 2θ range reveal two separate peaks, which can be associated, in principle, to VN-220 and Fe-200, see Figs. 4.3d-f. Diffractograms recorded in the 2θ range from 33° to 43°, using the method described in Section 2.4.2, from specimens nitrided for times beyond 15 h at 580 °C show the presence of a separate VN-111 reflection (see Fig. 4.4).

4.3.1.2 Analysis of the microstructure using TEM and HRTEM

The specimens nitrided for 2, 4 and 10 h at 580 °C consist of a ferrite matrix, as shown by the electron diffraction pattern given in Fig. 4.5b, exhibiting a kind of “tweed contrast” in the bright-field diffraction-contrast image shown in Fig. 4.5a. No separate VN spots are present in the electron diffraction patterns of these specimens. The theoretical diffraction pattern to be expected if the VN precipitates diffract independently is shown in Fig. 4.5c. Streaks of intensities along the $\langle 100 \rangle$ α -Fe directions are observed in the electron diffraction patterns, see Fig. 4.5b. This can be interpreted as a consequence of strain broadening, in particular in the $\langle 100 \rangle$ direction (cf. Section 4.3.1.1) and can be due to the development of nitride platelets

along $\{100\}$ α -Fe planes. Note that the precipitate/matrix misfit is particularly pronounced in the direction perpendicular to the nitrated platelets (cf. Section 4.1).

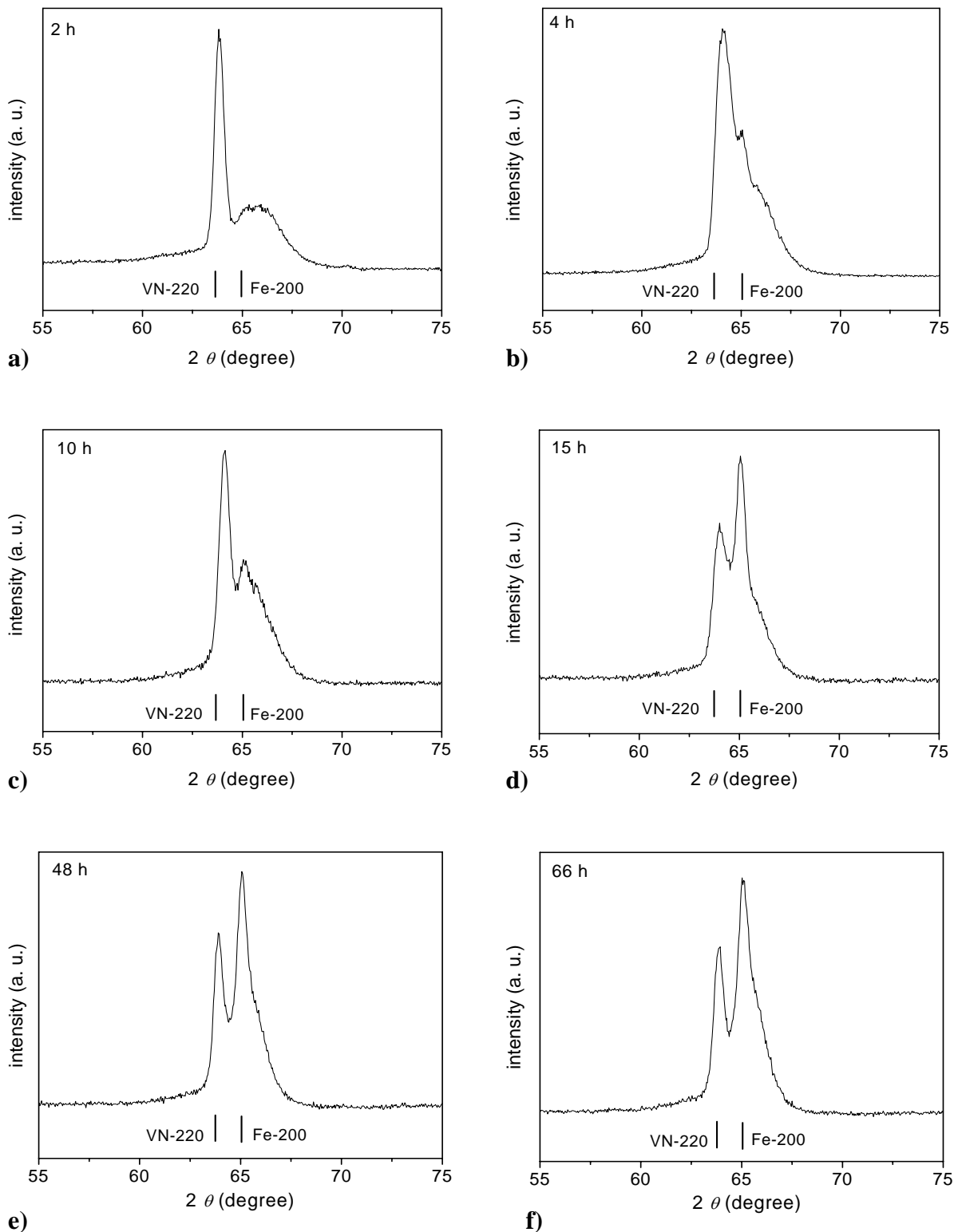


Fig. 4.3: X-ray diffractograms in the diffraction-angle, 2θ , range around the Fe-200 reflection for specimens of Fe-2 wt. % V alloy nitrided at 580 °C, $r_N = 0.104 \text{ atm}^{-1/2}$ for different nitriding times (a) nitrided for 2 h, (b) nitrided for 4 h, (c) nitrided for 10 h, (d) nitrided for 15 h, (e) nitrided for 48 h, (f) nitrided for 66 h. The hypothetical positions of the VN-220 and Fe-200 reflections (if VN and α -Fe diffract independently and if those phase are unstrained) have also been indicated.

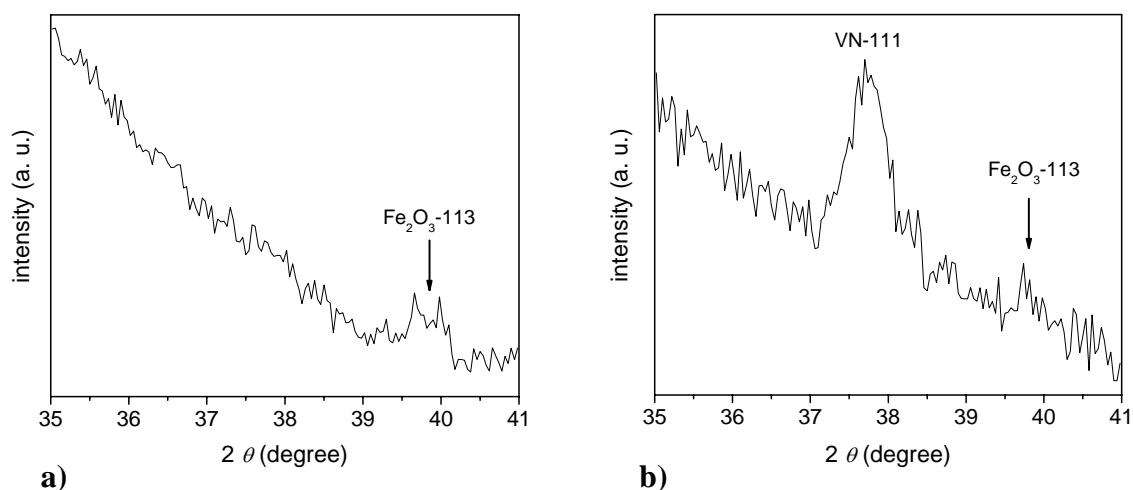


Fig. 4.4: X-ray diffractograms recorded from specimens of Fe-2.23 at.% V alloy nitrided at 580 °C and $r_N = 0.104 \text{ atm}^{-1/2}$ for 4 and 20h; **(a)** no VN-111 reflection is detectable for the specimen nitrided for 4 h; **(b)** a separate VN-111 reflection clearly occurs for the specimen nitrided for 20 h. A weak peak due to iron oxide at the surface can be discerned in both cases.

By examination of the microstructure of the nitrided specimens using HRTEM, extremely tiny VN platelets are observed in the whole specimen. These platelets are (indeed) oriented according to the Bain orientation relationship (cf. Section 4.1) and are extremely small, about 5 nm long and 1-2 atomic layers thick, see Figs. 4.6a-c. The lattice fringes shown in Figs. 4.6a and 4.6b bend across the platelets, which strongly suggests that the platelets at this stage of nitriding (10 h at 580 °C) are coherent but experience considerable misfit with the matrix.

For the specimens nitrided for 48 and 66 h at 580 °C, now also separate VN spots are discerned in the electron diffraction pattern (see Fig 4.7). The dark field images taken from the VN spots reveal the existence of small VN precipitates [around 20 nm diameter] in the specimen). Evidently, at these relatively long nitriding times coarsening (at least partially) of the originally very tiny VN platelets has occurred, leading to incoherent (separate) diffraction by the nitrides, in agreement with the XRD results (see Section 4.3.1.1).

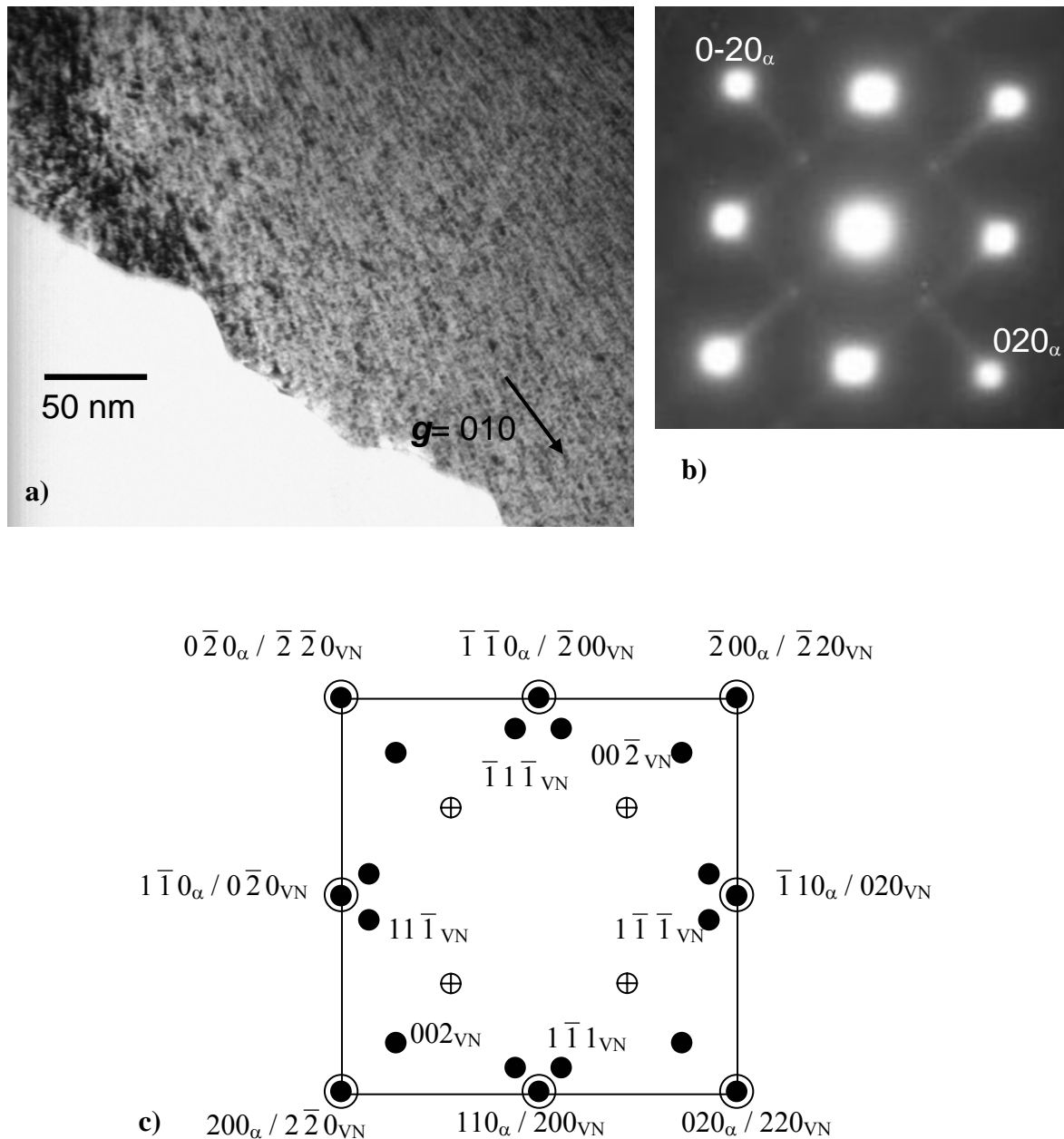


Fig. 4.5: TEM for a specimen of Fe-2.23 at.% V alloy nitrided for 2 h at 580 °C and $r_N = 0.104 \text{ atm}^{-1/2}$; electron beam direction: $[001]_{\alpha-Fe}$. **(a)** Bright field; the microstructure is representative for specimens nitrided up to 10 h, and consists of a tweed-like contrast with no observable separate precipitates; **(b)** corresponding electron diffraction pattern, no separate VN spots are visible (see **(c)**), only streaks occur along the $\langle 100 \rangle_{\alpha-Fe}$ directions and spots corresponding to Fe_3O_4 are observed; **(c)** schematic depiction of the theoretical diffraction pattern due to the ferrite matrix (open circles) and the VN precipitates (rock salt structure), assuming the Bain orientation relationship (black filled circles); spots corresponding to Fe_3O_4 are represented by crossed circles. The diffraction pattern takes into account all three variants possible for a VN precipitate following the Bain orientation relationship; see Ref. [18].

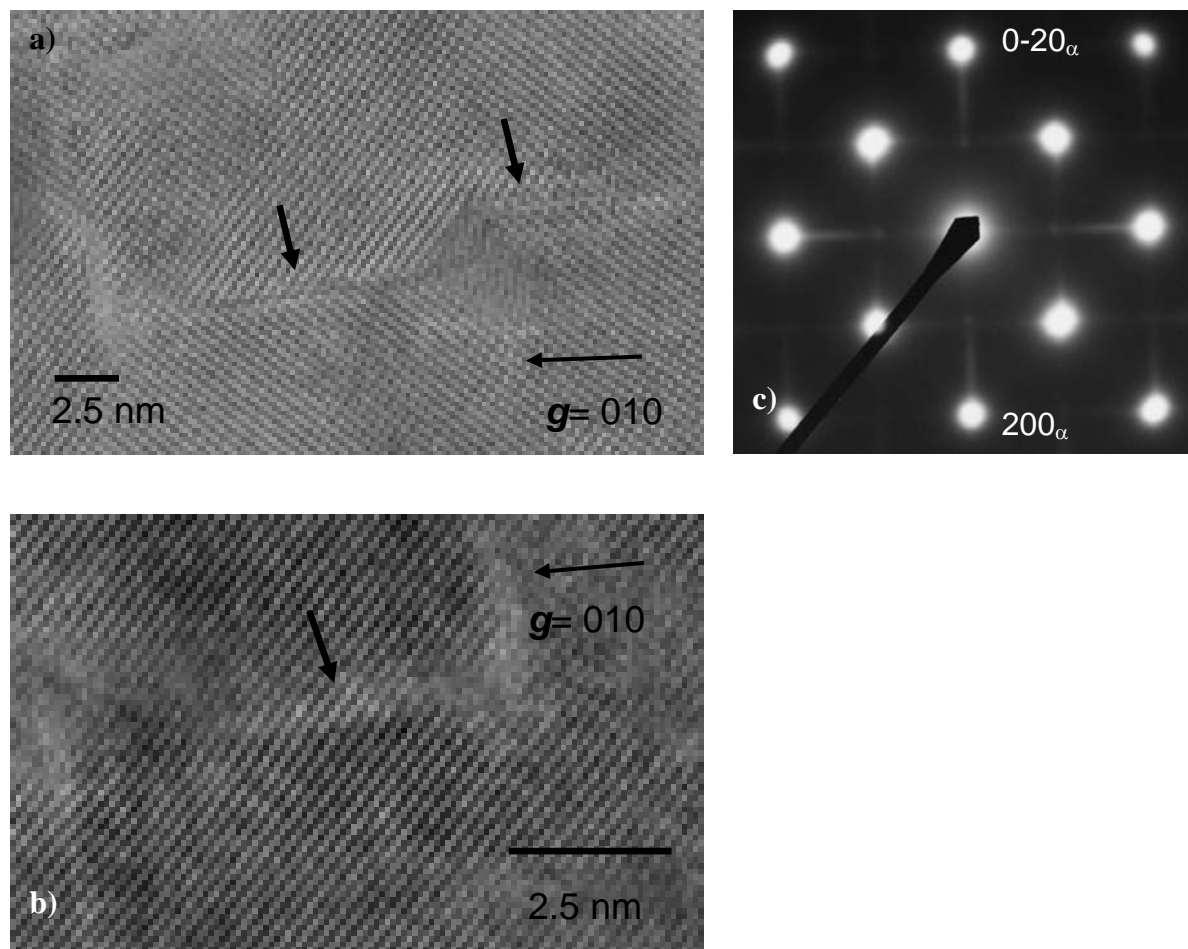


Fig. 4.6: HRTEM for a specimen of Fe-2.23 at.% V alloy nitrated for 10 h at 580 °C and $r_N = 0.104 \text{ atm}^{-1/2}$; electron beam direction: $[001]_{\alpha\text{-Fe}}$. **(a)** HRTEM image showing coherent, very tiny VN platelets oriented according to the Bain relationship (see arrows); the platelets are about 5 nm long and 1-2 monolayers thick. **(b)** detail of a single platelet (see arrow), revealing the bending of the lattice planes at the location of the platelet; **(c)** corresponding electron diffraction pattern, no separate VN spots are visible, only streaks along the $\langle 100 \rangle_{\alpha\text{-Fe}}$ directions.

4.3.2 Nitrated and annealed specimens

The purpose of annealing nitrated specimens is to study the stability of the microstructure. In particular, the transition of coherent nitride precipitates to semi-coherent/incoherent precipitates, as a function of the annealing temperature, and the associated diffraction effects are of interest.

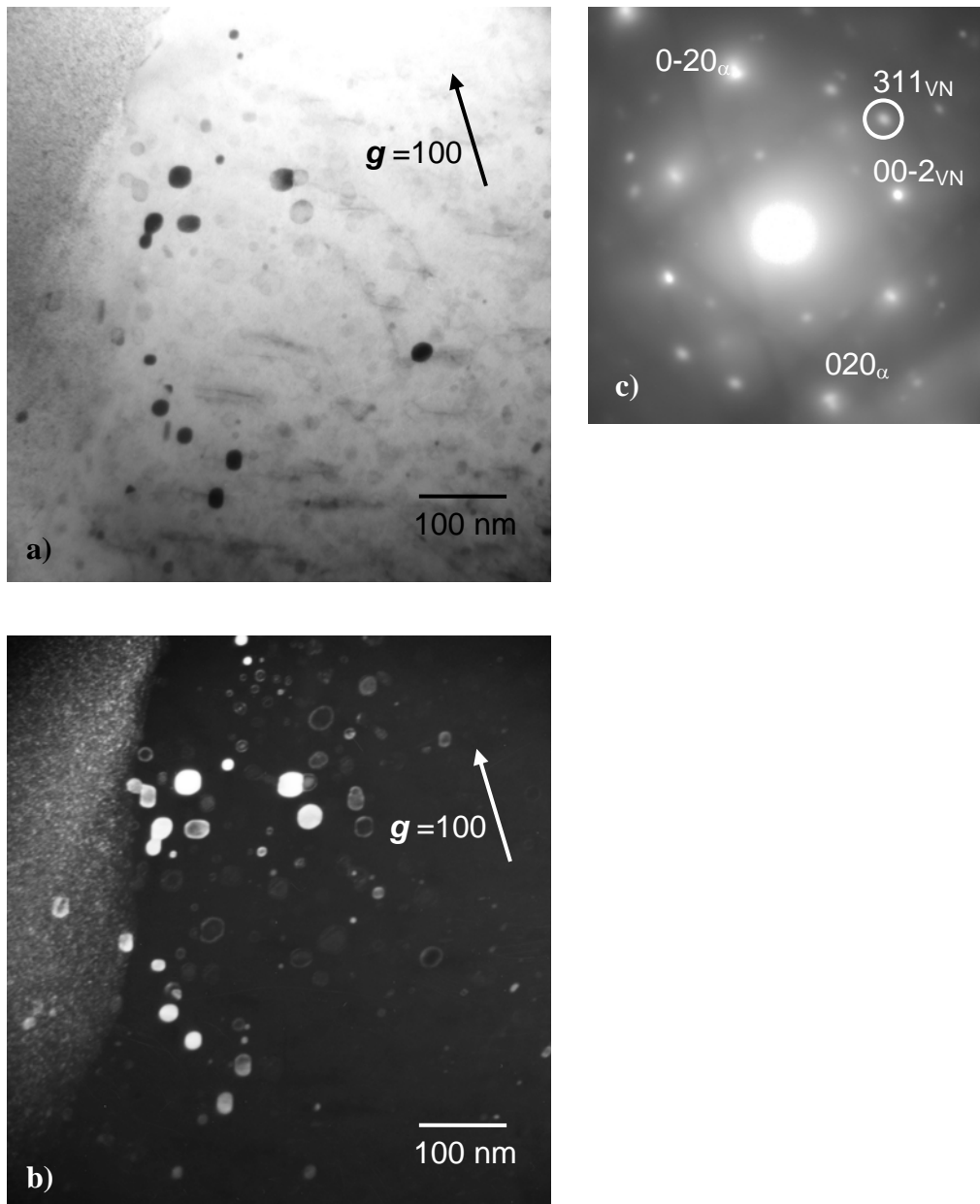


Fig. 4.7: TEM for a specimen of Fe-2.23 at.% V alloy nitrided for 66 h at 580 °C and $r_N = 0.104 \text{ atm}^{-1/2}$; electron beam direction near the $[001]_{\alpha\text{-Fe}}$ axis. **(a)** Bright field; **(b)** Dark field utilizing the VN-311 spot, individual VN particles can be observed; **(c)** corresponding electron diffraction pattern.

4.3.2.1 Phase analysis using X-ray diffraction (XRD)

Recognizing that a specimen nitrided for 15 h and longer at 580 °C gives rise to separate VN reflections in the diffraction patterns, one may expect that annealing for 10 h at 580 °C a specimen previously nitrided for 10 h at 580 °C would also lead to the occurrence of separate VN reflections in the diffractograms. However, after annealing for even 30 h at 580 °C of a specimen nitrided for 10 h at 580 °C no such change was detected in the diffractograms. Only

after annealing the specimen (originally nitrated for 10 h at 580 °C) at higher temperatures, for 20 h at 600 °C, 20 h at 620 °C and 20 h at 640 °C, a significant change in the peak shape was observed (compare Figs. 4.3c and 4.8a). Upon annealing at 700 °C only a diffraction peak apparently corresponding to Fe-200 and a trace of the VN-220 reflection are observed in the diffractogram (see Figs. 4.8c and 4.8d). Other VN reflections, besides the VN-220, are observed as well upon annealing at such elevated temperatures (see Fig. 4.9).

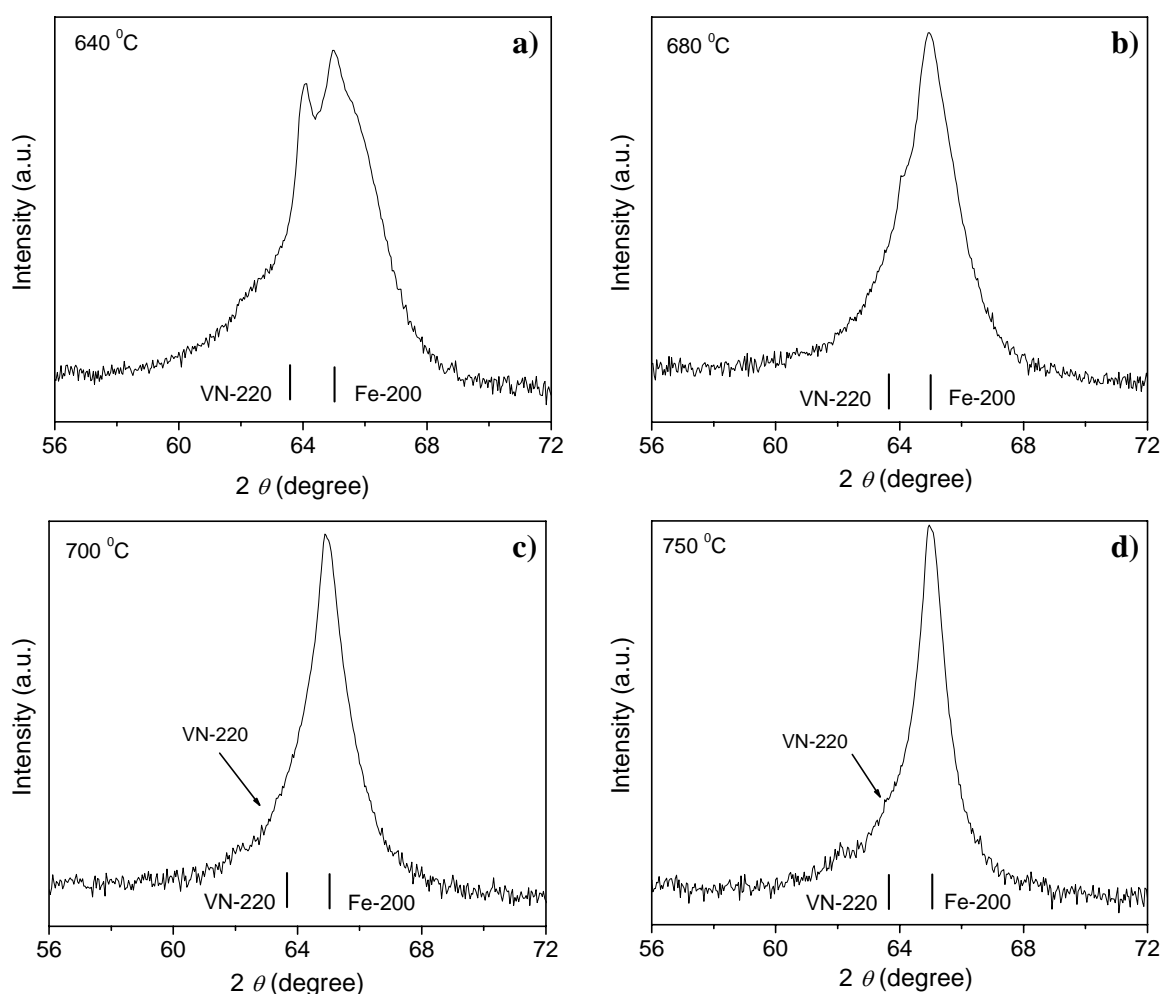


Fig. 4.8: Diffractograms in the diffraction-angle, 2θ , range around the Fe-200 reflection recorded from specimens of Fe-2.23 at.% V alloy nitrated for 10 hours at 580 °C and $r_N = 0.104 \text{ atm}^{-1/2}$ and subsequently subjected to consecutive annealing treatments: **(a)** annealed for 20 h at 640 °C; **(b)** annealed for 20 h at 680 °C; **(c)** annealed for 20 h at 700 °C; **(d)** annealed for 20 h at 750 °C. The hypothetical positions of the VN-220 and Fe-200 reflections (if VN and α -Fe diffract independently and if those phase are unstrained) have also been indicated.

4.3.2.2 Effects of denitriding

Denitriding involves that the nitrogen dissolved at the octahedral interstices of the ferrite lattice and the nitrogen *adsorbed* at the nitride platelet face is removed [15]. The main effect

of denitriding upon subsequently annealing is that the sequence of structural changes induced by the annealing, and as described in Section 4.3.2.1, occurs at an earlier stage of aging, i.e. at lower temperatures. The diffractograms in the diffraction-angle range around the Fe-211 reflection and recorded after annealing for 30 h at 580 °C, 20 h at 600 °C, 20 h at 620 °C and 20 h at 640 °C 20 h, of a specimen nitrided for 10 h at 580 °C and subsequently denitrided, show that only one pronouncedly broadened diffraction peak is present, whereas for the case of the nitrided + annealed sample still two diffraction maxima are visible (see Fig. 4.10a and compare with Fig. 4.8a).

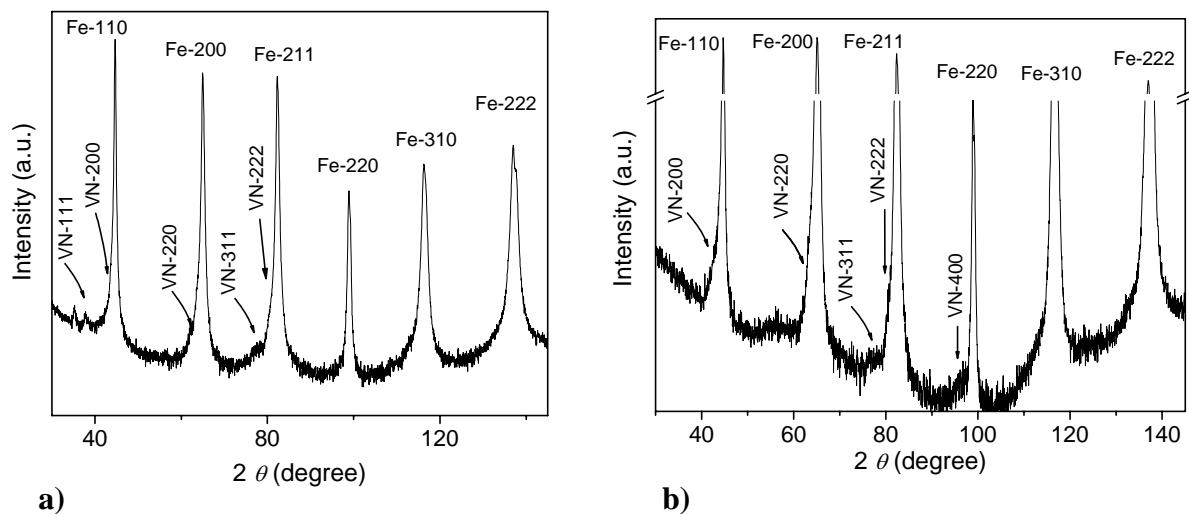


Fig. 4.9: Diffractograms recorded from specimens of Fe-2.23 at.% V alloy nitrided for 10 hours at 580 °C and $r_N = 0.104 \text{ atm}^{-1/2}$ and subsequently subjected to the following annealing treatments: **(a)** annealed at 580 °C for 10 h, then again at 580 °C for another 20 h, and subsequently at annealing temperatures increasing from 580 to 740 °C in steps of 20 °C for 20 h each time, and finally at 750 °C for 20 h; **(b)** annealed at 750 °C for 20 h.

4.3.2.3 Analysis of the microstructure using TEM and HRTEM

The microstructure of the nitrided specimen after the last annealing step (i.e. annealing for 10 hours at 750 °C) consists of elongated and relatively thin VN platelets, oriented according to the Bain orientation relationship, embedded in a ferrite matrix, see Fig. 4.11. The platelets are surrounded by strains fields, as revealed by specific diffraction contrast (see arrows in Fig. 4.11a). Separate VN diffraction spots can be observed in the electron diffraction pattern, see Fig. 4.11c (see also Fig. 4.5c). It may be suggested that the nitride platelets are (still) partially coherent with the matrix, evidently even after the relatively prolonged annealing, a (complete) relaxation of stress was not achieved. The length of the platelets is variable, but usually less than 100 nm, the thickness is around 5-10 nm; see the dark field images taken for a VN-002 spot in the electron diffraction pattern.

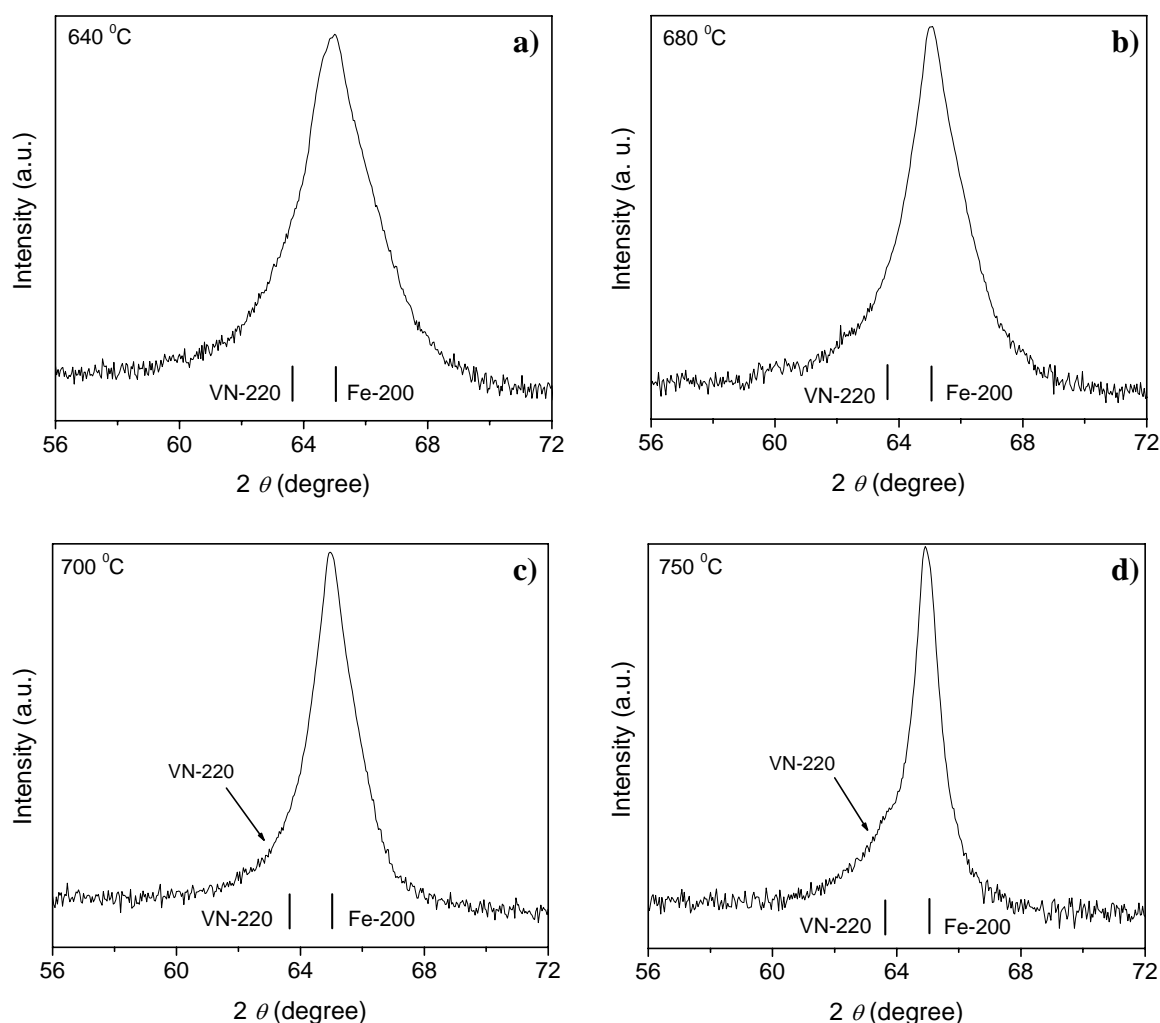


Fig. 4.10: Diffractograms in the diffraction-angle, 2θ , range around the Fe-200 reflection recorded from specimens of Fe-2.23 at.% V alloy nitrided for 10 hours at 580 °C and $r_N = 0.104 \text{ atm}^{-1/2}$ and subsequently denitrided, after which it was subjected to consecutive annealing treatments: (a) annealed for 20 h at 640 °C; (b) annealed for 20 h at 680 °C; (c) annealed for 20 h at 700 °C; (d) annealed for 20 h at 750 °C. The hypothetical positions of the VN-220 and Fe-200 reflections (if VN and α -Fe diffract independently and if those phase are unstrained) have also been indicated.

The microstructure of the nitrided + *denitrided* specimen after the last annealing step (i.e. annealing for 20 hours at 750 °C) shows an identical morphology as described above; no significant difference due to the absence of dissolved and adsorbed nitrogen in the ferrite lattice was observed.

The (transmitted/diffracted) intensity is not uniform along a single platelet; i.e. some regions of a single platelet are brighter and other regions of the same platelet appear darker. Tilting of the foil in the electron microscope shows that upon tilting the specimen over small angles ($\sim 0.5^\circ$) the maximum of diffracted intensity in the VN dark field images shifts along

the single platelet; regions that at first are bright in the dark field image turn dark(er) upon tilting (see Fig. 4.12). HRTEM micrographs reveal that, yet, such VN platelets are continuous, but that the atomic planes are slightly bent, and defects as dislocations can be discerned in the platelets, concentrated at specific locations, see Fig. 4.13. The bent lattice in the nitride precipitates is responsible for the variation of the diffraction conditions along the platelets: upon tilting the specimen parts of the bent lattice become (in)visible in the diffraction-contrast image. Therefore, it can be concluded that each VN platelet is composed of smaller, almost perfect parts, which are separated by distorted regions.

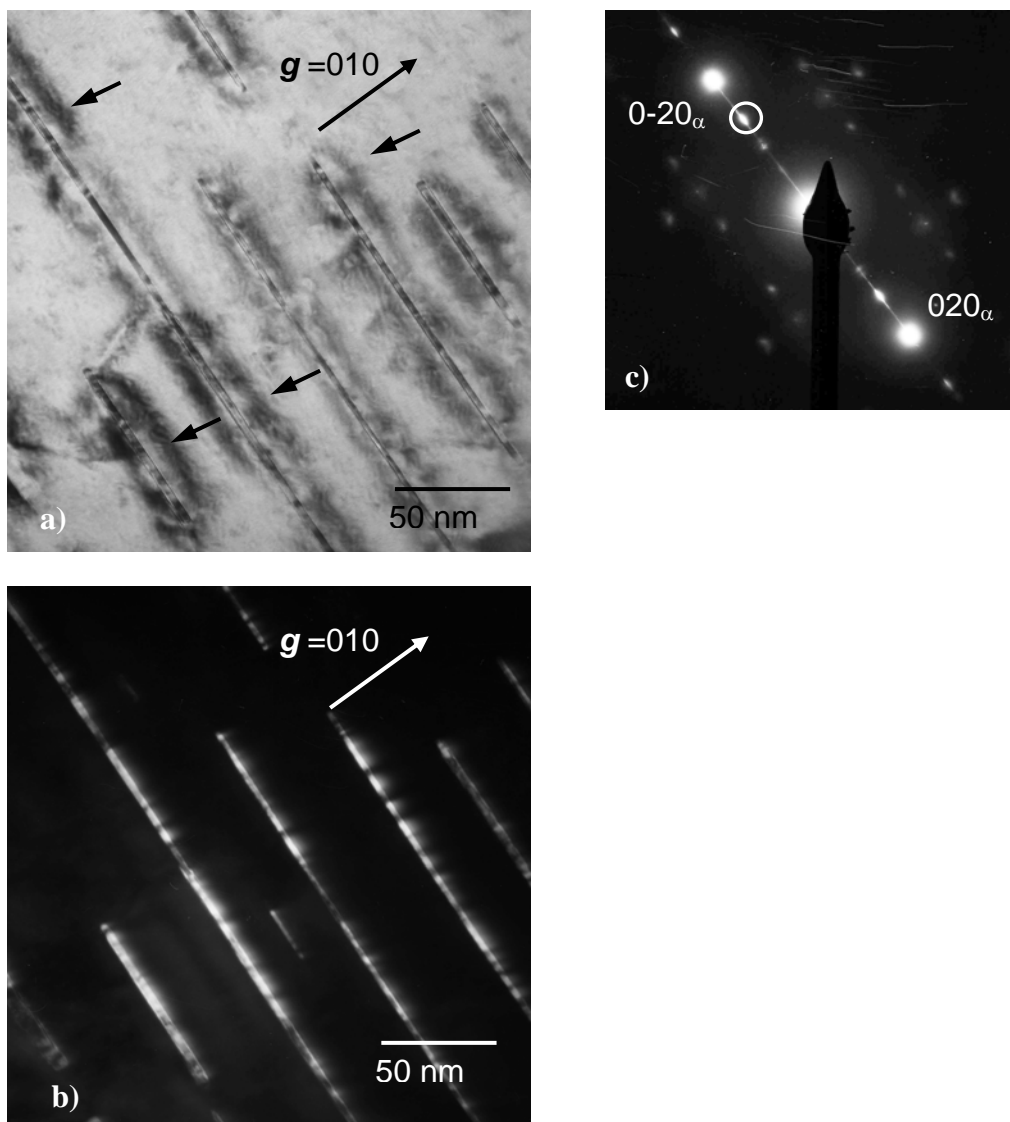


Fig. 4.11: TEM for a specimen of Fe-2.23 at.% V alloy nitrided for 10 h at 580 °C and $r_N = 0.104 \text{ atm}^{-1/2}$ and subsequently annealed under Ar atmosphere at 750 °C for 10 h; electron beam direction near the $[001]_{\alpha\text{-Fe}}$ axis. **(a)** Bright field: the microstructure consists of relatively long and thin VN platelets, surrounded by strain fields (see dark arrows), embedded in a ferrite matrix. **(b)** Dark field taken from the VN-0 $\bar{2}0$ spot (white circle) in the corresponding electron diffraction pattern (cf. Fig. 4.5c), shown in **(c)**.

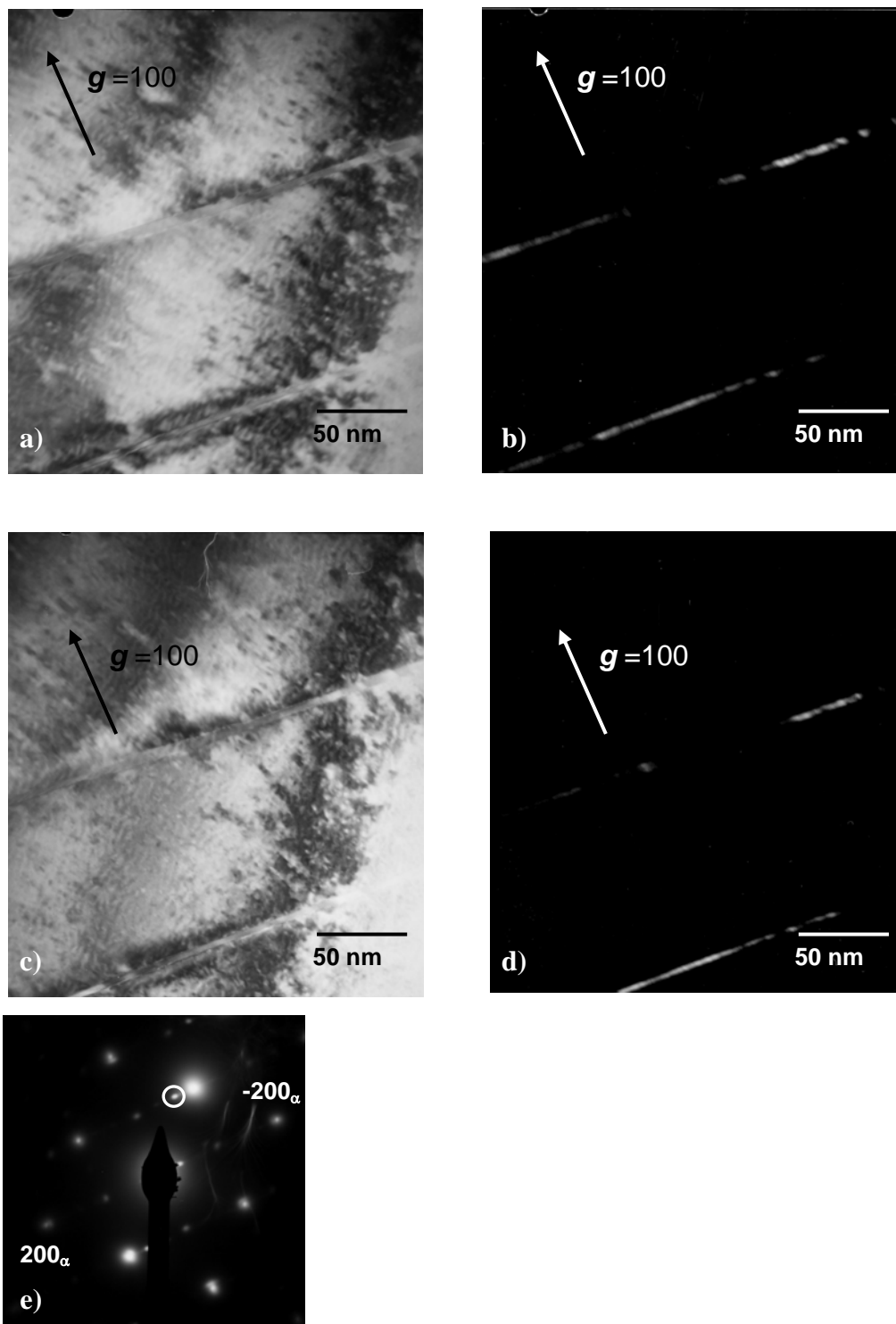


Fig. 4.12: TEM for a specimen of Fe-2.23 at.% V alloy nitrided for 10 h at 580 °C and $r_N = 0.104 \text{ atm}^{1/2}$ and subsequently denitrided for 48 h at 700 °C under H_2 atmosphere, and then annealed under Ar atmosphere at 750 °C for 10 h; electron beam direction near the $[001]_{\alpha\text{-Fe}}$ axis. (a) Bright field; (b) corresponding dark field; (c) bright field recorded after tilting the specimen 0.50° along the longitudinal and transversal axes in the foil surfaces; (d) corresponding dark field; (e) electron diffraction pattern corresponding to (a) and (b), upon tilting the pattern does not change significantly. Dark field images were recorded using the $\text{VN-}\bar{1}\bar{1}\bar{1}$ spot (see white circle, cf. Fig. 4.5c).

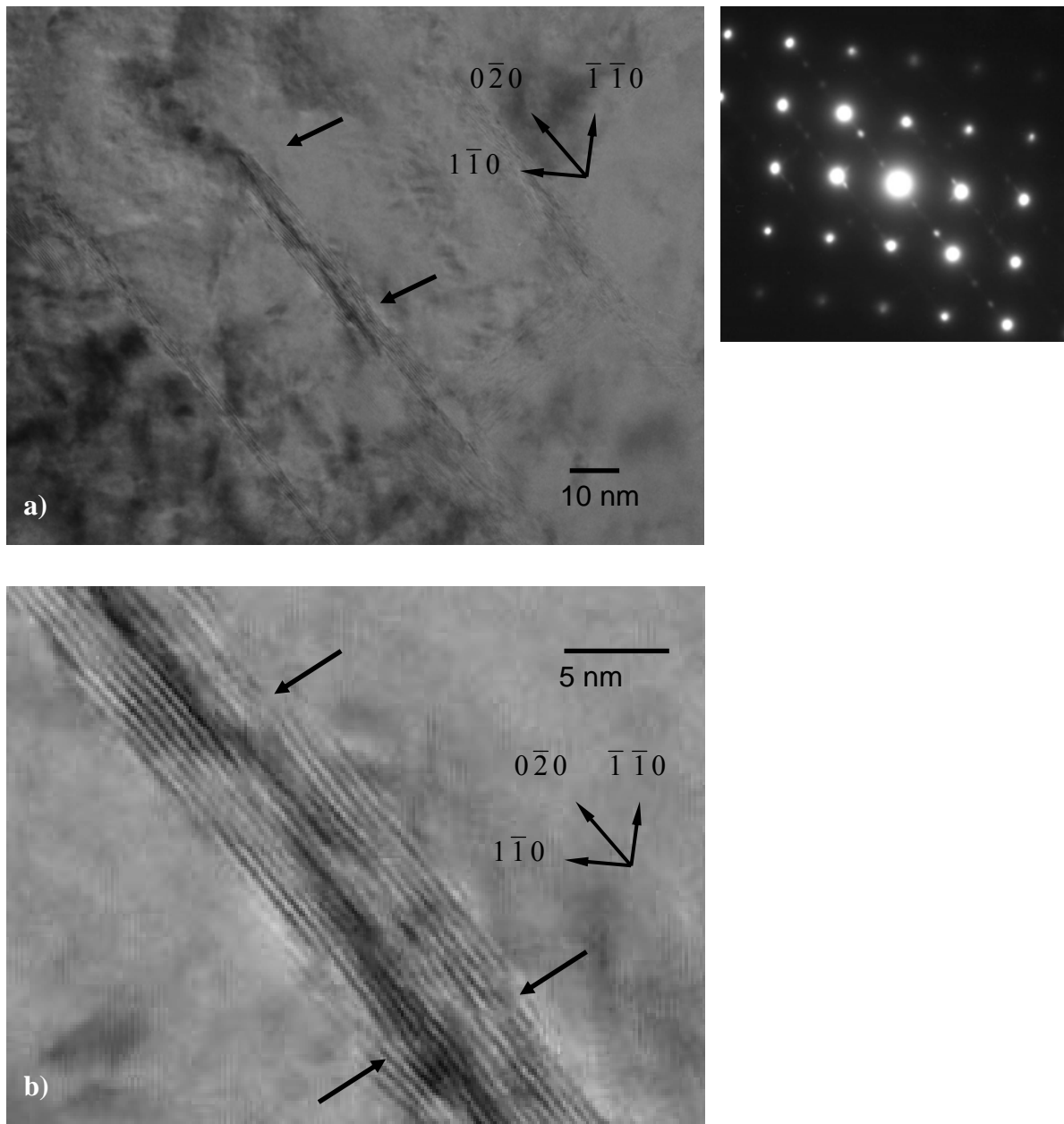


Fig. 4.13: HRTEM for a specimen of Fe-2.23 at.% V alloy nitrided for 10 h at 580 °C and $r_N = 0.104 \text{ atm}^{-1/2}$ and subsequently denitrided for 48 h at 700 °C under H_2 atmosphere, and then annealed under Ar atmosphere at 750 °C for 10 h; electron beam direction: $[001]_{\alpha\text{-Fe}}$. **(a)** HRTEM image; the arrows indicate a VN platelet; **(b)** detail of the VN platelet revealing bent lattice planes and defects (see arrows; the lattice fringes in the VN platelet run parallel to its (010) lattice planes); **(c)** corresponding electron diffraction pattern (cf. Fig. 4.5c).

4.3.3 Stoichiometry of the nitride platelets; evidence for absorbed nitrogen of types I, II and III

Nitrogen absorption isotherms are determined for a particular nitriding temperature and indicate the amount of nitrogen absorbed by the specimen at a given nitriding potential [7, 15]. During the determination of the absorption isotherms it is crucial that the precipitation

morphology does not change. Therefore the specimens are pre-nitrided at a temperature above the temperature of the isotherm concerned, thereby fixing the precipitation morphology. Afterwards, the specimens are denitrided (under H₂ atmosphere). By weighing the specimen before and after denitriding the amount of nitrogen bonded in the nitride particles (i.e. nitrogen of Type I) can be determined, since nitrogen adsorbed at the nitride-platelet faces (nitrogen of type II) and nitrogen dissolved in the ferrite matrix (i.e. nitrogen of type III) is removed by denitriding (cf. Section 4.1).

An absorption isotherm for Fe-2.23 at.% V, determined in this project, is shown in Fig. 4.14. After through nitriding at 580 °C for 24 h and denitriding at 470 °C in pure H₂ for 42 h it followed that the remaining nitrogen content can be fully attributed to nitrogen strongly bonded to vanadium in the corresponding nitride VN (see Fig. 4.1). A small amount of vanadium (0.19 ± 0.08 at.%) did not take part in the formation of VN, possibly because it is present in the form of oxides already before nitriding (oxides are generally more stable than nitrides). In any case, formation of some mixed nitride, as (Fe, V)N is ruled out as this would correspond to larger amounts of nitrogen of type I than corresponding with the precipitation of all vanadium as VN.

The amount of nitrogen dissolved interstitially in the ferrite matrix (nitrogen of type III) depends linearly on the nitriding potential, r_N , [19] and comprises the equilibrium amount of nitrogen dissolved in stress-free ferrite (see dashed-dotted line in Fig. 4.14) plus the excess dissolved nitrogen due to the misfit-stress field induced by the misfitting nitride precipitates. Evidently (see Fig. 4.14), this part of the excess nitrogen can be as large as the equilibrium amount of dissolved nitrogen.

Taking the value for the amount of nitrogen obtained by extrapolation of the linear part of the absorption isotherm to $r_N = 0$, and subtracting from this value the amount of type I nitrogen (i.e. the amount of nitrogen remaining in the specimen after denitriding), provides a value for the amount of nitrogen adsorbed at the faces of the nitride platelets (nitrogen of type II). Assuming that at the interface of the ferrite matrix with the VN platelet every octahedral interstice of the ferrite contains one adsorbed (trapped) excess nitrogen atom (see Fig. 4.1a), it follows from the amount of type II nitrogen in the specimen nitrided for 24 h at 580 °C that the nitride platelet thickness is about 2 nm (cf. reasoning in Ref. [15]).

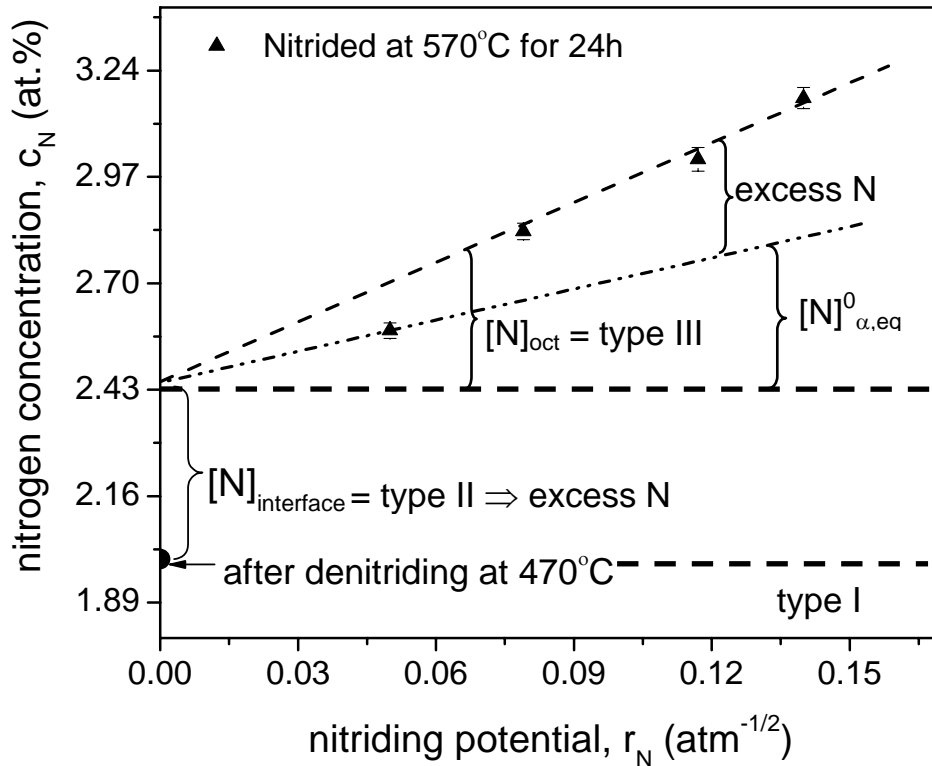


Fig. 4.14: Nitrogen absorption isotherm corresponding to a specimen of Fe-2.23 at.% V alloy prenitrided at 580 °C for 24 h and subsequently denitrided at 470 °C for 42 h, and afterwards nitrated at 570 °C for 24 h using four different nitriding potentials, r_N . The linear portion of the absorption isotherm is indicated by the dashed line. The amount of nitrogen absorbed by pure iron subjected to the same nitriding procedures as the specimen of the iron-vanadium alloy is indicated by the inclined dashed-dotted line (data also obtained in this project). After denitriding only the nitrogen bonded to VN remains (type I); nitrogen adsorbed at the faces of the nitride platelets, $[N]_{\text{interface}}$, corresponds to type II nitrogen. The “excess nitrogen” comprises type II nitrogen plus the part of type III nitrogen that exceeds the equilibrium solubility of nitrogen in pure, stress-free ferritic iron.

4.3.4 Analysis of the X-ray diffraction profiles

4.3.4.1 Diffraction model

On the basis of the (HR)TEM and absorption-isotherm evidence, presented in Sections 4.3.1.2, 4.3.2.3 and 4.3.3, it is concluded that for nitriding times shorter than 10 h at 580 °C already all vanadium has precipitated as coherent VN platelets exhibiting a Bain orientation relationship with the nitrogen *supersaturated* ferrite matrix. At this stage no separate VN diffraction spots are observed neither in the X-ray diffraction patterns nor in the electron diffraction patterns. It is concluded that the VN platelets at this stage diffract coherently with the surrounding ferrite matrix. Because of the strong, tetragonally anisotropic misfit between platelet and matrix (see Section 4.1), the coherently diffracting domain, comprising the platelet and the surrounding matrix, can be considered as a b.c.t. “phase” (see Fig. 4.15). Thus it is proposed to describe the X-ray diffraction patterns obtained from specimens

nitrided at 580 °C for nitriding times shorter than 10 h as originating from diffraction from a b.c.t. “phase” (VN platelets plus the surrounding tetragonally distorted ferrite) and a b.c.c. “phase” (cubic ferrite), see Fig. 4.16.

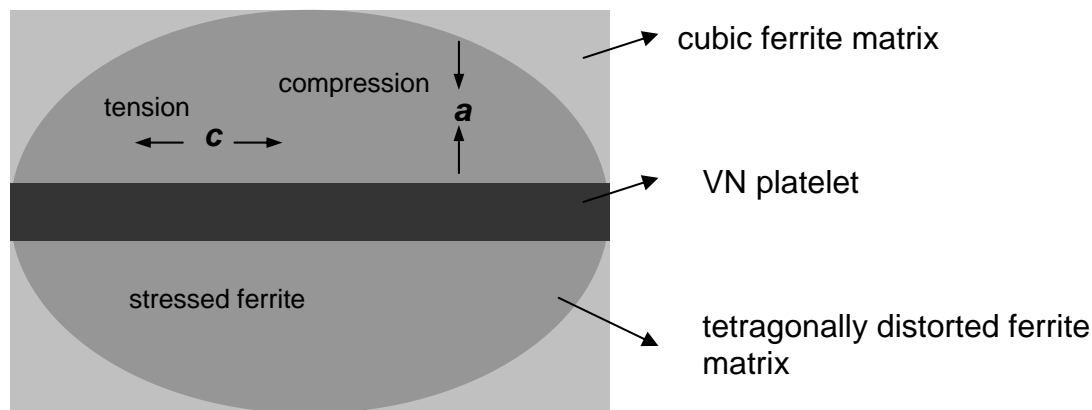


Fig. 4.15: Schematic view of a VN platelet coherent with the surrounding ferritic matrix. Due to the specific misfit between the ferrite and the VN precipitate, there is an expansion in the lattice spacing of ferrite parallel to the platelet and a (corresponding) compression in the perpendicular direction, leading to a tetragonal distortion of the ferrite matrix surrounding the precipitate.

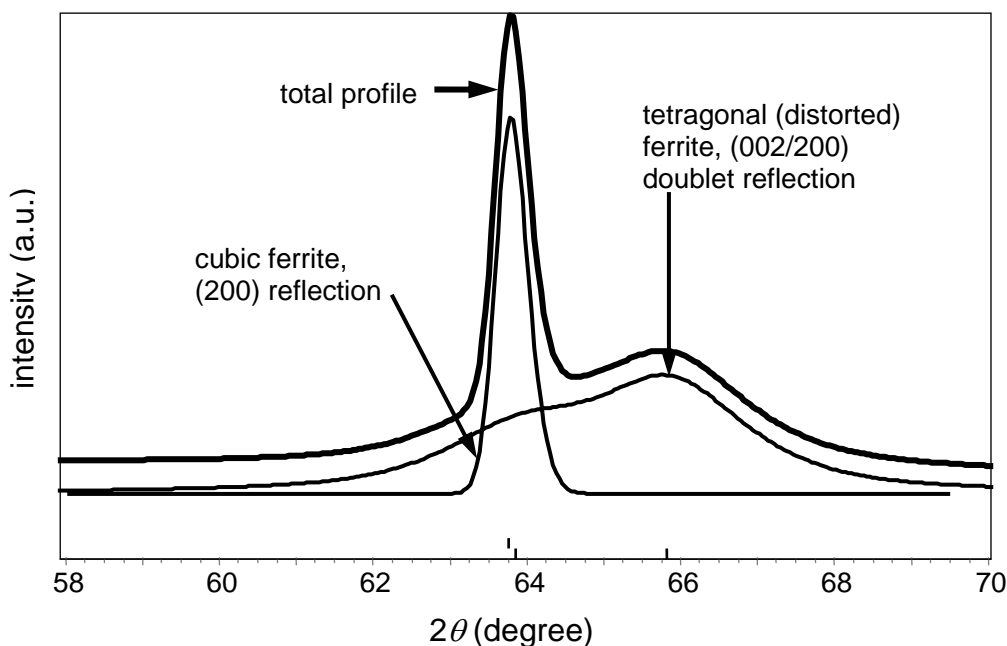


Fig. 4.16: Schematic view of the contributions of the cubic b.c.c. “phase” (cubic ferrite) and the tetragonally distorted b.c.t. “phase” (VN platelet plus surrounding ferrite) to the total diffraction profile.

For specimens nitrided for times longer than 10 h at 580 °C and for nitrided specimens annealed after nitriding at temperatures lower than 680 °C, it followed that part of the VN precipitates diffract incoherently with the matrix (cf. Section 4.3.1.2 and Fig. 4.7). Thus, to simulate the X-ray diffraction patterns it is proposed to conceive the nitrided (and annealed)

microstructure as composed of a b.c.t. “phase” (coherent VN platelets diffracting coherently with the tetragonally distorted surrounding ferrite), a b.c.c “phase” (cubic ferrite) and a f.c.c. phase (incoherently diffracting VN platelets).

For nitrided specimens that were subsequently annealed at temperatures above 680 °C all VN is diffracting incoherently (cf. Section 4.3.1.2 and Fig. 4.11). Thus, to simulate the X-ray diffraction patterns one can depart from a b.c.c. phase (cubic ferrite) and a f.c.c. phase (incoherently diffracting VN platelets).

The fitting of the measured diffraction line profiles on the above basis requires starting values for the lattice parameters. These have been determined as follows. The starting value of the lattice parameter of the cubic ferrite, $a_{\alpha-Fe}$, has been calculated taking into account the dilation produced in the ferrite matrix due to the nitrogen dissolved in the octahedral sites, using equations and data in [20, 21]. The starting value of the lattice parameters of the b.c.t. “phase” (VN platelets + surrounding ferrite) has also been determined from using data for the nitrogen martensite [21].

The starting value of the lattice parameter for the f.c.c. phase (VN) has been determined directly from Ref. [22]. For the specimens that after nitriding were subjected to a denitriding process (see Section 4.2.2), the starting value of the lattice parameter of the b.c.c. phase has been taken as the lattice parameter of unstrained, pure ferrite [22]. Proposing starting values of the lattice parameters for the b.c.t. “phase” in the denitrided specimens is less obvious; sound results were obtained by adopting the same lattice parameters as for the specimens that were only nitrided.

The diffraction profiles were simulated using the software Topas, which is based on the Rietveld method. The input data required to perform the simulation are the lattice parameters and crystalline structure of the phases, the atomic positions and occupancies pertaining to the lattice concerned and the function to simulate the profiles, in this case a Thompson-Cox-Hasting function [23] was employed.

During the simulation the lattice parameters are refined. As a result of the simulation also values of the volume fraction of each phase are obtained.

4.3.4.2 Results of the fitting and discussion

Fitting, on the basis of the model described in Section 4.3.4.1, of calculated diffraction profiles to measured ones gives satisfactory results (see Fig. 4.17).

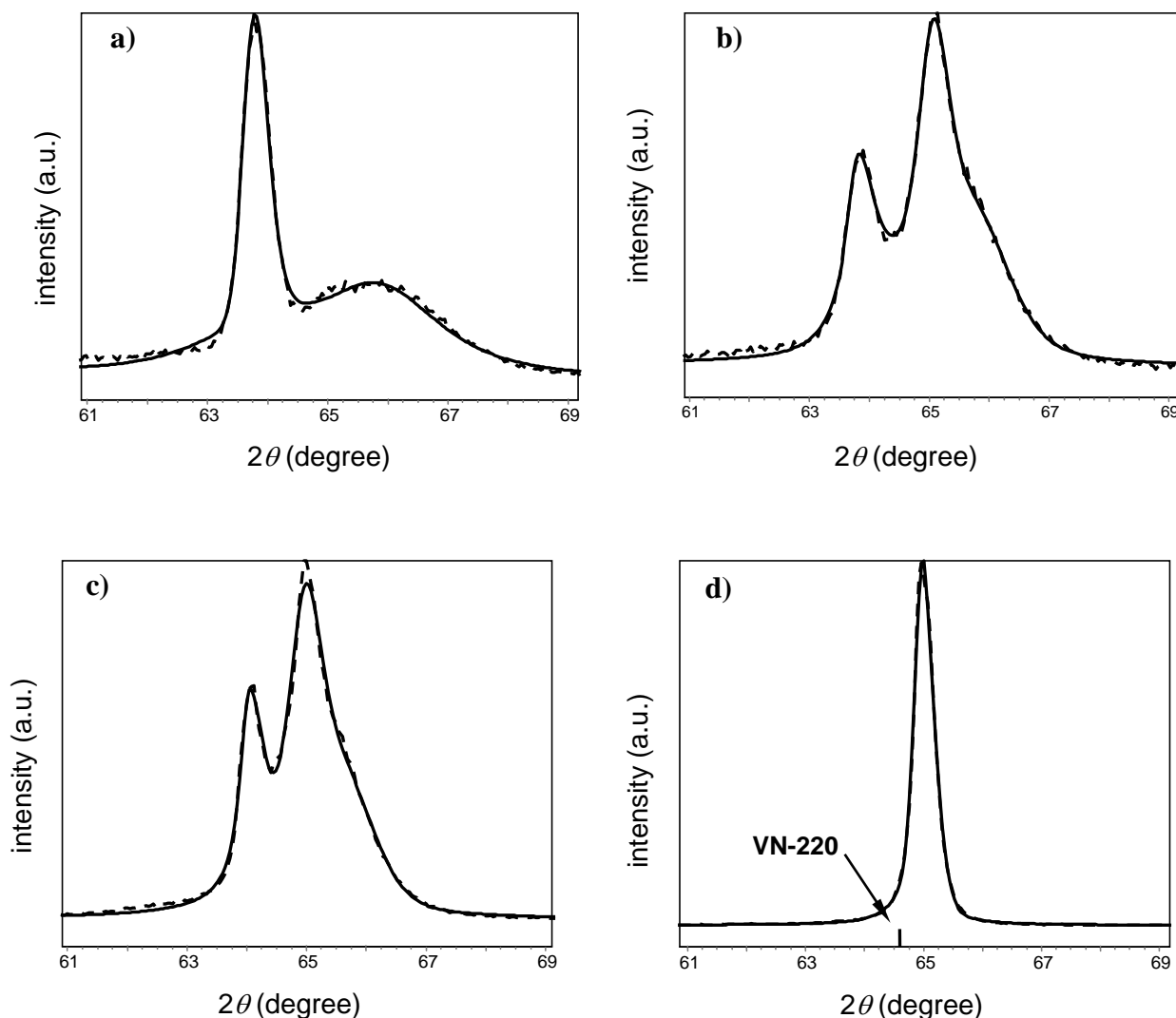


Fig. 4.17: Measured (dashed line) and simulated (full line) X-ray diffraction-line profiles, in the diffraction-angle, 2θ , range around the Fe-200 reflection recorded from specimens of Fe-2.23 at.% V alloy (a) nitrided for 2 hours at 580 °C; (b) nitrided for 66 h at 580 °C; (c) nitrided for 10 hours at 580 °C and subsequently annealed 10 h at 580 °C, again 20h at 580 °C, and subsequently at annealing temperatures increasing from 600 to 640 °C in steps of 20 °C for 20 h each time; (d) nitrided for 10 hours at 580 °C and subsequently annealed 10 h at 580 °C, again 20h at 580 °C, and subsequently at annealing temperatures increasing from 600 to 740 °C in steps of 20 °C for 20 h each time, and finally at 750 °C for 20 h. All specimens were nitrided using a nitriding potential $r_N = 0.104 \text{ atm}^{-1/2}$.

Incoherency of diffraction depends on the length of the diffraction vector (and on the predictability of the distances between the scatterers, i.e. the correlation in the positions of the scatterers); e.g. see Ref. [24]. Hence, the size of the coherently diffracting b.c.t. and b.c.c. domains, as discussed in Section 4.3.4.1, will depend on the reflection considered. Thus, only relative amounts of these “phases”, as determined by fitting to a single reflection, can be meaningfully discussed as function of e.g. aging time.

The ratio of the volume fraction of b.c.t. “phase” to the volume fraction of b.c.c. “phase” for nitriding times not exceeding 10 h at 580 °C (i.e. before the VN phase starts to diffract separately) is, for the Fe-200 reflection, about 3 (see Fig. 4.18). Upon continued coarsening the volume ratio of b.c.t. to b.c.c. decreases: about 1.5 for 48-66 h at 580 °C, which reflects the emergence of a (now) separately diffracting VN phase. Annealing at high temperatures reduces this ratio further, becoming nil for annealing at 700 °C. The volume fraction of VN phase calculated after simulating the diffraction-line profile around the Fe-200 reflection is about 10 %. The expected volume fraction of VN phase for the Fe-2.23 at.% V alloy is approximately 4% (calculated following Ref. [7]). Recognizing that the volume fraction of VN is derived from the integrated intensity of the VN-220 reflection neighbouring the Fe-200 reflection, the difference can be explained as a consequence of the textured ferrite matrix.

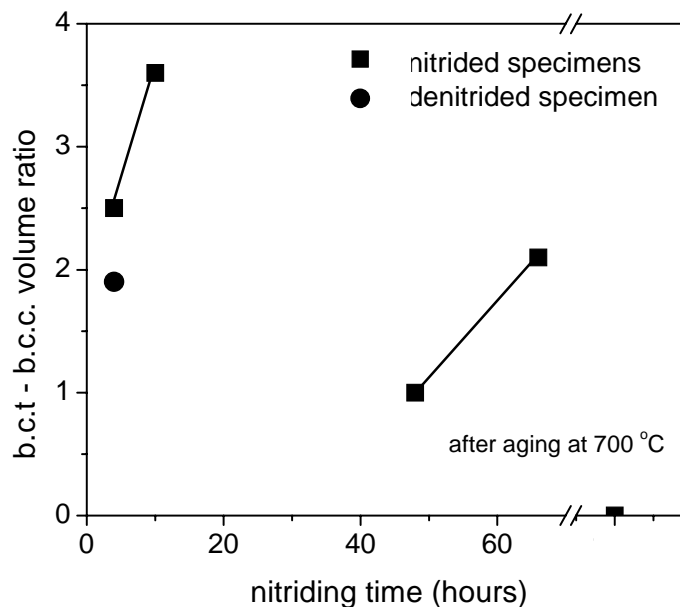


Fig. 4.18: Plot of the b.c.t. – b.c.c. volume ratio for specimens nitrided for 4, 10, 48 and 66 h at 580 °C (squares), for a specimen nitrided for 4 h at 580 °C and subsequently denitrified (full circle) and for a specimen nitrided for 10 h at 580 °C and subsequently annealed 10 h at 580 °C, again 20h at 580 °C, and subsequently at annealing temperatures increasing from 600 to 700 °C in steps of 20 °C for 20 h each time. All specimens were nitrided using a nitriding potential $r_N = 0.104 \text{ atm}^{-1/2}$.

The volume fraction of b.c.t. “phase” is less for denitrified specimens as compared with otherwise similarly treated specimens: e.g. after nitriding for 4 h at 580 °C the b.c.t. - b.c.c. volume ratio is 2.5 for the only nitrided specimen and 1.9 for the nitrided + denitrified specimens (see Fig. 4.18); for explanation see end of Section 4.4.

The diffractograms, for the 2θ range around the Fe-200 reflection, recorded from an unnitrided, annealed specimen, a nitrided specimen (for 4 h at 580 °C) and nitrided (for 4 h at

580 °C) and then denitrated specimen, can be compared in Fig. 4.19; the corresponding lattice parameters have been gathered in Table 4.1.

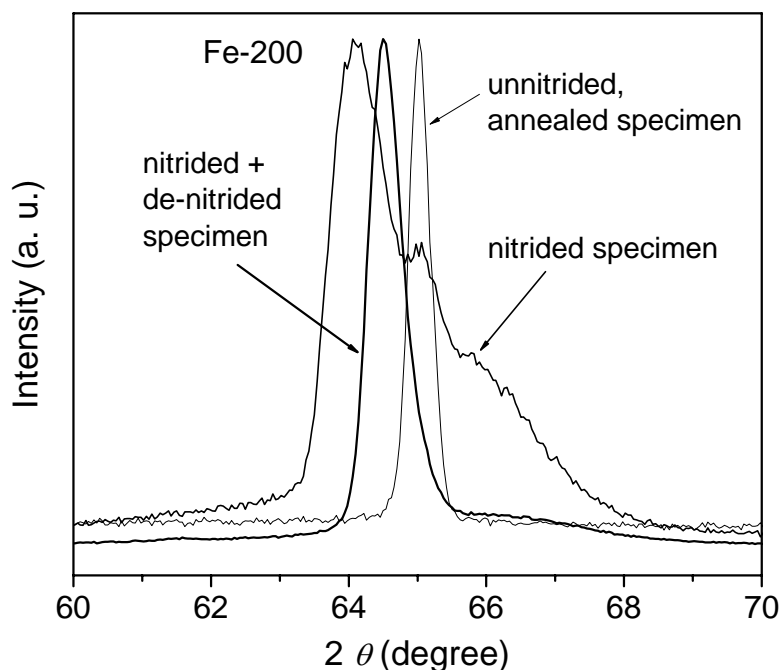


Fig. 4.19: X-ray diffraction-line profiles in the diffraction-angle, 2θ , range around the Fe-200 reflection, recorded from specimens of Fe-2.23 at.% V alloy subjected to different treatments: an annealed, unnitrided specimen; a specimen nitrided for 4 hours at 580 °C and $r_N = 0.104 \text{ atm}^{-1/2}$, and a specimen nitrided for 4 hours at 580 °C and $r_N = 0.104 \text{ atm}^{-1/2}$ and subsequently denitrated for 48 h at 700 °C under H_2 atmosphere. The diffraction-line profiles are normalized with respect to their maximum intensity.

Table 4.1: Lattice parameters, as determined by fitting experimental X-ray diffraction line profiles using the model described in Section 3.4.1, of cubic, α -ferrite and tetragonally distorted ferrite (t -ferrite) corresponding to several specimens of Fe-2.23 at.% alloy: an annealed, unnitrided specimen, a specimen nitrided for 4 h at 580 °C and $r_N = 0.104 \text{ atm}^{-1/2}$ and a specimen nitrided for 4 h at 580 °C and $r_N = 0.104 \text{ atm}^{-1/2}$ and subsequently denitrated during 48 h at 700 °C under H_2 atmosphere.

	unnitrided specimen	nitrided specimen			nitrided + denitrided specimen		
	$a_{\alpha\text{-Fe}}$	$a_{\alpha\text{-Fe}}$	$a_{t\text{-Fe}}$	$c_{t\text{-Fe}}$	$a_{\alpha\text{-Fe}}$	$a_{t\text{-Fe}}$	$c_{t\text{-Fe}}$
lattice parameter (Å)	2.8683	2.9051	2.8615	2.8636	2.8871	2.8351	2.8696

The lattice parameter of the unnitrided, annealed specimen is slightly larger (2.8683 Å) than the equilibrium (stress-free) lattice parameter of pure iron b.c.c. ferrite (2.8665 Å [22], see Table 4.1), which can be ascribed to the presence of dissolved vanadium. Upon nitriding the peak maximum shifts to lower 2θ values (cf. Fig. 4.19), corresponding to an increase of the lattice parameter (see Table 4.1). This increase of lattice parameter can only partly be ascribed to the nitrogen dissolved in the ferrite lattice: according to the model described in Ref. [7], the elastically accommodated misfit of the VN precipitates with the ferrite matrix leads to the introduction of an overall, hydrostatic tensile stress in the matrix, which leads to an overall increase of the lattice parameter of the matrix, i.e. also of the lattice parameter of the cubic ferrite (cf. Section 4.3.4.1). Hence, as long as the misfit between the VN precipitates and the matrix is accommodated elastically, the cubic ferrite indicated in Fig. 4.15 is “distorted” as well. Only if the VN precipitates are incoherent with the matrix (all misfit accommodated plastically, e.g. by dislocations) and diffract separately, the cubic ferrite will have the lattice parameter of pure, stress-free α -Fe, no longer containing dissolved vanadium (2.8665 Å).

Upon denitriding, the ferrite peak shifts to higher 2θ values (see Fig. 4.19), corresponding to, in particular, the removal of dissolved (excess) nitrogen (nitrogen adsorbed at the platelet faces, type II nitrogen, is removed as well by denitriding). The lattice parameter determined for the cubic ferrite is smaller than the lattice parameter determined for the nitrided specimen (see Table 4.1), but larger than the lattice parameter determined for the annealed, unnitrided specimen (see Table 4.1). This demonstrates the occurrence of lattice expansion due to the hydrostatic tensile distortion caused by the misfitting precipitates, as discussed above (as there is no dissolved nitrogen that also leads to lattice expansion).

4.4 General discussion: “sidebands” and coarsening

In the early stages of nitride precipitation, the coherent precipitates may be conceived as part of the matrix crystal lattice. If considerable precipitate/matrix (volume) misfit occurs, such precipitate/matrix lattice integrity can only be realized at the cost of severe lattice deformation at the location of the precipitate and its immediate surroundings. Such strongly distorted regions, comprising the coherent precipitate and its immediate surroundings can diffract coherently and give rise to diffraction profiles which are easily misinterpreted (e.g. as due to diffraction by a new phase [25]).

In the case of the coherent, sub-microscopical VN platelets formed for nitriding times shorter than 10 h at 580 °C, the mismatch between the ferrite matrix and the VN precipitates is

such that the ferrite matrix surrounding the nitride platelets is, strongly anisotropically, tetragonally deformed (Fig. 4.15). This causes in the diffractograms (see Fig. 4.16) the appearance of strongly broadened tetragonal doublets due to coherent diffraction from the coherent platelets and the surrounding matrix. The matrix remote from the precipitates gives rise to the singlet, cubic ferrite reflection (see Fig. 4.16). It follows that the tetragonal doublet, which is strongly broadened, visually gives rise to distinct diffracted intensity at both sides of the much sharper cubic ferrite reflection, which has been described as “sidebands” before in the literature in association with explanations based on spinodal decomposition [9]. As the nitride platelets are oriented in the matrix following the Bain orientation relationship, the sidebands are more easily observed for Fe-(2h 0 0) reflections than for other reflections.

Upon continued nitriding (=aging; as the specimens are through nitrided after 2 h at 580 °C; cf. Section 4.2.2) coarsening occurs relatively slowly. After nitriding for 48 and 66 h at 580 °C a considerable fraction of tetragonally distorted regions, comprising coherent VN platelets and their immediate ferrite surroundings still remains in the specimens, as follows from the fitting of the diffractograms (cf. Fig. 4.17). At this stage VN diffraction profiles are observed in the X-ray diffractograms (see Fig. 4.4) if an appropriate set of tilt and rotation angles is applied to locate a maximum of diffracted VN intensity (recognizing the Bain orientation relationship and the texture of the matrix), which indicates that the volume fraction of the incoherent VN particles is, at this stage, relatively small.

After annealing at relatively high temperatures (680-750 °C) only VN reflections and cubic ferrite matrix reflections are present in the diffractograms. The incoherent platelets are still relatively small and surrounded by distinct strains fields as revealed by the TEM analysis (see Fig. 4.11).

The coarsening process involves in particular that the platelet length increases. The coarsening process occurs in a strained matrix. Thus, upon growth (in particular, lengthening) of a platelet its associated strain field interacts with the strain fields of the neighbouring VN platelets. As a consequence, the growing (lengthening) VN platelets exhibit pronounced deformations as a result of compliance with the strongly varying pronounced microstrains: local bending of lattice planes and dislocations can be observed. The bending and disruptions of the lattice planes in the VN platelets change the local diffraction conditions, leading to the occurrence of regions of strongly different diffracted intensity in a single nitrided platelet, as observed in the bright and (particularly) dark field micrographs (cf. Fig. 4.13b and Section 4.3.2.3).

Coarsening of the VN platelets occurs at lower temperatures for denitrided specimens (cf. Section 4.3.2.2), suggesting that nitrogen plays a role in stabilizing the tetragonally distorted regions in the matrix. Nitrogen atoms occupy preferentially the 2b-type octahedral interstices of the b.c.t. lattice, which are located in the middle of the edges parallel to the c-axis (as these interstices offer a larger volume than the 4c-type octahedral sites). The preferential occupancy of the 2b-type octahedral interstices stabilizes the tetragonal nature of the lattice, i.e. the experienced volume misfit between platelets and the surroundings is smaller than in the absence of dissolved nitrogen. Hence, in the absence of dissolved nitrogen less b.c.t. “phase” occurs (cf. Section 4.3.4.2) and incoherence by coarsening will occur at an earlier stage than with dissolved nitrogen.

4.5 Conclusions

1. Upon nitriding ferritic Fe-2.23 at.% V alloy precipitation of nitride platelets occurs. The platelets have the stoichiometric composition VN (analysis of nitrogen-absorption isotherm) and are oriented with respect to the matrix according to the Bain orientation relationship (TEM). The nitrogen absorbed in the nitrided specimens can be divided in three types: (i) type I nitrogen is strongly bonded to the nitride precipitates; (ii) type II nitrogen is adsorbed at the interface between the nitride platelet and the ferrite matrix; (iii) type III nitrogen is dissolved in the octahedral interstitial sites of the ferrite matrix.
2. Three stages in the development of the VN platelets are observed: (i) For specimens nitrided for times shorter than 10 h at 580 °C, VN platelets are extremely small (5nm length, 1-2 atomic layers thick) and coherent with the surrounding ferrite matrix, which is distorted tetragonally due to the misfit between the VN platelets and the ferrite lattice. For this stage, the X-ray diffraction profiles can be successfully modeled by considering two “phases”: a b.c.c. “phase” for the cubic ferrite and a b.c.t. “phase” comprising the coherent VN platelets and the distorted surrounding ferrite. (ii) For specimens nitrided for times longer than 10 h at 580 °C and specimens nitrided + annealed at annealing temperatures lower than 680°C, some VN platelets have coarsened to the extent that they diffract separately (i.e. independent of the matrix), whereas a considerable amount of VN is still coherent. Consequently three “phases” must be considered for successful modeling of the X-ray diffraction profiles: a b.c.c. “phase” for the cubic ferrite, a

b.c.t. “phase” for the coherent VN platelets and the distorted surrounding ferrite and a f.c.c. phase for the incoherent VN platelets. (iii) For specimens nitrated + annealed at annealing temperatures higher than 680°C the VN precipitates are incoherent and in this case two phases are considered for successful modeling of the X-ray diffraction profile: a b.c.c. phase for the cubic ferrite and a f.c.c. phase for the incoherent VN platelet. The b.c.c. “phase” in stages (i) and (ii) is subjected to the hydrostatic tensile stress component due to misfit between the precipitates and the matrix. The b.c.c. phase in stage (iii) can be considered as undistorted.

3. “Sidebands”, formerly ascribed to e.g. spinodal decomposition, can now be explained as due to the coherent diffraction by the system composed of coherent VN platelets and their tetragonally distorted ferrite surroundings.
4. Coarsening, in particular lengthening, of the VN platelets occurs in strong and strongly varying surrounding strains fields, which leads to local bending of the lattice planes and disruptions of the lattice integrity (dislocations) in the VN precipitates. As a consequence, strong variations are observed in the diffracted intensity in diffraction-contrast images of single platelets. Denitrating (= removal of nitrogen dissolved in the ferrite matrix) accelerates the coarsening, i.e. coarsening occurs already at lower annealing temperatures, because nitrogen dissolved in the 2b octahedral interstitial sites of the b.c.t. lattice stabilizes the tetragonal nature of the lattice; in the presence of dissolved nitrogen the volume misfit between the VN platelets and the surrounding ferrite matrix is smaller than in the absence of dissolved nitrogen.

Aknowledgments

The authors wish to thank Mr. J. Köhler and Mr. P. Kress for assistance with the nitriding experiments, Mr. W. Sigle for assistance during the first stage of the TEM characterization of the specimens and Mr. F. Phillipp for assistance during the HRTEM analysis.

References

- [1] ASM Handbook, volume 4, ASM International, Metals Park, Ohio (1991).

- [2] D. Liedtke: Wärmebehandlung von Eisenwerkstoffen. Nitrieren und Nitrocarburieren, Expert Verlag, Renningen (2006).
- [3] E.J. Mittemeijer (Ed): Mat. Sci. Forum 102-104 (1992) 223.
- [4] K.H. Jack, in: Proc. Conf. on Heat Treatment, The Metals Society, London (1975) 39.
- [5] B.J. Lightfoot, D.H. Jack, in: Proc. Conf. on Heat Treatment, The Metals Society, London (1975) 59.
- [6] E.J. Mittemeijer: J. Heat Treat. 3 (1983) 114.
- [7] M.A.J. Somers, R.M. Lankreijer, E.J. Mittemeijer: Phil. Mag. A 59 (1989) 353.
- [8] D.S. Rickerby, S. Henderson, A. Hendry, K.H. Jack: Acta Metall. 34 (1986) 1687.
- [9] D.H. Jack: Acta Metall. 24 (1976) 137.
- [10] D.S. Rickerby, A. Hendry, K.H. Jack: Acta Metall. 34 (1986) 1925.
- [11] T.C. Bor, A.T.W. Kempen, F.D. Tichelaar, E.J. Mittemeijer, E. van der Giessen: Phil. Mag. A 82 (2002) 971.
- [12] M. Gouné, T. Belmonte, A. Redjaimia, P. Weisbecker, J.M. Fiorani, H. Michel: Mat. Sci. Eng. A 351 (2003) 23.
- [13] S.S. Hosmani, R.E. Schacherl, E.J. Mittemeijer: Acta Mater. 35 (2005) 2069.
- [14] M. Sennour, P.H. Jouneau, C. Esnouf: J. Mat. Sci. 39 (2004) 4521.
- [15] M.H. Biglari, C.M. Brakman, E.J. Mittemeijer, S. van der Zwaag: Phil. Mag. A 72 (1995) 931.
- [16] S.S. Hosmani, R.E. Schacherl, E.J. Mittemeijer: Acta Mater. 54 (2006) 2783.
- [17] P.M. Hekker, H.C.F. Rozendaal, E.J. Mittemeijer: J. Mat. Sci. 20 (1985) 718.
- [18] M.H. Biglari, C.M. Brakman, E.J. Mittemeijer: Phil. Mag. A 72 (1995) 1281.
- [19] E.J. Mittemeijer, J.T. Slycke: Surf. Eng. 12 (1996) 152.
- [20] E.J. Mittemeijer, M.A.J. Somers: Surf. Eng. 13 (1997) 483.
- [21] L. Cheng, A. Böttger, Th.H. de Keijser, E.J. Mittemeijer: Scripta Metall. et Mater. 24 (1990) 509.
- [22] P. Villars (Ed.): Pearson's Handbook. Desk edition. Crystallographic data for intermetallic phases. ASM International, Metals Park, Ohio (1997).
- [23] P. Thompson, D.E. Cox, J.B. Hastings: J. Appl. Cryst. 20 (1987) 79.
- [24] J.G.M. van Berkum, R. Delhez, Th.H. de Keijser, E.J. Mittemeijer: Acta Cryst. A, 52 (1996) 730.
- [25] C.R. Houska: Acta Cryst. A 49 (1993) 771.

Chapter 5

Zusammenfassung

5.1 Einleitung

Das Nitrieren stellt ein wichtiges thermochemisches Oberflächenbehandlungsverfahren von Eisenbasislegierungen, zur Verbesserung des Ermüdungsverhaltens, der mechanischen Eigenschaften und der Korrosionsbeständigkeit von Bauteilen dar. Eines der wichtigsten Verfahren zur Nitrierung von Eisenbasislegierungen ist das Gasnitrieren. Beim Gasnitrieren wird die Probe in einer NH_3 / H_2 Atmosphäre wärmebehandelt, wodurch Stickstoff in die Probe eindiffundiert und sich eine Nitrierschicht an der Probenoberfläche ausbildet. In Abhängigkeit des NH_3 Anteils in der Atmosphäre und der Prozesstemperatur kann die Nitrierschicht aus einer Verbindungsschicht, bestehend aus Eisennitriden an der Probenoberfläche, und einer darunter liegenden Diffusionszone (Stickstoff gelöst auf Oktaederlücken des Ferritgitters) zusammengesetzt sein. Bei Anwesenheit von Legierungselementen M mit einer Affinität gegenüber Stickstoff (M: Ti, Al, V, Cr) können sich MN_x Nitride in der Diffusionszone ausscheiden.

Im Anfangsstadium bilden sich Nitride mit einer Kohärenten Grenzfläche zur umgebenden Eisenmatrix aus. Dies bewirkt eine relativ hohe Härte, hervorgerufen durch Spannungsfelder in der Umgebung der Nitridausscheidungen. Die Spannungsfelder werden durch die Fehlpassung zwischen MN_x Ausscheidungen und der Ferritmatrix hervorgerufen, was eine starke Behinderung von Versetzungsbewegungen zur Folge hat. Mit fortschreitender Nitrierdauer findet eine Vergrößerung, kombiniert mit dem Verlust der Kohärenz, der Ausscheidungen statt. Dies führt zu einer Reduzierung der Spannungsfelder und dem Granzflächenanteil, sowie zum Verlust der Übersättigung von Stickstoff. Die Vergrößerung erfolgt durch 2 Mechanismen: (i) Bei „kontinuierliche Vergrößerung“ erfolgt das Wachstum von relativ großen Ausscheidungen auf Kosten kleinerer Ausscheidungen; (ii) „Diskontinuierliche Vergrößerung“ beinhaltet die Bildung einer lamellaren Mikrostruktur, bestehend aus Ferrit und MN_x Lamellen.

Eine erhöhte Stickstofflöslichkeit in Nitrierschichten von Fe-M Legierungen kann reproduzierbar nachgewiesen werden. Dieser erhöhte Stickstoffanteil wird als Überschusstickstoff bezeichnet. Überschusstickstoff bezeichnet dabei die Differenz zwischen der ermittelten Gesamtstickstoffkonzentration und der normalen Stickstoffaufnahmekapazität der Nitrierschicht. Die Normale Kapazität setzt sich aus 2

Beiträgen zusammen: (i) Auf den Oktaederlücken von spannungsfreiem Ferrit gelöster Stickstoff; (ii) Stickstoff gebunden in den ausgeschiedenen Nitriden. Überschussstickstoff kann in 3 Kategorien unterteilt werden: (i) Stickstoff gebunden an Versetzungen. (ii) An der Grenzfläche Ausscheidung / Matrix adsorbierter Stickstoff, (iii) auf den Oktaederlücken der Ferrit Matrix überschüssig gelöster Stickstoff.

Diffusionszonen von Nitrierschichten in Fe-M Legierungen weisen deutliche Eigenspannungen auf. Eigenspannungen können durch Änderungen in der Zusammensetzung, thermische Effekte, Gitterdefekte und / oder Ausscheidungsreaktionen verursacht werden. Eigenspannungen haben einen sehr großen Einfluss auf die mechanischen Eigenschaften nitrierter Proben. Dies gilt insbesondere für die Ermüdungseigenschaften: Die Anwesenheit von Druckeigenspannungen parallel zur Probenoberfläche wirkt der Rissbildung und dem Risswachstum entgegen.

5.2 Experimentelles

Eisen-Chrom (4, 8, 13 und 20 Gew. %) und Eisen-Vanad (2 Gew.%) Legierungen wurden aus reinen Fe (99,98 Gew. %) und reinen Cr (99,999 Gew. %) bzw. reinen V (99,98 Gew. %) in einem Induktionsofen hergestellt.

Die Legierungen wurden nach dem Abgießen zu Blechen gewalzt: die Eisen-Chrom Legierung wurden zu einer Dicke von 1,2 mm und die Eisen-Vanad Legierung zu einer Dicke von 0,2 mm gewalzt. Anschließend wurden die Bleche in rechteckige Probenstücke ($2 \times 1 \text{ mm}^2$ für Eisen-Chrom Legierungen, $2 \times 2 \text{ mm}^2$ für Eisen-Vanad Legierung) geschnitten. Die Proben aus den Eisen-Chrom Legierungen wurden zu einer Enddicke von 1 mm gefräst. Die Proben wurden unter Schutzgas (Argon mit einer Reinheit von 99,999 vol. %) bei 700 °C für zwei Stunden rekristallisiert.

Vor dem Nitrieren wurden die Proben geschliffen, poliert (letzte Stufe mit 1 μm Diamantsuspension) und im Ultraschallbad gereinigt.

Das Nitrierverfahren wurde in einem vertikal angeordneten Mehrzonenofen unter einem Ammoniak/Wasserstoff Gasstrom durchgeführt. Die Stickstoffaufnahme an der Probeoberfläche hängt vom Ammoniakanteil in der Nitrieratmosphäre ab. Der ammoniakanteil kann über das Verhältnis der Strömungsgeschwindigkeiten von Ammoniak und Wasserstoff geregelt werden. Die Regelung der Gasströme erfolgt durch „Mass Flow-Controller“. Am Ende der Nitrierung wurden die Proben in Wasser abgeschreckt.

Die Mikrostruktur der nitrierten Schichten wurden durch Licht-Elektronen-Mikroskopie, Härtemessungen und Röntgendiffraktometrie untersucht. Die Zusammensetzung der Nitrierschichten wurde mittels Elektronstrahlmikroanalyse bestimmt. Die Messungen von Eigenspannungen in Eisen-Chrom Legierungen wurden mittels Röntgendiffraktometrie durchgeführt.

5.3 Ergebnisse und Diskussion

5.3.1 Mikrostruktur der Nitrierschicht von Fe-Cr Legierungen

Nach dem Nitrieren von Fe-Cr Legierungen mit unterschiedlichen Chromkonzentrationen konnten in Abhängigkeit der Konzentration zwei unterschiedliche Mikrostrukturarten festgestellt werden.

1. Mikrostruktur 1 setzt sich aus dunklen Körnern im Bereich der Probenoberfläche und aus hellen Körnern in dem darunterliegenden Bereich der Nitrierschicht zusammen, und tritt bei Fe-Cr Legierungen mit einem Cr Gehalt zwischen 4 und 8 Gew.% Cr auf. Die dunklen Körner weisen eine lamellare Mikrostruktur, bestehend aus Ferrit und CrN Lamellen, auf. In diesem Bereich wurde das ursprünglich aus submikroskopisch kleinen kohärenten / teilkohärenten Ausscheidungen bestehende Gefüge durch die gröbere lamellare Morphologie ersetzt. Die hellen Körner weisen kohärente / teilkohärente submikroskopische Ausscheidungen auf.
2. Mikrostruktur 2 besteht ausschließlich aus der vergrößerten lamellaren Morphologie. Diese Mikrostruktur tritt bei Nitrierschichten von Fe-Cr Legierungen mit einem Cr Anteil zwischen 13 und 20 Gew.% Cr auf.

Für Beide Mikrostrukturen konnte eine Abhängigkeit der Lamellenabstände und Koloniegröße von der Schichttiefe festgestellt werden. Im Bereich der Probenoberfläche treten größere Kolonien und Lamellenabstände als an der Grenzfläche zwischen Nitrierschicht und nicht nitriertem Kern auf. Am deutlichsten tritt dieser Effekt bei Proben mit relativ hohen Cr Gehalten auf.

Härtetiefenprofile nitrierter Fe-Cr Legierungen mit Cr Konzentrationen zwischen 4 und 8 Gew.% Cr zeigen relativ geringe Härtewerte für die diskontinuierliche vergrößerten Bereiche an der Probenoberfläche, wohingegen in den darunterliegenden Schichten mit submikroskopisch kleinen Ausscheidungen deutlich höhere Härtewerte auftreten (siehe Abb.

5.2a). Die Härtetiefenprofile nitrierter Fe-Cr Legierungen mit Cr Konzentrationen zwischen 13 und 20 Gew.% Cr weisen einen Abfall der Härte von der Probenoberfläche bis zur Grenzfläche Nitrierschicht / nicht nitrierter Kern der Probe (siehe Abb. 5.2b). Parallel dazu nimmt auch die Stickstoffkonzentration von der Probenoberfläche zur Grenzfläche der Nitrierschicht ab.

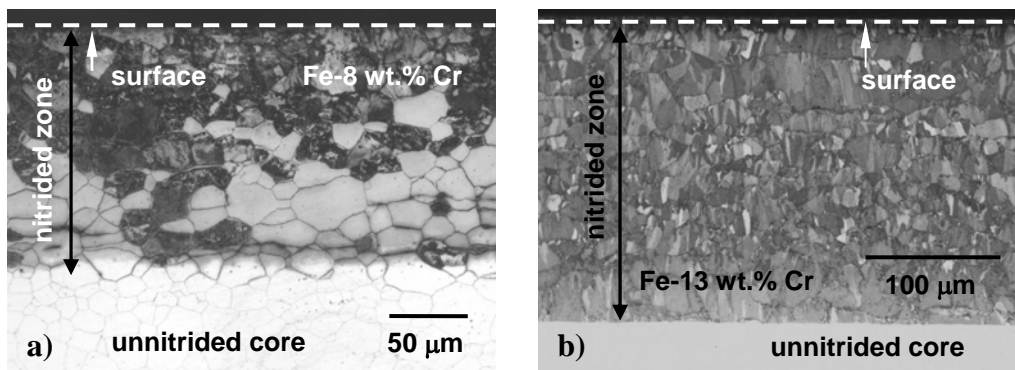


Abb. 5.1: Morphologie der Nitrierschichten von Fe-Cr Legierungen. (a) Lichtmikroskopische Aufnahme der Nitrierschicht einer Fe-8 Gew.% Cr Legierung (Nitrierdauer: 6 h), bestehend aus einer vergrößerten Morphologie im Bereich der Probenoberfläche und dem darunterliegenden Bereich mit submikroskopische Ausscheidungen. (b) Lichtmikroskopische Aufnahme der Nitrierschicht einer Fe-13 Gew.% Cr Legierung (Nitrierdauer: 6 h), bestehend aus einer komplett vergrößerte lamellaren Mikrostruktur.

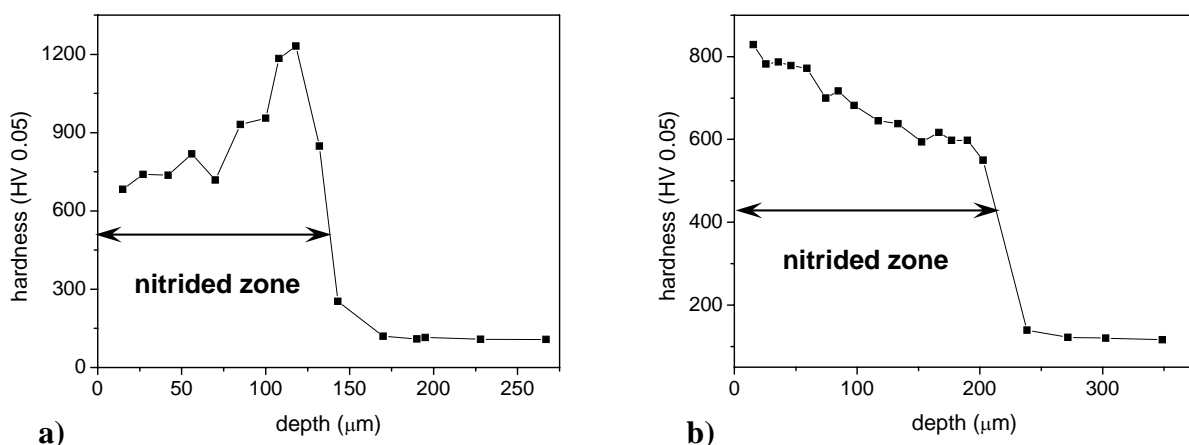


Abb. 5.2: (a) Härtetiefenprofil der Nitrierschicht einer Fe-8 Gew.% Cr Legierung (Nitrierzeit: 6 h). Wie unter 5.3.1. beschrieben setzt sich die betrachtete Nitrierschicht aus Mikrostruktur 1 und 2 zusammen. (b) Härtetiefenprofil der Nitrierschicht einer Fe-13 Gew.% Cr Legierung (Nitrierzeit: 24 h). Die Nitrierschicht besteht in diesem Fall ausschließlich aus einer diskontinuierlich vergrößerten Mikrostruktur. Beide Proben wurden unter einem Nitrierpotential von $r_N = 0.104 \text{ atm}^{-1/2}$ bei einer Nitrieretemperatur von 580 °C nitriert.

5.3.2 Der Einfluss des Cr Gehaltes und des Überschussstickstoffes auf die Mikrostruktur der Nitrierschichten in Fe-Cr Legierungen

Die Morphologie der Nitrierschichten von Fe-Cr Legierungen wird von 2 Prozessen beeinflusst: (1) das Wachstum der Nitrierschicht sowie (2) dem Wachstum der diskontinuierlich vergrößerten Region. Bei Fe-Cr Legierungen mit relativ geringen Cr Konzentrationen kann das Wachstum der Nitrierschicht schneller ablaufen als der diskontinuierliche Vergrößerungsprozess. Daher setzt sich die Nitrierschicht dieser Legierungen aus einer diskontinuierlich umgewandelten Mikrostruktur im Bereich der Oberfläche und einer darunter liegenden Schicht mit kohärenten submikroskopischen CrN Ausscheidungen zusammen. Mit höheren Cr Anteilen in der Legierung verringert sich die Wachstumsgeschwindigkeit der Nitrierschicht. Erreicht die Cr Konzentration einen bestimmten Wert ist die Wachstumsgeschwindigkeit der Nitrierschicht geringer oder gleich der Wachstumsgeschwindigkeit der diskontinuierlich vergrößerten Zone. Dies hat zur Folge, dass die Nitrierschichten komplett aus der diskontinuierlich vergrößerten Mikrostruktur bestehen. Des weiteren nimmt die Stickstoffübersättigung in der Nitrierschicht mit steigendem Cr Gehalt zu.

Die Triebkraft des diskontinuierlichen Vergrößerungsprozesses nimmt mit steigender Stickstoffübersättigung zu, wodurch die diskontinuierliche Vergrößerung der CrN Ausscheidungen begünstigt wird. Da die Stickstoffübersättigung an der Probenoberfläche am größten ist bilden sich in diesem Bereich die meisten Keime zur Bildung der lamellaren Ausscheidungskolonien, wodurch kleinere Lamellen und Kolonien entstehen. Dies hat zur Folge, dass die Lamellen- und Koloniegröße in richtung Grenzfläche Nitrierschicht / nicht nitrierter Kern größer wird. In Abb. 5.3 ist dieses Verhalten schematisch dargestellt.

5.3.3 Einfluss der Mikrostruktur nitrierter Schichten in Fe-Cr Legierungen auf die Eigenspannungen

Zur Untersuchung des Einflusses der Mikrostruktur auf die Eigenspannungen wurden Spannungstiefenprofile erstellt. Für Fe-Cr Legierungen mit einer Cr Konzentration zwischen 4 und 8 Gew.% Cr hat sich dabei der folgende Zusammenhang zwischen Mikrostruktur und Eigenspannung in der Anfangsphase des Nitrierens herausgestellt: Oberhalb der Grenzfläche Nitrierschicht / nicht nitrierter Kern sind überwiegend Kompressionsspannungen vorhanden. Die Mikrostruktur besteht in diesem Bereich im Wesentlichen aus kohärenten oder

teilkohärenten submikroskopischen CrN Ausscheidungen. In den darüber liegenden Schichten tritt vor allem die diskontinuierlich vergrößerte Morphologie auf. In diesem Bereich werden überwiegend Zugrestspannungen beobachtet.

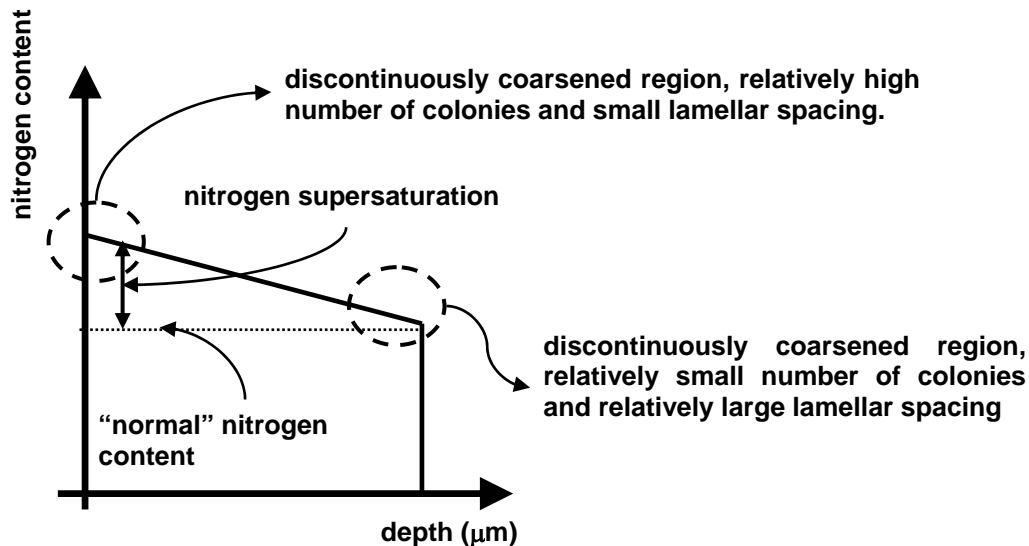


Abb. 5.3: Schematische Darstellung des Stickstoff – Konzentrations- Tiefenprofils der Nitrierschicht einer Hoch Cr haltigen Legierung mit Beschreibung der auftretenden Lamellen- und Koloniegröße bei der jeweiligen Schichttiefe.

Bei Fortführung des Nitrierprozesses treten komplexere Restspannungstiefenprofile auf (siehe Abb. 5.4). Zur Erklärung dieser Profile wird das Folgende Modell, für die Nitrierschichten von Fe-Cr Legierungen mit ein Cr Anteil < 13 Gew.% Cr, eingeführt:

- a. Im Anfangsstadium der Nitrierung bilden sich zunächst kohärente oder teilkohärente CrN Ausscheidungen. Aufgrund der Fehlpassung zwischen Ausscheidungen und der umgebenden Matrix besteht die Tendenz der lateralen Ausdehnung dieser Schicht. Der angrenzende nicht nitrierte Kern der Probe wirkt diesem bestreben entgegen, wodurch Kompressionsspannungen in der Schicht hervorgerufen werden.
- b. Durch die diskontinuierliche Vergrößerung werden die kohärenten submikroskopischen Ausscheidungen durch inkohärenten CrN Lamellen ersetzt. Durch den Verlust der Kohärenz an den Grenzflächen tritt eine Relaxation der Kompressionsspannungen in der Schicht auf. Dieser Effekt kommt insbesondere an der Probenoberfläche zum Tragen, da sich die Schicht hier senkrecht zur freien Oberfläche ausdehnen kann. Entsprechend können in tieferen Schichten noch Kompressionsspannungen auftreten. Parallel werden mit dem Wachstum der Nitrierschicht neue Ausscheidungen mit kohärentem Charakter entstehen. Daher werden in diesem Bereich, wie unter a. geschildert, erneut Kompressionsspannungen

auftreten. Damit das mechanische Gleichgewicht erhalten bleibt hat dies die Folgenden 2 Reaktionen zur Folge: (i) Im Bereich der Probenoberfläche treten Restspannungen mit Zugcharakter auf und (ii) an der Grenzfläche Nitrierschicht / nicht nitrierter Kern treten im nicht nitrierten Teil ebenfalls Restspannungen mit Zugcharakter auf.

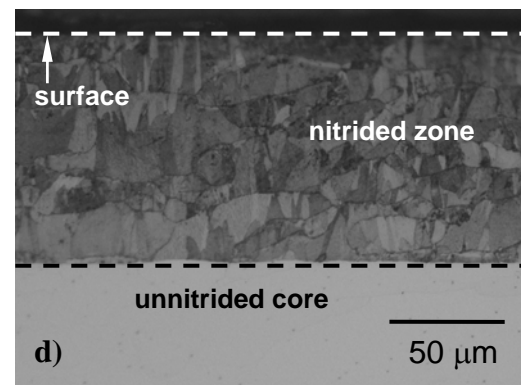
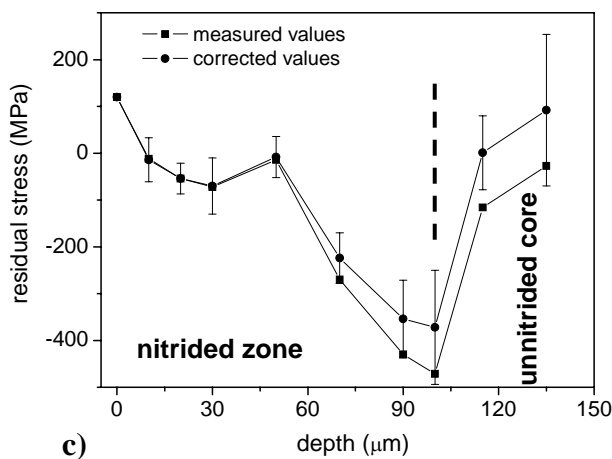
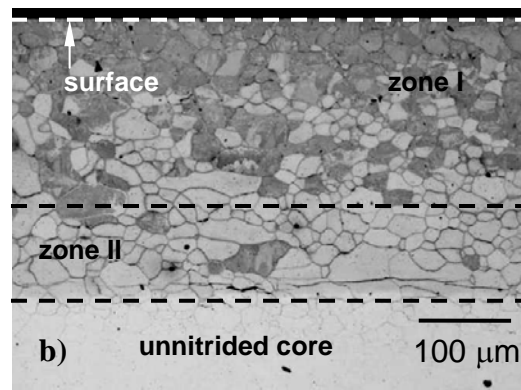
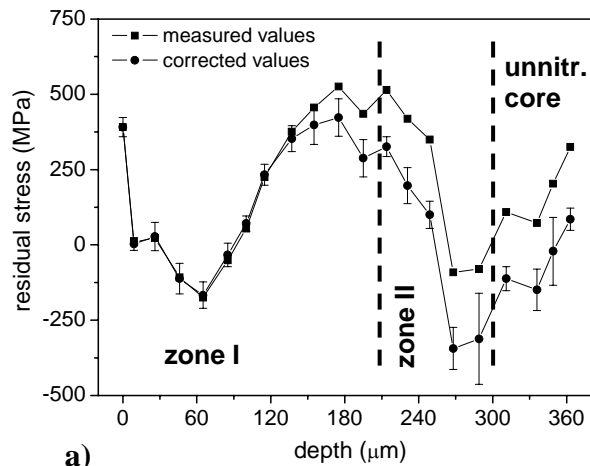


Abb 5.4: (a) Restspannungstiefenprofil der Nitrierschicht einer Fe-8 Gew.% Cr Legierung (Nitrierdauer 24 h). (b) Lichtmikroskopische Aufnahme des Querschnitts der unter (a) beschriebenen Nitrierschicht, wobei Zone I und II den Bereichen mit diskontinuierlich Vergrößerter Mikrostruktur und die Schicht mit kohärenten submikroskopischen Ausscheidungen entsprechen. (c) Restspannungstiefenprofil der Nitrierschicht einer Fe-13 Gew.% Cr Legierung (Nitrierdauer 6 h). (d) Lichtmikroskopische Aufnahme des Querschnitts der unter (c) beschriebenen Nitrierschicht, wobei in diesem Fall die komplette Nitrierschicht aus der diskontinuierlich vergrößerten Morphologie besteht.

Auf Basis des entworfenen Modells können Restspannungstiefenprofile von Nitrierschichten, bestehend aus diskontinuierlich vergrößerten Regionen (siehe Zone I in Abb. 5.4b) und Bereichen mit submikroskopisch kohärenten Ausscheidungen (siehe Zone II in Abb. 5.4b) diskutiert werden. Bei fortschreitender Nitrierdauer tritt im Bereich von Zone II eine Kompensation der vorhandenen Kompressionsspannungen auf. Diese Kompensation

wird durch die Zugspannungen an den Grenzflächen zu Zone I und zum nicht nitrierten Kern verursacht.

Wie schon unter Punkt (b) diskutiert tritt eine Relaxation der Kompressionsspannung, bedingt durch diskontinuierliche Vergrößerung auf. Die Relaxation kann dabei besonders leicht an der Probenoberfläche ablaufen. Dieser Sachverhalt gilt auch für Nitrierschichten von Fe-Cr Legierungen mit einem relativ hohen Cr Gehalt (siehe Abb. 5.4c und 5.4d). An der Probenoberfläche stellt sich ein Spannungszustand mit Zugcharakter ein, während in tieferen Schichten Druckspannungsfelder beobachtet werden können. Diese Druckspannungen sind im Vergleich zu den Proben mit einer kohärent submikroskopischen Ausscheidungsstruktur wesentlich größer.

5.3.4 Nitridausscheidungen und Ausscheidungsvergrößerungen in Fe-2 Gew. % V Legierungen

Beim Nitrieren von Fe-2 Gew.% V Legierungen entstehen Vanadiumnitrid Plättchen in der Nitrierschicht. Die Plättchen haben die stöchiometrische Zusammensetzung VN und sind im Bezug zur Ferritmatrix gemäß der Bain Orientierung ausgerichtet (siehe Abb. 5.5). Der in der Nitrierschicht aufgenommene Stickstoff kann in drei Kategorien unterteilt werden: (i) Stickstoff gebunden in den VN Ausscheidungen, (ii) absorbiert an der Grenzfläche zwischen den VN Plättchen und der Matrix, (iii) Stickstoff gelöst auf den Oktaederlücken der Ferritmatrix.

Der Ausscheidungsvorgang der VN Plättchen kann in drei Fälle eingeteilt werden: (i) Bei Nitrierzeiten kleiner als 10 h und einer Nitriertemperatur von 580°C treten sehr kleine (5 nm entspricht 1-2 Atomlagen) kohärente Ausscheidungen auf. Durch die kohärente Grenzfläche erfährt die umgebende Eisenmatrix eine starke tetragonale Verzerrung, was sich durch das Auftreten von so genannten „Sidebands“ in den Röntgendiffraktogrammen äußert. Diese können unter Berücksichtigung eines tetragonal verzerrten Anteiles in der Eisenmatrix modelliert werden. (ii) Für Nitrierzeiten größer als 10 h und einer Nitriertemperatur von 580°C sowie einer Glühbehandlung (Temperatur unter 680°C) im Anschluss, können sowohl feine kohärente Ausscheidungen als auch vergrößerte Ausscheidungen beobachtet werden. Dies äußert sich in den Röntgendiffraktogrammen durch das Auftreten von separaten VN Reflexen. Zur Modellierung des gemessenen Röntgendiffraktogrammes muß daher die Präsenz der Folgenden „Phasen“ in der Nitrierschicht angenommen werden: Kubischer Ferrit, tetragonal verzerrter Ferrit sowie kohärente VN Ausscheidungen. (iii) Für nitrierten Proben,

welche zusätzlich bei Temperaturen $> 680^\circ\text{C}$ Wärmebehandelt wurden, treten nur noch inkohärente VN Nitridausscheidungen in der Nitrierschicht auf. Zur Modellierung der gemessenen Röntgendiffraktogramme wurde daher die Präsenz von separaten VN Ausscheidungen in der Eisenmatrix angenommen. In allen drei geschilderten Fällen konnten die gemessenen Diffraktogramme erfolgreich modelliert werden. Die kubisch raumzentrierte Phase der Eisenmatrix kann in den Fällen (i) und (ii) einem hydrostatischen Spannungsfeld zugeordnet werden, hervorgerufen durch die Fehlpassung zwischen den Ausscheidungen und der Eisenmatrix. Im Fall (iii) ist die Eisenmatrix spannungsfrei. Das Auftreten von „Sidebands“ wurde bislang spinodalen Entmischungsvorgängen zugeschrieben. Die vorliegenden Ergebnisse zeigen, dass „Sidebands“ durch die kohärente Diffraktion an VN Ausscheidungen in einer tetragonal verzerrten Eisenmatrix verursacht sein können.

Vergrößerung, speziell das Wachstum der VN Ausscheidungen in die Länge, tritt in starken und sich stark verändernden Spannungsfelder auf. Dies führt lokal zu Krümmungen der Netzebenen und dem auftreten von Versetzungen in den VN Ausscheidungen. Als Folge treten deutliche Intensitätsschwankungen in Beugungskontrastbildern der VN Ausscheidungen auf. Denitrieren beschleunigt den Vergrößerungsprozess bzw. erfolgt schon bei relativ geringeren Temperaturen, da gelöster Stickstoff auf den 2b Plätzen der Eisenmatrix die tragonale Verzerrung stabilisiert. Im Vergleich zu einer Eisenmatrix ohne gelöstem Stickstoff auf den Zwischengitterplätzen ist die Volumenfehlpassung mit gelöstem Stickstoff zwischen Matrix und Ausscheidung geringer.

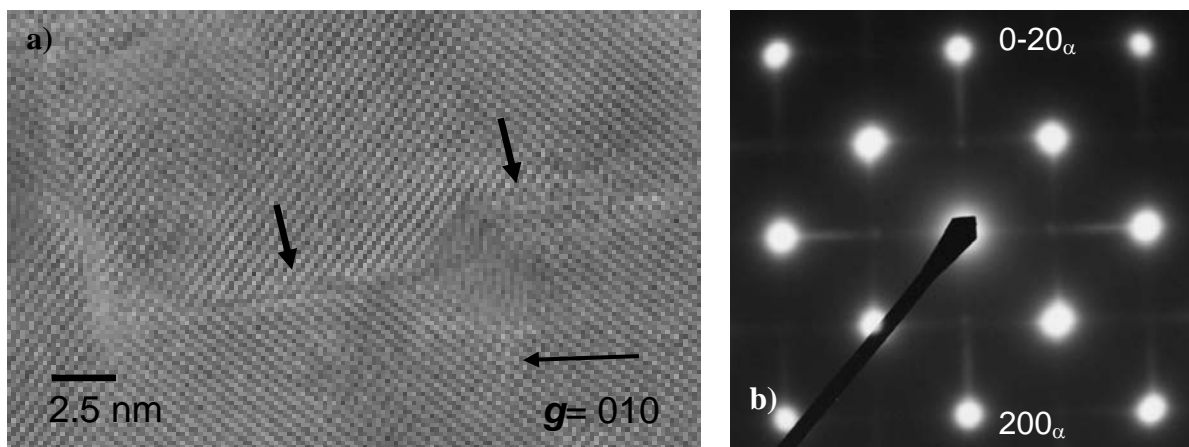


Abb. 5.5: HRTEM Untersuchung einer Fe-2.23 at. % V Legierung nitriert bei einer Temperatur von 580°C und einer Nitrierkennzahl von $r_N = 0.104 \text{ atm}^{-1/2}$ für 10 h. Die Einstrahlrichtung des Elektronenstrahles ist $[001]_{\alpha\text{-Fe}}$. (a) HRTEM Aufnahme von kohärenten VN Plättchen mit einer Bain Orientierung bezüglich der Eisenmatrix (siehe Pfeile in der Abbildung). Die Plättchen weisen eine Länge von ca. 5 nm und eine Dicke von ca. 1-2 Monolagen auf. (b) Im Beugungsbild zu Abbildung (a) treten „streaks“ entlang der $\langle 100 \rangle_{\alpha\text{-Fe}}$ Richtungen aber keine VN Reflexe auf.

Curriculum Vitae

Nicolás Vives Díaz

born on January 7th 1979 in Rosario, Argentina

School:

1985-1991 Primary school: Colegio La Salle, Rosario, Argentina
1992-1996 High school: Instituto Politécnico Superior “Gral. San Martín”,
Rosario, Argentina

Academic studies:

1997-1999 National University of Rosario, Rosario, Argentina
Faculty of Sciences, Engineering and Surveying
Study of Electronic Engineering

1999-2003 National University of Gral. San Martín, San Martín, Argentina
Institute of Technology “Prof. Jorge Sabato”
Study of Materials Engineering

2003 Institute of Technology “Prof. Jorge Sabato” and University of Buenos
Aires, Buenos Aires, Argentina
Diploma thesis: *Structural characterization of nano-quasicrystalline
alloys*

Dissertation:

2003-2007 PhD student at the Max Planck Institute for Metals Research,
Institute for Materials Science, University of Stuttgart
Promoter: Prof. Dr. Ir. Eric J. Mittemeijer
Research Theme: *Nitriding of Iron-based alloys; residual stresses and
internal strain fields*

Danksagung

Die vorliegende Arbeit wurde am Institut für Metallkunde der Universität Stuttgart und am Max-Planck-Institut für Metallforschung angefertigt.

In erster Linie möchte ich mich bei Herrn Prof. Dr. Ir. E.J. Mittemeijer für die Aufnahme in seine Abteilung und für sein Interesse an dieser Arbeit besonders bedanken. Insbesondere bedanke ich mich bei ihm für sein außergewöhnliches Engagement bei der fachlichen Betreuung. Die zahlreichen und regelmäßigen wissenschaftlichen Diskussionen mit ihm haben ganz wesentlich zum Erfolg dieser Arbeit beigetragen.

Herrn Prof. Dr. F. Aldinger danke ich für die freundliche Übernahme des Mitberichts, sowie Herrn Prof. Dr. E. Roduner für die Zusage den Prüfungsvorsitz zu übernehmen.

Meinem täglichen Betreuer, Herrn Dr. R. Schacherl, danke ich für die stete Diskussionsbereitschaft und seine wertvollen Ratschläge. Zum erfolgreichen Durchführen und Abschließen der Arbeit hat er in großem Maße beigetragen.

Herzlich bedanken möchte ich mich bei allen Mitarbeitern des Max-Planck-Instituts für Metallforschung, insbesondere den Kollegen der Abteilung Mittemeijer, für die gute Zusammenarbeit und freundliche Unterstützung bei den Problemen des Forschungsalltages und für die angenehme Arbeitsatmosphäre. Dabei gilt mein besonderer Dank Arno Clauß, meinem langjährigen Zimmerkollegen.

Ermöglicht wurde diese Arbeit durch die finanzielle Unterstützung der „International Max Planck Research School for Advanced Materials (IMPRS-AM)“.

Am Schluss möchte ich einen besonderen Dank für meine Familie aussprechen. Sie war immer da als Unterstützung aus der Ferne. Meinen Freunden und Bekannten danke ich für das Verständnis, die sie mir in dieser Zeit entgegengebracht haben.

